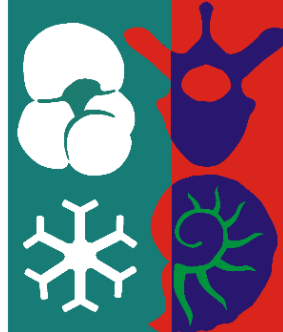




ARISTOTLE UNIVERSITY OF THESSALONIKI

Interinstitutional Program of Postgraduate Studies in

PALAEONTOLOGY - GEOBIOLOGY



ANGELOS TAMVAKIS

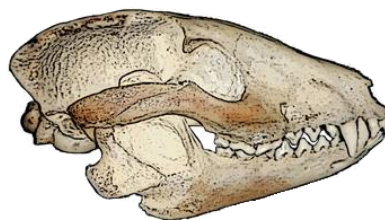
Geologist

SYSTEMATICS AND FUNCTIONAL MORPHOLOGY OF THE
SKULL IN GREEK FOSSIL AND EXTANT NYCTEREUTES

MASTER THESIS

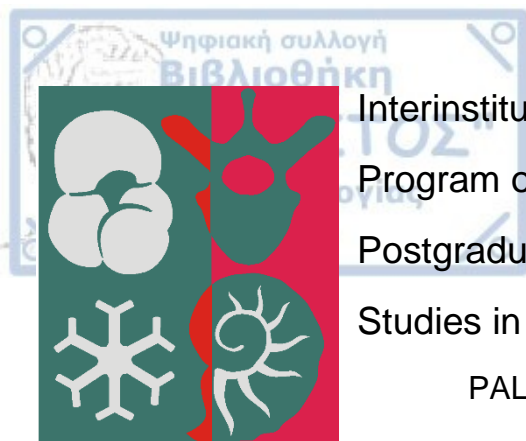
Direction: Macropalaeontology

Directed by Aristotle University of Thessaloniki



THESSALONIKI 2021





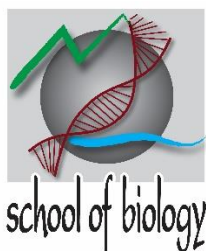
Interinstitutional
Program of
Postgraduate
Studies in

PALAEONTOLOGY – GEOBIOLOGY

supported by:



Τμήμα Γεωλογίας ΑΠΘ
School of Geology AUTH



Τμήμα Βιολογίας ΑΠΘ
School of Biology AUTH



National and
Kapodistrian
University of Athens
Faculty of Geology and
Geoenvironment

Τμήμα Γεωλογίας & Γεωπεριβάλλοντος ΕΚΠΑ
Faculty of Geology & Geoenvironment NKUA



Τμήμα Γεωλογίας Παν/μίου Πατρών
Department of Geology, Patras Univ.



UNIVERSITY OF THE AEGEAN

Τμήμα Γεωγραφίας Παν/μίου Αιγαίου
Department of Geography, Aegean Univ.





ANGELOS TAMVAKIS
ΑΓΓΕΛΟΣ ΤΑΜΒΑΚΗΣ
Πτυχιούχος Γεωλόγος

SYSTEMATICS AND FUNCTIONAL MORPHOLOGY OF THE SKULL IN GREEK
FOSSIL AND EXTANT NYCTEREUTES

ΣΥΣΤΗΜΑΤΙΚΗ ΚΑΙ ΜΟΡΦΟΛΕΙΤΟΥΡΓΙΚΗ ΑΝΑΛΥΣΗ ΤΟΥ ΚΡΑΝΙΟΥ
ΣΥΓΧΡΟΝΩΝ ΚΑΙ ΕΛΛΗΝΙΚΩΝ ΑΠΟΛΙΘΩΜΕΝΩΝ NYCTEREUTES

Υποβλήθηκε στο ΔΠΜΣ Παλαιοντολογία-Γεωβιολογία

Ημερομηνία Προφορικής Εξέτασης: 20/05/2021
Oral Examination Date: 20/05/2021

Three-member Examining Board

Professor Dionisios Youlatos, Supervisor
Professor Dimitrios S. Kostopoulos, Member
Professor Nikolai Spassov, Member

Τριμελής Εξεταστική Επιτροπή

Καθηγητής Διονύσιος Γιουλάτος, Επιβλέπων
Καθηγητής Δημήτριος Κωστόπουλος, Μέλος Τριμελούς Εξεταστικής Επιτροπής
Καθηγητής Nikolai Spassov, Μέλος Τριμελούς Εξεταστικής Επιτροπής



© Angelos Tamvakis, Geologist, 2021

All rights reserved.

SYSTEMATICS AND FUNCTIONAL MORPHOLOGY OF THE SKULL IN GREEK
FOSSIL AND EXTANT NYCTEREUTES – *Master Thesis*

© Άγγελος Ταμβάκης, Γεωλόγος, 2021

Με επιφύλαξη παντός δικαιώματος.

ΣΥΣΤΗΜΑΤΙΚΗ ΚΑΙ ΜΟΡΦΟΛΕΙΤΟΥΡΓΙΚΗ ΑΝΑΛΥΣΗ ΤΟΥ ΚΡΑΝΙΟΥ

ΣΥΓΧΡΟΝΩΝ ΚΑΙ ΕΛΛΗΝΙΚΩΝ ΑΠΟΛΙΘΩΜΕΝΩΝ NYCTEREUTES – *Μεταπτυχιακή*

Διπλωματική Εργασία

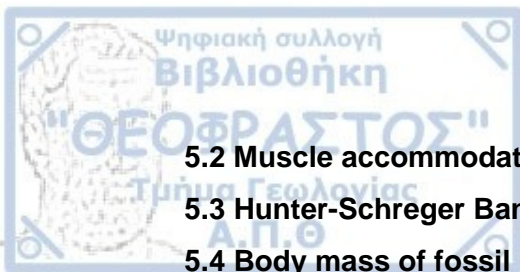
Citation:

Tamvakis, A., 2021. –Systematics and Functional morphology of the skull in Greek fossil and extant Nyctereytes. Master Thesis, Interinstitutional Program of Postgraduate Studies in Palaeontology-Geobiology. School of Geology, Aristotle University of Thessaloniki, 114 pp.

It is forbidden to copy, store and distribute this work, in whole or in part, for commercial purposes. Reproduction, storage and distribution are permitted for non-profit, educational or research purposes, provided the source of origin is indicated. Questions concerning the use of work for profit-making purposes should be addressed to the author. The views and conclusions contained in this document express the author and should not be interpreted as expressing the official positions of the Aristotle University of Thessaloniki.



Acknowledgements	9
ABSTRACT	10
ΠΕΡΙΛΗΨΗ	11
1. INTRODUCTION	12
1.1 Aims of Study	13
1.2 Presence of <i>Nyctereutes</i> in Greece and fauna assemblage in Greek <i>Nyctereutes</i> fossil sites	14
1.3 Geological background of Dafnero fossil site	16
2. The extant <i>Nyctereutes procyonoides</i>	17
2.1 Morphology of the extant raccoon dog <i>Nyctereutes procyonoides</i>	17
2.2 Extant varieties	18
2.3 Dispersal	19
2.4 Range and Habitat	19
2.5 Diet of extant and fossil <i>Nyctereutes</i>	19
2.6 Physical competitors and threats	20
3 Materials and Methods:	21
3.1 Studied specimens and comparative sample:	21
3.2 Measurements and statistical analyses	21
3.3 Functional analysis	27
3.3.1 From carnivory towards herbivory	27
3.3.2 Methods	30
4 Systematic Paleontology:	40
4.1 Descriptions	40
DFN3-155:	40
DFN3-342:	42
DFN3-154:	43
DFN3-8:	45
DFN3-8a-b:	46
4.2 Metric Data	47
4.3 Comparison	51
4.4 Discussion on phylogenetic relationships and evolutionary trends	57
5 Functional Morphology of fossil <i>Nyctereutes</i>	61
5.1 Geometric Morphometric analysis in <i>Nyctereutes</i> crania	61



5.2 Muscle accommodation in <i>Nyctereutes</i>	62
5.3 Hunter-Schreger Bands pattern in <i>Nyctereutes</i>	64
5.4 Body mass of fossil <i>Nyctereutes</i>	67
5.5 Bite Force Estimation in Fossil <i>Nyctereutes</i>	68
5.6 Prey Size Estimation in Fossil <i>Nyctereutes</i>	69
5.7 Cranial muscle accommodation in <i>Nyctereutes</i>	70
5.8 Cranial shape variation in <i>Nyctereutes</i>	70
5.9 The effect of the subangular lobe.....	72
5.10 Pre-postglenoid process and bite force	75
5.11 Bite Force, Prey Size Variation in <i>Nyctereutes</i>	76
6 CONCLUSIONS	78
REFERENCES.....	82
APPENDIX.....	91



Acknowledgements

Firstly, I would like to express my sincere appreciation to my supervisors, Professors Dimitrios S. Kostopoulos (Geology Department, Aristotle University of Thessaloniki) and Dionisios Youlatos (Biology Department, Aristotle University of Thessaloniki). Dimitrios S. Kostopoulos for entrusting me with the examined material. His guidance was crucial and beneficial, especially in the systematic section of the current thesis. Dionisios Youlatos for mentoring me during my first encounter with functional morphology subject. His advice and suggestions both on methodological part but also throughout the whole text were really helpful. I would also like to thank Dr. George Koufos, Professor Emeritus of Palaeontology and Stratigraphy (Geology Department, Aristotle University of Thessaloniki) for sharing his knowledge with me. I am deeply thankful to Professor Nikolai Spassov (Bulgarian Academy of Sciences), member of my examining board for providing me samples as comparative material part of the collection of the National Museum of Natural History of Sofia (NMNHS) but also for his suggestions on my text. I would like also to thank Gildas Merceron (Senior Researcher of French National Centre for Scientific Research, CNRS), CNRS, France [grant number PICS5185;2010-2013]; and the National Geographic Society [grant 9903-16; 2016-2017] for supporting the excavations in Dafnero site, as well all the researchers participating at the excavations in Dafnero site. Secondly, I am deeply grateful to Dr. Fay Penrose (School of Veterinary Science, University of Liverpool) for sharing photographs of her work with me, providing me helpful comparative material for my thesis. Last but not least I would like to thank my family and all my friends for their support.



ABSTRACT

The present thesis studies the newly excavated *Nyctereutes* material from Dafnero, as well as the functional morphology of the skull in fossil and extant *Nyctereutes*. The new material includes two complete skulls, one partially preserved skull and two hemimandibles. *Nyctereutes* has been previously documented in various sites of Greece with the presence of *N. megamastoides* and *N. tingi*. The findings of Dafnero extend the presence of *N. tingi* in Europe until the middle Villafranchian. Moreover, the co-existence of *N. tingi* and *N. megamastoides* is reported for the first time in Europe. Furthermore, the metric data of *N. tingi* from Dafnero, imply a relation between *N. tingi* and *N. vulpinus* as supported by previous studies. The morpho-functional study includes the analysis of endocranial volume and bite force variation, the geometric morphometric examination of the skull, and the HSB structure of *Nyctereutes* dentition. The endocranial volume variation indicates the development of a bigger temporalis muscle in the more carnivorous species, *N. tingi* and *N. donnezani*. The geometric morphometric analysis revealed differences in the crania of *Nyctereutes*, with the more omnivorous species possessing a more horizontally aligned cranium, and the more carnivorous a more vertically aligned one. Larger bite forces were estimated for the larger species, but no specialized bony structures, aiming to increase bite force, were observed. The Hunter Schreger Bands structure is similar in all *Nyctereutes* species, suggesting equal bone consumption. The dietary plasticity of *Nyctereutes* allowed it to co-exist with larger and similar sized carnivores.



ΠΕΡΙΛΗΨΗ

Η παρούσα εργασία μελετά το νέο υλικό *Nyctereutes* από την θέση Δαφνερό, από συστηματική άποψη, καθώς και την οικομορφολογική ανάλυση του κρανίου τόσο απολιθωμένου όσο και του σύγχρονου *Nyctereutes*. Το νέο υλικό αποτελείται από δύο ολόκληρα κρανία, ένα μερικώς διατηρημένο κρανίο και δύο ημιγνάθους. Η παρουσία του *Nyctereutes* έχει καταγραφεί προηγουμένως σε διάφορες θέσεις στον Ελλαδικό χώρο κυρίως με το είδος *N. megamastoides* και *N. tingi*. Τα ευρήματα του Δαφνερού μαρτυρούν την παρουσία του *N. tingi* στην Ευρώπη μέχρι το μέσο Βιλαφράγκειο. Επιπρόσθετα, δείχνουν την συνύπαρξη του *N. tingi* και του *N. megamastoides* στην Ευρώπη για πρώτη φορά. Επιπλέον, τα μετρικά δεδομένα των δειγμάτων *N. tingi* από το Δαφνερό προτείνουν μία σχέση μεταξύ του *N. tingi* και του *N. vulpinus* όπως έχει προταθεί στο παρελθόν από προηγούμενους ερευνητές. Η μορφολειτουργική ανάλυση περιλαμβάνει μελέτη της διακύμανσης ενδοκρανιακού όγκου και της δύναμης δαγκώματος, της γεωμετρικής μορφομετρικής ανάλυσης των κρανίων διαφόρων ειδών *Nyctereutes* και της δομής των HSB γραμμών στην οδοντοστοιχία του *Nyctereutes*. Η διακύμανση του ενδοκρανιακού όγκου προτείνει πως ο κροταφικός μυς ήταν μεγαλύτερος στις πιο σαρκοφάγες μορφές, *N. tingi* και *N. donnezani*. Η γεωμετρική μορφομετρική ανάλυση αναδεικνύει διαφορές στα κρανία των *Nyctereutes*, με τις πιο παμφάγες μορφές να έχουν ένα οριζοντίως προσανατολισμένο κρανίο, ενώ οι πιο σαρκοφάγες μορφές να έχουν ένα πιο κάθετα προσανατολισμένο κρανίο. Μεγαλύτερες δυνάμεις κατά το δάγκωμα περιμένουμε στις πιο εύρωστες μορφές, χωρίς να έχουν παρατηρηθεί εξειδικευμένες μορφολογικές προσαρμογές προς την ενίσχυση του δαγκώματος. Η δομή των Hunter Schreger Bands είναι παρόμοια σε όλα τα είδη *Nyctereutes*. Το μεγάλο εύρος διατροφικών επιλογών του *Nyctereutes* του επέτρεψε να συνυπάρξει με μεγαλύτερα ή και ισομεγέθη σαρκοφάγα.

1. INTRODUCTION

The genus *Nyctereutes* belongs to the family Canidae. The clade of Canidae originates back in the Eocene with the first representatives of Canini dated to the late Miocene of North America (Tedford et al., 2009). Around 7 Ma canids migrated from North America to Eurasia via the Beringian land bridge (Tedford et al., 2009). There, one of these canid immigrants diversified giving rise to the first representatives of the genus *Nyctereutes*. It not clear yet which is the ancestor of *Nyctereutes*. The oldest fossils of *Nyctereutes* in both Europe (France, Spain) and Asia (Yushe basin in China) are considered to date from the early Pliocene (Ruscinian) and they are referred to the species *N. donnezani* and *N. tingi* respectively (Lucenti, 2018).

The European descendant of this radiation is considered to be the extinct species *N. megamastoides*, a form which is similar to the Asiatic *N. sinensis* (Bartolini Lucenti, 2017; Ward and Wurster-Hill, 1990). The European taxon disappeared by the end of the Pliocene, while the Asiatic form survived and decreased in body size to the point of the extant raccoon dog, *N. procyonoides* (Ward and Wurster-Hill, 1990). Based on recent studies, 8 to 10 fossil species are recognized and related to the extant *Nyctereutes procyonoides* (Daguenet and Sen, 2019). The oldest species with the most primitive features, is *Nyctereutes tingi* (Lucenti et al., 2018). The Asian fossil record includes *Nyctereutes tingi* (Late Miocene to Middle Pliocene) and *N. sinensis* (Middle Pliocene to Middle Pleistocene) (Asahara et al., 2015). According to Lucenti (2017), *N. sinensis* is considered as the closest phylogenetic relative to the extant *Nyctereutes procyonoides*, but further research must be done on this topic. In Europe three fossil species are known: *N. donnezani* from Western Europe (Ruscinian) (Lucenti, 2017) and Turkey (Daguenet and Sen, 2019), *N. tingi* known from Greece (Bartolini Lucenti, 2018; Koufos, 1997) but also from Bulgaria with *N. cf. tingi* (Monguillon et al., 2004; Spassov, 2003, 1997), *N. vulpinus* from St. Vallier, France (Monguillon et al., 2004) and *N. megamastoides* from the middle-late Villafranchian faunas of Italy, France, Georgia, Greece and Hungary (Koufos, 1993; Lucenti, 2018, 2017). Regarding the European fossil record, the origins of *N. megamastoides* has been attributed into *N. donnezani* lineage (Lucenti, 2017), while the relations of *N. vulpinus* with the rest of the known fossil species are yet unclear. The newly excavated material from Dafnero comes to aid further information regarding the presence of *N. tingi* and the systematic status of *N. vulpinus* in the European region.

Extant *Nyctereutes* is thought to be a small fox-like canid with omnivorous diet and distinct opportunistic behaviour (Asahara and Takai, 2017; Kauhala et al., 1998). This dietary plasticity of *Nyctereutes* has been highlighted in its fossil representatives by previous studies mainly by the study of m2/m1 area of the lower dentition (Asahara and Takai, 2017; Bartolini Lucenti, 2019; Lucenti et al., 2018). Over the years specific morphological adaptations in *Nyctereutes* have been associated in response to specific diet preferences, such as the more triangular shaped molars or the development of the subangular lobe (Asahara and Takai, 2017; Bartolini Lucenti, 2019; Monguillon et al., 2004). It is believed that the more primitive *Nyctereutes* species (*N. tingi*, *N. donnezani*) were adapted to a more carnivorous diet in comparison with the more derived species such as *N. megamastoides* and *N. sinensis* (Bartolini Lucenti, 2019). Nevertheless, the variation of *Nyctereutes* skull morphology regarding its diet preferences has not been fully explored yet.

1.1 Aims of Study

This study has two main goals. Firstly, to identify the newly excavated material from Dafnero site and provide additional information regarding the presence of *Nyctereutes* in Europe. Moreover, we attempt to investigate the possible affinities between the primitive *N. tingi* and the more derived *N. megamastoides* and *N. vulpinus* (Monguillon et al., 2004). *Nyctereutes tingi* in Asia co-occurred with its successor *N. sinensis* (Farjand et al., 2020). In Europe, *N. tingi* is represented by two skulls of Pliocene age from Megalo Emvolo (Koufos and Kostopoulos, 1997), while Spassov (2003) mentions an early Pleistocene presence of *N. cf. tingi* from the locality of Varshets in Bulgaria. It has been previously suggested that *N. vulpinus* may have originated by a possible European clade of *N. tingi* (Monguillon et al., 2004). Two *N. megamastoides* skulls have been previously described from Dafnero (Koufos, 1993). The recent finding of a robust skull with distinct cranial characters raised different questions regarding its taxonomy. Secondly, we attempt to clarify the functional morphology of the skull of *Nyctereutes*. A shift towards more omnivorous diet in the more derived species has been suggested by different authors (Asahara & Takai, 2017, 2019; Lucenti, 2019). The gradient development of the subangular lobe in *Nyctereutes* has been associated with an increased ability for mastication (Bartolini Lucenti, 2019; Curtis and Santana, 2018; Dagenet and Sen, 2019; Ewer, 1973). Here we attempt to investigate any structural differences between the more carnivorous and the more omnivorous *Nyctereutes* species and their functional importance. Studies have revealed that the different skull morphology of the Carnivorans affects the accommodation of the adductor muscles within the cranium (Penrose et al., 2016), but also their mechanical advantage (Figueirido et al., 2010; Penrose, 2018). Differences in the mastication ability related with variation of temporalis muscle size in canids have been previously addressed by other studies, as that of the skull morphology in a red fox population of Hokkaido (Amaike et al., 2015). We hypothesize that the more omnivorous species will invest towards enhancing the masseter muscle which is the primary muscle in transverse chewing as observed in the herbivores (Popowics and Herring, 2006). On the contrary, the more carnivorous species may have opted for the enhancement of the temporalis muscle which is mainly utilized for the infliction of a lethal bite (Van Valkenburgh, 2007). To test our hypothesis, specific skull characters will be studied: (a) we expect lower brain-volumes in the more carnivorous species while the Miller's index is constant, allowing the more carnivorous species to accommodate a bigger temporalis. Contrariwise, the more omnivorous species will be probably characterized by skull structures providing more available attachment surface area for the masseter, such as the subangular lobe; (b) greater mechanical advantage for the temporalis is expected in the more carnivorous species by the more vertical aligned crania, and on the other hand for the masseter in the more omnivorous species with a horizontally aligned crania or the elevation of the zygomatic arches; and (c) a shorter rostrum is expected in the more carnivorous species increasing the strength of the bite force, while the more omnivorous species will probably exhibit a more elongated muzzle able for rapid chewing.

1.2 Presence of *Nyctereutes* in Greece and fauna assemblage in Greek *Nyctereutes* fossil sites

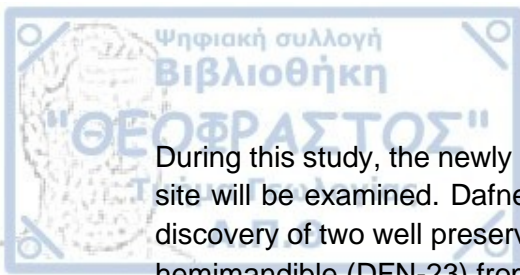
Fossil *Nyctereutes* is reported in Greece by two species that of *N. tingi* and *N. megamastoides* (Koufos, 2013), while the extant *N. procyonoides* has not yet been reported in the Greek landscape. The localities with *Nyctereutes* in Greece are depicted in Fig. 1 and in Table 1.



Fig. 1. Geographic map indicating the positions of the *Nyctereutes* presence in Greece.

Table 1. List of *Nyctereutes* fossil species from Greek sites.

Species	Locality	Age
<i>Nyctereutes tingi</i>	Megalo Emvolo (MEV)	MN-15
<i>Nyctereutes megamastoides</i>	Dafnero 1-3 (DFN1-3)	MN-17
<i>Nyctereutes megamastoides</i>	Sesklon (SES)	MN-17
<i>Nyctereutes megamastoides</i>	Volax (VOL)	MN-17
<i>Nyctereutes megamastoides</i>	Vatera- F (VAT F)	MN-17
<i>Nyctereutes cf. megamastoides</i>	Vatera- E (VAT E)	MN-17



During this study, the newly excavated material of *Nyctereutes* from Dafnero-3 (DFN3) site will be examined. Dafnero has provided *Nyctereutes* material previously with the discovery of two well preserved *N. megamastoides* skulls (DFN-17 and DFN-20) and a hemimandible (DFN-23) from DFN1 site (Koufos, 1993).

The fauna of Dafnero includes numerous carnivores: *Homotherium latidens*, *Chasmaporthetes lunensis*, *Baranogale cf. helbingi*, *Nyctereutes megamastoides*, *Vulpes alopecoides*, *Ursus cf. etruscus*, whereas the herbivorous species are: *Paradolichopithecus aff. arvernensis*, *Equus stenorhis cf. vireti*, *Palaeotragus inexpectatus*, *Metacervoceros ex gr. rhenanus*, *Eucladoceros tegulensis*, *Gallogoral meneghinii*, *Gazella bouvraine* and *Gazellospira torticonis* (Hermier et al., 2020; Kostopoulos et al., 2019). The faunal assemblage of Dafnero is similar to that of Sesklo, Vatera and Volakas from Greece and Saint Vallier from France and La Puebla from Spain (Koufos and Kostopoulos, 1997; Kostopoulos et al., 2019). Paleoenvironmental reconstructions show a relatively dry and open habitat with the presence of giraffids and various bovid species like *Gazellospira* along with *Equus stenorhis* and on the same time the absence of suids (Athanassiou, 1996; de Vos et al., 2002). Typically, the existence of a deer (*Eucladoceros*) indicates the presence of forest or a closed habitat. In this case this may not be true as *Eucladoceros* was a browser that could feed with herbaceous monocotyledons and thus could survive in open wooded habitats (Berlioz et al., 2018). In summary, the paleoenvironment of Dafnero area must have been a mosaic of open landscapes with parts of wooded areas with dry climate.

The Megalo Emvolo fossil area is situated in Thermaikos bay, 20 Km southwest of Thessaloniki (Boev and Koufos, 2000; George D. Koufos et al., 1991). The Megalo Emvolo site has yielded two *Nyctereutes* skulls, referred to as *N. tingi* (Koufos, 1997). Three fossiliferous sites have been discovered, "Megalo Emvolo 1", "Megalo Emvolo 2" and "Megalo Emvolo 3". The geological formation consist of sedimentary rocks like sands, gravels, silts, sand-silts, and sandstones with calcitic concretions (Boev and Koufos, 2000). According to Koufos (2006), the fauna assemblage of Megalo Emvolo includes: *Testudo cf. graeca*, *Testudo sp.*, *Pavo bravardi*, *Dolicopithecus rusciniensis*, *Trischizolagus dumitrescuae*, *Trischizolagus cf. maritsae*, *Oryctolagus cf. laynensis*, *Microspalax odessanus*, *Hipparion longipes*, *Sus minor*, *Parabos, macedoniae*, *Gazella borbonica*, *Koufotragus bailloudi* and the only carnivoran found *Nyctereutes tingi*. This site has been dated to late Ruscinian (MN 15) (Koufos, 2013).

Sesklon is a village 15km west of Volos. This fossil area is situated in a basin consisted of Mesozoic metamorphic rocks filled with clay (Athanassiou, 2002). The carnivores reported in Sesklon are: *Nyctereutes megamastoides*, *Vulpes cf. alopecoides*, *Ursus cf. etruscus*, *Pliohyaena perrieri*, *Homotherium crenatidens*, cf. *Homotherium crenatidens* (Athanassiou, 2002; Koufos, 2013). The presence of herbivores is also abundant. The majority of the herbivore taxa belong to *Equus stenorhis*, *Gazellospira torticornis*, *Gazella bouvrainae*, *Gazella borbonica*, and *Euthyceros thessalicus* (Athanassiou, 2002). The fauna is also consisted by many cervids such as *Croizetoceros ramosus*, *Eucladoceros ctenoides* and *Metacervoceros aff. rhenanus* (Koufos, 2013). The presence of *Anancus arvernensis* and *Mammuthus meridionalis* has also been reported. The Sesklon locality is dated in MN17 (Lower Pleistocene) (Koufos, 2013).

Volax fossil site is located in Drama basin, in Macedonia Greece close to the Falakro Mountain. The fauna of Volax locality is consisted by several carnivores, including: *Nyctereutes megamastoides*, *Vulpes praecorsac*, *Bosdagius felinus*, *Megantereon megantereon* and *?Lynx issiodorensis*, a single Equidae and Giraffidae, *Equus stenorhis* cf. *vireti* and *Mitlanotherium martinii* respectively, numerous bovids: cf. *Leptobos*, *Gazellospira* cf. *torticornis*, *Gallogoral meneghinii sickenbergi*, *Gazella* sp., *?Procamptoceras* sp. and some cervids like *Eucladoceros ctenoides*, *Metacervoceros rhenanus*, *Croizetoceros ramosus*. The fossil site is dated in MN17 (Lower Pleistocene) (Koufos, 2013).

Vatera locality is located in the southern parts of Lesvos island (Lyras and van der Geer, 2007). Numerous fossil sites have been found in Vatera, with the presence of *Nyctereutes* been recorded in VTR-F and VTR-E. Overall Vatera fauna includes: *Paradolichopithecus arvernensis*, *Nyctereutes megamastoides*, *Meles thoralis*, *Anancus* cf. *arvernensis*, *Equus* cf. *stenorhis*, *Equus* sp., *Metacervoceros* cf. *rhenanus*, *Mitlanotherium* cf. *inexpectatum*, *Gazella* aff. *borbonica*, *Gazella* cf. *bouvrainae*, *Gazellospira* cf. *torticornis*, cf. *Leptobos* sp., Antilopinae indet. A. and Antilopinae indet. D, *Mammuthus* cf. *meridionalis*, *Stephanorhinus* cf. *etruscus*, *Machairodontinae* indet. and *Testudo* sp.. Vatera fauna is dated around ~2 Ma (Lower Plesitocene) (Lyras and van der Geer, 2007).

This study involves fossil *Nyctereutes* material from Megalo Envolo and Dafnero sites.

1.3 Geological background of Dafnero fossil site

The fossiliferous site of Dafnero is located near Dafnero Village of Western Macedonia, Greece, close to the Aliakmon river, on the southwest slopes of Mt. Vourinos (Fig. 2).

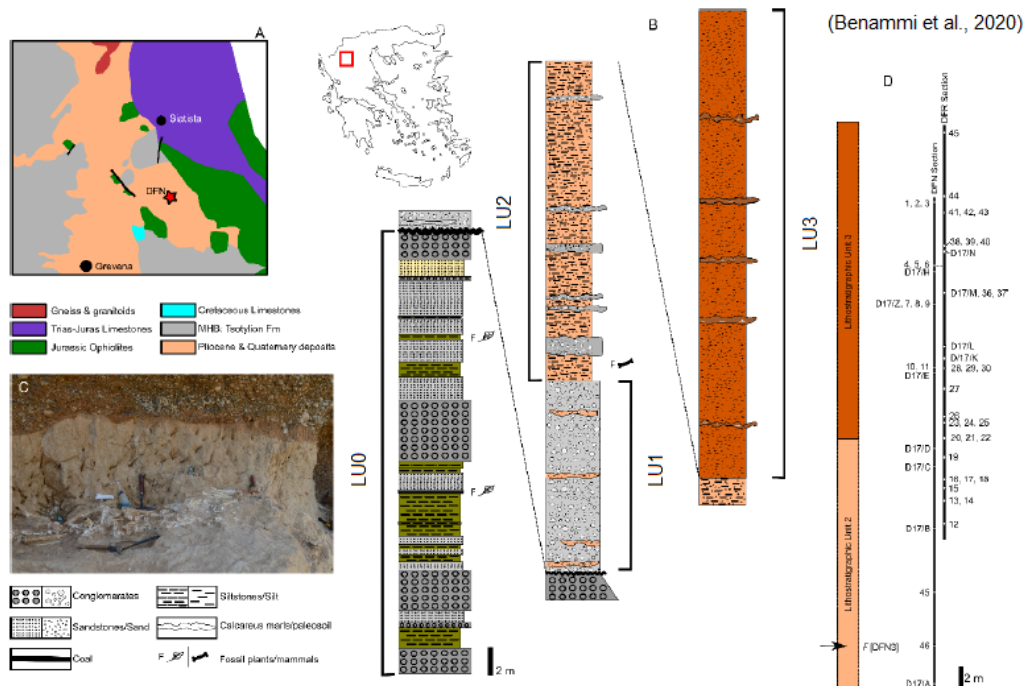
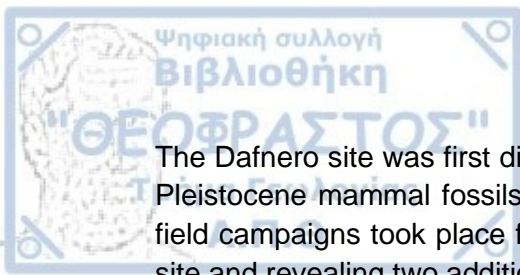


Fig. 2. Geological and geographic setting for Dafnero fossil site. A: Simplified geological map of the examined area, B: Stratigraphic composition of Dafnero sedimentological sequence, C: Local sedimentological setting as indicated by the fossil accumulation of DFN3, D: Palaeomagnetic sampling and correlation of the two sampled sections of Dafnero area (from: Benammi et al., 2020).



The Dafnero site was first discovered in the 1990s yielding important but scarce Early Pleistocene mammal fossils (Benammi et al., 2020; Koufos, 1993). More systematic field campaigns took place from 2010 on improving the fossil assemblage of Dafnero site and revealing two additional sites (Dafnero-2, DFN2; Dafnero-3, DFN3) (Benammi et al., 2020; Koufos et al., 2020). The finding of a nearly intact cercopithecoid cranium, upgraded the importance of Dafnero site, to a primate-bearing locality (Kostopoulos et al., 2018). Dafnero is located near the eastern margins of the Mesohellenic Basin (MHB) (Benammi et al., 2020). In the studied area fossiliferous deposits overlay Tsiotyliion formation which is represented by a lithostratigraphic unit (LU0) of approximately 30m, consisting of gray-green conglomerates with siltstone and sandstone intercalations (Benammi et al., 2020) (Fig. 4).

A ~60m thick unit of sands, gravels conglomerates and clays of fluvio - terrestrial origin is placed unconformably on LU0 (Koufos et al., 1991; Benammi et al. 2020). This unit is subdivided in three separate subunits (LU1-3; Benammi et al. 2020). The fossiliferous sites (DFN, DFN2, DFN3) are situated at the very base of LU2. DFN and DFN3 sites are on the the same fossiliferous layer at the opposite slopes of a hill (Kostopoulos et al. 2018). The majority of fossil specimens found in DFN3 were subjected to deformation. Initial biochronological data from DFN1 suggested a middle Villafranchian age (Koufos et al., 1991), but recent magnetostratigraphic results estimate a 2.3 Ma age for Dafnero fauna (Benammi et al., 2020).

2. The extant *Nyctereutes procyonoides*

2.1 Morphology of the extant raccoon dog *Nyctereutes procyonoides*

Nyctereutes procyonoides is a small fox-like canid that originated in Asia (Fig. 3) (Japan, Vietnam, Korea, eastern Siberia) (Kauhala and Kowalczyk, 2011; Naderi et al., 2020; Sheldon, 1992). A distinguished feature of the species is a facial black mask, resembling the appearance of a raccoon (*Procyon lotor*). It has a short and pointy muzzle, typical of a canid and small, rounded ears (Ward and Wurster-Hill, 1990). Its tail is about 1/3 of its total body length. It is generally a small animal, with body mass varying from 4 to 5 kg (Ward and Wurster-Hill, 1990), with a total length of about 60-68 cm (Sheldon, 1992) while the height at the tip of its shoulders can reach a maximum of 50 cm (Naderi et al., 2020). Considering its small size, *Nyctereutes* has a stout structure, distinguishable post-cranial skeleton, consisted of hefty cervical vertebrae and stout appendicular bones, characteristics that do not match those of a typical cursorial canid like *Canis lupus* or *Canis latrans* (Ward and Wurster-Hill, 1990). *Nyctereutes* is not considered an agile swift canid. Thick fur covers its body, giving it the appearance of a robust animal. Depending on the climate, fur thickness changes. Its fur operates as thermal insulation and helps to control its body temperature (Ward and Wurster-Hill, 1990). In cold climates it is dense and soft, giving the impression that the animal's legs are extremely short. During summer, or in the southern range of the species distribution with warmer climates, its fur is thinner (Ward and Wurster-Hill, 1990). *Nyctereutes* can also alter its metabolism to endure colder climates (Ward and Wurster-Hill, 1990). It is the only canid reported to hibernate (Naderi et al., 2020). Its teeth are generally small, with the carnassial blade being reduced compared to that of a typical canid. On the contrary, its upper molars are large and in some occasions an

extra molar has been observed giving a different dental formula: I/l 3/3, C/c 1/1, P/p 4/4, M/m 2-3/3 and not the usual of canids with M/m: 2/3. *Nyctereutes procyonoides* depends basically on its olfaction, as its sight is not very reliable (Ward, 1959). It is characterized as a nocturnal animal, whereas during the day it spends most of its time in its den (Abe et al., 2006; Ward, 1959). On some occasions it can be active during daytime if it feels threatened or hungry.



Fig. 3. *Nyctereutes procyonoides*, from Hanover, Germany. Photo taken by Michael Gäbler.

2.2 Extant varieties

The single living representative of *Nyctereutes*, *N. procyonoides* includes several subspecies based on phenotypic, craniometric and behavioral differences (Castelló, 2018). According to Asahara et al. (2015) there are six geographically separated subspecies:

- *N. p. procyonoides* (West southwest China and north Indonesia)
- *N. p. orestes* (Gansu, Guizhou, Shaanxi, Sichuan, and Yunnan provinces in China)
- *N. p. ussuriensis* (southeast Russia, northeast China, east Mongolia)
- *N. p. koreensis* (Korea)
- *N. v. viverrinus* (Japan except Hokkaido)
- *N. v. albus* (Hokkaido, Japan)



2.3 Dispersal

Raccoon dog originally comes from Asia, South eastern Siberia and China (Sheldon, 1992). It was introduced to Europe after 9,000 individuals were released in the western areas of the former Soviet Union, in order to exploit its fur (Drygala et al., 2010; Kauhala, Kaarina, Kowalczyk, 2012). The species is now found in most parts of Europe like Finland, Sweden, Germany, parts of eastern Europe (Sheldon, 1992) even in the Balkan region (Bulgaria) (Natchev, 2016), while recently, it was recorded in Turkey (Naderi et al., 2020). Its ability to withstand most of the climate conditions alongside with its omnivorous opportunistic diet allows *Nyctereutes* to disperse easily and accommodate in new habitats.

2.4 Range and Habitat

Nyctereutes procyonoides can live in a wide range of climates, from the subtropical climate of Japan, Vietnam and Indonesia to the arid continental climate of Siberia and Mongolia with extremely cold winters (Kauhala and Kowalczyk, 2011) as it is the only canid with the ability to hibernate (Naderi et al., 2020). Most of the time, it chooses as habitat mixed or conifer forests with thick undergrowth that can be used as a cover, river valleys, fields, meadows or marshlands (Kauhala, Kaarina, Kowalczyk, 2012; Kauhala and Kowalczyk, 2011; Naderi et al., 2020; Sheldon, 1992) while sometimes it also ranges in urban areas (Kauhala and Kowalczyk, 2011). Whenever feasible, it chooses areas nearby to water, like river shores or lakes, as it can also dive into water to flee from a potential threat. Furthermore water provides plenty of food sources like fish or small amphibians (Mulder, 2012; Sheldon, 1992). It typically avoids dense forests and areas with sparse undergrowth (Mulder, 2012). Raccoon dogs can manage with most types of environments if they are given shelter and enough food (Sutor et al., 2014).

2.5 Diet of extant and fossil *Nyctereutes*

Despite their name, Carnivorans exhibit a variety of food choices. Depending on their preferences the representatives of the group are categorized into five groups: hypercarnivorous (>70% diet with meat), mesocarnivorous (50-70% diet with meat), hypocarnivorous (<50% diet with meat), omnivorous (diet based on insects, plant material), and herbivorous. *Nyctereutes* is an omnivorous animal with a wide spectrum of food preferences (Kauhala and Kowalczyk, 2012), contrary to its main competitor the red fox (*Vulpes vulpes*) (Drygala et al., 2014). The main food sources of *Nyctereutes procyonoides* are small mammals (basically rodents), plants (maize, fruits, berries and human crops like potatoes), carrion, small amphibians and sometimes fish and birds (Hirasawa et al., 2006; Mulder, 2012). The absolute absence of prey like hares (*Lepus spp.*) and rabbits (*Oryctolagus cuniculus*) is noticeable, as speed and strength is required for their capture, reflecting the inability of *Nyctereutes procyonoides* to hunt them, as it lacks on agility and speed and shows lack of predatory expertise (Mulder, 2012). The diet of *Nyctereutes procyonoides* varies depending on spatial and seasonal food availability. Data from studies of *Nyctereutes procyonoides* stomach remains and feces show the seasonal variation of raccoon's dog diet (Fig. 4).

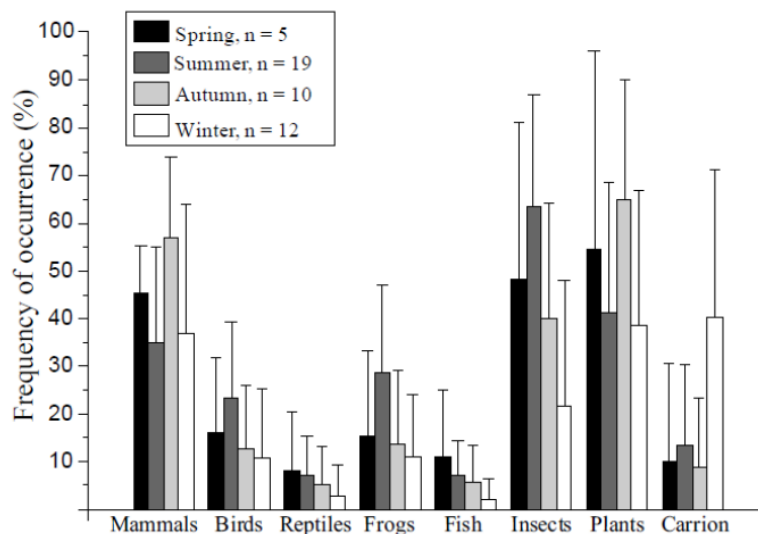


Fig. 4. *Nyctereutes procyonoides* diet variation during each season (from: Kauhala, Kowalczyk, 2012).

During spring, the main food source comes from plants like leaves and fruits while the main prey is insects. In summer, it is similar to that of spring, with the difference that more amphibians and insects are available for hunting. In autumn, *N. procyonoides* depends basically on different fruits and plants and small mammals. In winter plants are difficult to find, so raccoon dogs depend mostly on predation of small mammals and the detection of carcasses and carrion.

The diet of the raccoon dog also depends on the area. During the winter *N. procyonoides* feeds mostly on carrion in Northern Germany, during the winter, (Drygala et al., 2014), while in Japan, where plant is abundant due to better climate conditions, it consumes more fruits, berries, and crops (Hirasawa et al., 2006). Both seasonal and spatial diet variation highlight the opportunistic behavior of this animal (Mulder, 2012).

2.6 Physical competitors and threats

Nyctereutes procyonoides is a medium sized canid. Its main competitors are other medium sized omnivores like badgers, foxes (Kauhala, Kaarina, Kowalczyk, 2012), and in Japan the invasive raccoon *Procyon lotor* (Matsuo and Ochiai, 2009). The fact that these animals have a wide variety of food choices allows the coexistence of these species with no potential population decrease in either species (Drygala et al., 2014; Kauhala, Kaarina, Kowalczyk, 2012). However, the lack of muscularity and speed in raccoon dogs make them vulnerable to predators. There are many occasions where *Nyctereutes* pups have been killed by badgers or foxes, because raccoon dogs nest in burrows or dens, where they have easy access, or by bigger predators, such as lynx or wolves and bears, when in lairs built in the undergrowth (Mulder, 2012). During the winter, when finding prey is scarce, many predators habitually scavenge for carcasses. This may result in lethal attacks from other larger predators like wolf, lynxes or even eagles (Kowalczyk et al., 2009). It is clear that *N. procyonoides* is unable to compete in brute strength or agility with other carnivorans, even the ones of similar size. In this way, raccoon dogs adopt a strategy of remaining undetected rather than engaging in fights with them.

3 Materials and Methods:

3.1 Studied specimens and comparative sample:

The present study examines the fossil material of *Nyctereutes* from the fossiliferous site DFN3 in Western Macedonia, Greece. The fossil material is housed in the Museum of Geology-Palaeontology-Palaeoanthropology, School of Geology, Aristotle University of Thessaloniki (LGPUT). Fossil specimens from the sites of DFN1 and Megalo Emvolo, along with two extant skulls of *N. procyonoides* from Bulgaria, kindly provided by Prof. Nicolai Spassov, were used as comparative material. Moreover, additional published material of *Nyctereutes* was also used for quantitative comparative analyses. The studied cranial material is shown in Table 1. The complete list of material along with photos from the rest Greek fossil *Nyctereutes* used in this thesis is presented in the Appendix (Table 20-22) (Fig. 35-42) and Table 2.

Table 2. List of examined crania material used in this study.

Specimens	Species	Age	Source	Location
Bulgaria 1	<i>N. procyonoides</i>	modern	NMNHS	Bulgaria
Bulgaria 2	<i>N. procyonoides</i>	modern	NMNHS	Latvia
DFN3-155	<i>N. megamastoides</i>	2.3 Ma	LGPUT	Dafnero
DFN-17	<i>N. megamastoides</i>	2.3 Ma	LGPUT	Dafnero
DFN-20	<i>N. megamastoides</i>	2.3 Ma	LGPUT	Dafnero
MG 29-2013/457 (K220)	<i>N. megamastoides</i>	3.07 Ma	GNM	Kvabebi
MG 29-2013/581 (K219)	<i>N. megamastoides</i>	3.07 Ma	GNM	Kvabebi
MNHN.F.ACA 291	<i>N. donnezani</i>	4.2-3.2 Ma	MNHN	Çalta
MNHN.F.ACA 292	<i>N. donnezani</i>	4.2-3.2 Ma	MNHN	Çalta
MNCN63662	<i>N. donnezani</i>	3.91 Ma	MNCN	Layna
DFN3-154	<i>N. tingi</i>	2.3 Ma	LGPUT	Dafnero
MEL-1	<i>N. tingi</i>	4.2-3.2 Ma	LGPUT	Megalo Emvolo
MEL-2	<i>N. tingi</i>	4.2-3.2 Ma	LGPUT	Megalo Emvolo

Institutional Abbreviations:

NMNHS: National Museum of Natural History, Sofia (Bulgaria), MNHN: Natural History Museum of Paris, (France), GNM: Georgian Natural Museum, Tbilisi (Georgia), MNCN: Museo Nacional de Ciencias Naturales-CSIC, Madrid (Spain),

3.2 Measurements and statistical analyses

Photos of the physical samples were taken using a digital camera Nikon D5200 in order to take the essential measurements for the estimation of bite force and brain volume with the dry skull method following Damasceno et al. (2013) and Finarelli (2006) as well

as for the geometric morphometric analysis and the computation of the HSB angles. Digital measurements were computed with the software ImageJ (Schneider et al., 2010). Physical measurements of the cranium, dentition and mandible were taken using a digital caliper to the nearest of 0.1 mm following von den Driesch's (1976) method. All measurements are displayed in Fig. 5-8. The abbreviations and full descriptions of the measurements used in this analysis are given in Table 3.

In order to examine the importance of specific morphologies in distinguishing the different functional properties in *Nyctereutes*, an analysis of variance one-way ANOVA was conducted in specific measurements inferred from the available literature. Differences between the various *Nyctereutes* species were tested with Tukey's post hoc tests. The differences of specific morphologies between *Nyctereutes* were shown with boxplots constructed by specific measurements highlighted by ANOVA. For all statistical analyses we used the PAST software ver. 3.26b (Hammer et al., 2001).

The dental nomenclature for the upper dentition used in this study follows Farjand et al., 2020 (Fig. 9). The nomenclature for the lower dentition was based on Tedford et al., 2009 (Fig. 10). The osteological and muscle nomenclature is according to Howard & de Lahunta, 2013; Penrose, 2018.

Complete measurements of various *Nyctereutes* specimens skull, upper and lower dentition are provided in the Appendix in Tables 20-22.

Table 3. Skull and dental measurements used in this study (measurements are displayed in Fig. 5-8).

	Abbreviation	Measurement	Definition
Skull	SKL	Total skull length	Distance from prosthion to inion
	MSW	Maximum squamosal width	Maximum width of the zygomatic arch (from the exterior border)
	BCL	Braincase length	Apex of nuchal crest to postorbital constriction
	BCW	Braincase width	Maximum width across the braincase posterior to zygomatic arches and dorsal to tympanic bullae
	SKH	Skull height	Maximum height between the sagittal crest and basion
Upper Dentition	P1L	P1 length	Anteroposterior distance of upper first premolar
	P1W	P1 width	Buccolingual width of the upper first premolar
	P2L	P2 length	Anteroposterior distance of upper second premolar
	P2W	P2 width	Buccolingual width of the upper second premolar
	P3L	P3 length	Anteroposterior distance of upper third premolar
	P3W	P3 width	Buccolingual width of the upper third premolar
	P4L	P4 length	Anteroposterior distance of upper fourth premolar
	P4W	P4 width	Buccolingual width of the upper fourth premolar

Lower Dentition	M1L	M1 length	Anteroposterior distance of upper first molar
	M1W	M1 width	Buccolingual width of the upper first molar
	M2L	M2 length	Anteroposterior distance of upper second molar
	M2W	M2 width	Buccolingual width of the upper second molar
	p2L	p2 length	Anteroposterior distance of lower second premolar
	p2W	p2 width	Buccolingual width of the lower second premolar
	p3L	p3 length	Anteroposterior distance of lower third premolar
	p3W	p3 width	Buccolingual width of the lower third premolar
	p4L	p4 length	Anteroposterior distance of lower fourth premolar
	p4W	p4 width	Buccolingual width of the lower fourth premolar
	m1L	m1 length	Anteroposterior distance of lower first molar
	m1W	m1 width	Buccolingual width of the lower second molar
	m2L	m2 length	Anteroposterior distance of lower second premolar
	m2W	m2 width	Buccolingual width of the lower second molar

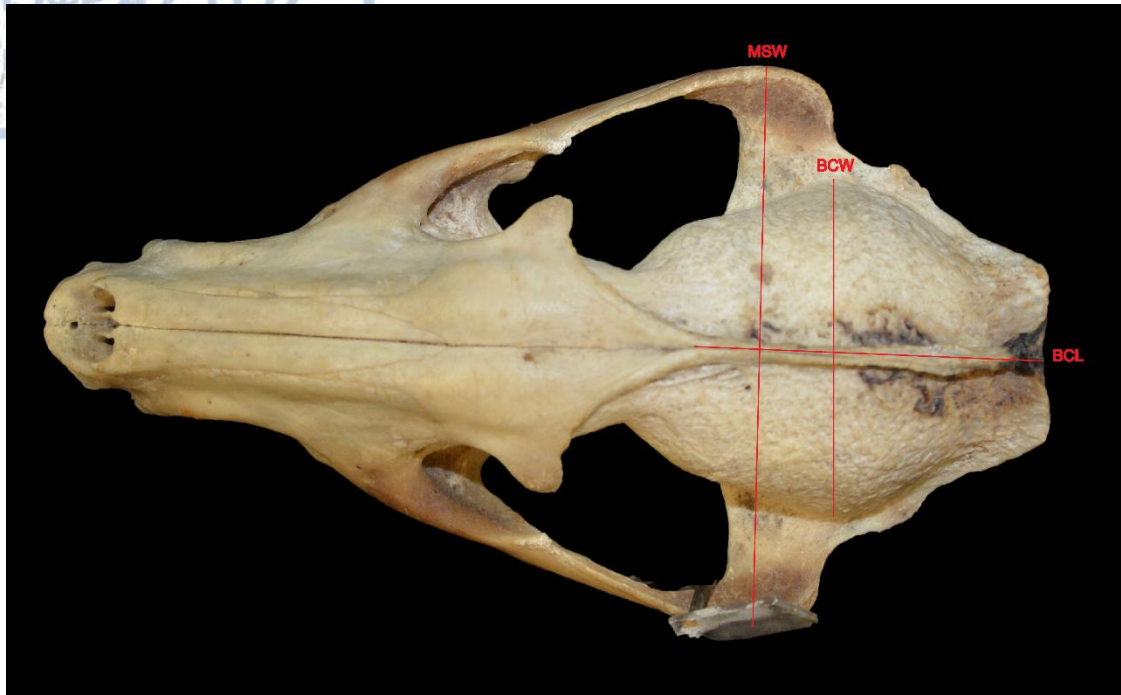


Fig. 5. Dorsal view of the *Nyctereutes* cranium. Red lines indicate the skull measurements taken during this study.



Fig. 6. Rostral view of the *Nyctereutes* cranium. Red lines indicate the skull measurements taken during this study.

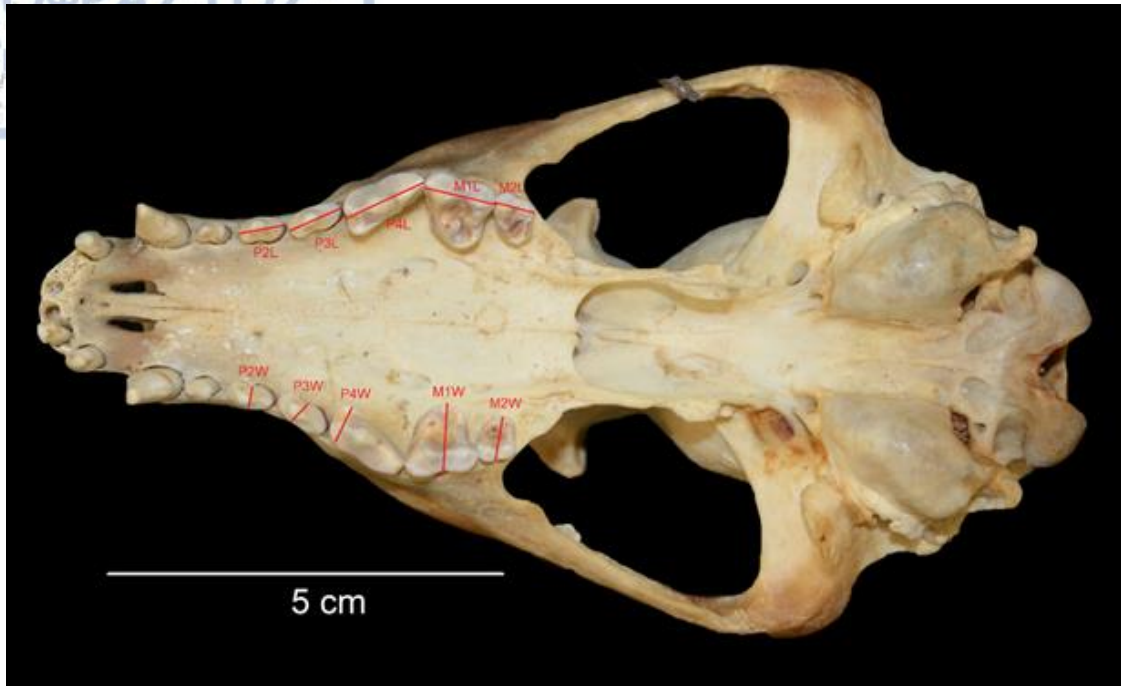


Fig. 7. Ventral view of the *Nyctereutes* cranium. Red lines upper dental measurements taken during this study.



Fig. 8. Occlusal view of the *Nyctereutes* mandible. Red line indicated the lower dental measurements taken for this study.

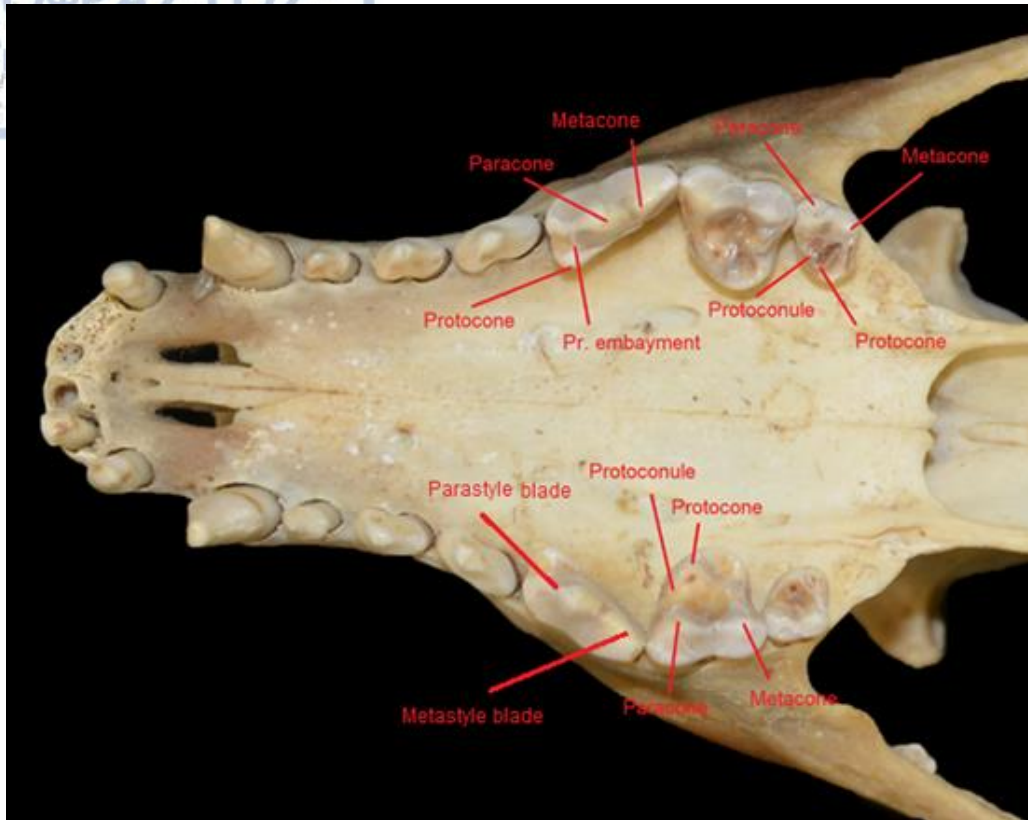


Fig. 9. Occlusal view of the *Nyctereutes* skull. Nomenclature used for the upper dentition for the current study.

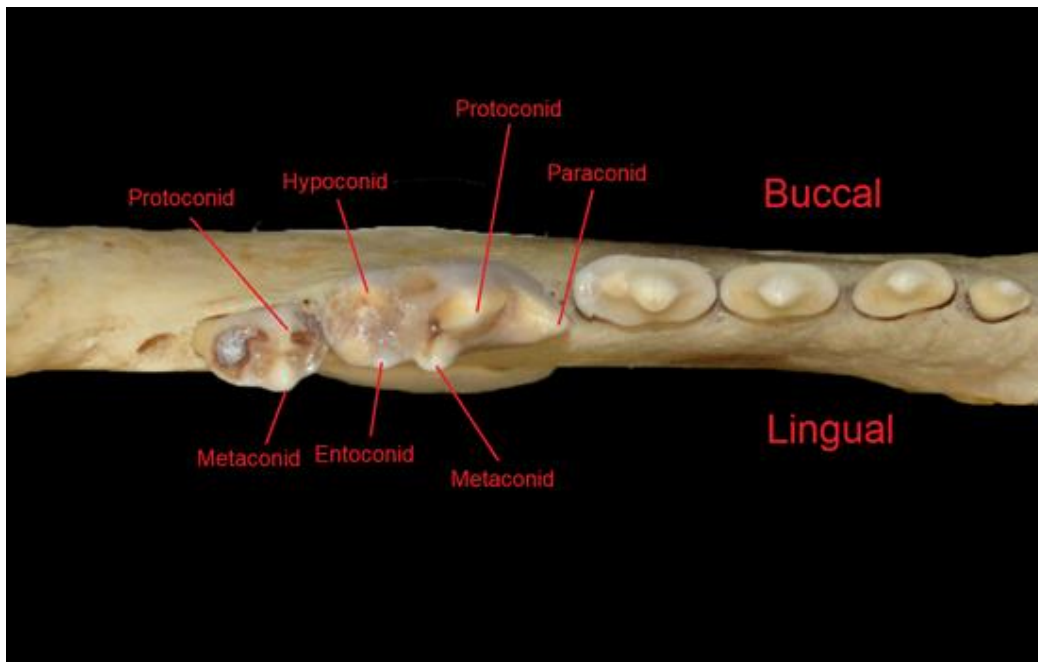


Fig. 10. Occlusal view of the *Nyctereutes* lower mandible. Nomenclature for the lower molars used for this study.

A Principal Component Analysis (PCA) was conducted using the measurements of the upper and lower dentition of the studied *Nyctereutes* sample for the discrimination between species (see Table 3).

3.3 Functional analysis

3.3.1 From carnivory towards herbivory

Exploiting their extreme ability to adapt in order to satisfy their energetic demands, carnivorans are found almost in every possible ecological niche from tropical forest to deserts across the globe (Meloro, 2008; Van Valkenburgh, 2007). This remarkable ecological diversity is expressed through a variety of morphological changes, leading to the linkage of various craniodental characteristics to specific dietary preferences (Christiansen and Wroe, 2007; Davis, 2014; Figueirido et al., 2010; Meloro, 2011, 2008; Palmqvist et al., 2007; Sacco and Van Valkenburgh, 2004; Van Valkenburgh, 2007). Dietary shifts in the carnivoran guild are not unusual, with the transition from carnivory to a more plant based diet being the least frequent (Price et al., 2012). Typical examples of such divergence in the extant carnivores can be found within the Ursidae family, with the hypercarnivorous polar bear (*Ursus maritimus*) preying mainly on seals and its Asian relative, the giant panda (*Ailuropoda melanoleuca*) feeding on bamboo (Sacco and Van Valkenburgh, 2004). Hunting a live prey requires different mechanics than the processing of plant food material, leading to different craniodental structures. Acquiring its food is a more challenging process for a hypercarnivorous animal, but the processing of the food is more demanding for a herbivorous animal instead, as plant food material is tougher regarding its material properties. This led meat consumers to favor the development of the temporalis muscle, responsible mostly for vertical jaw movements, enhancing prey capture ability and the infliction of a lethal bite (Davis, 2014; Penrose, 2018; Popowics and Herring, 2006). On the other hand, herbivores have invested in the masseter muscle, as they mainly utilize transverse jaw movements, especially during chewing, which is associated with food grinding (Fig. 11) (Davis, 2014; Fraser and Rybczynski, 2014).

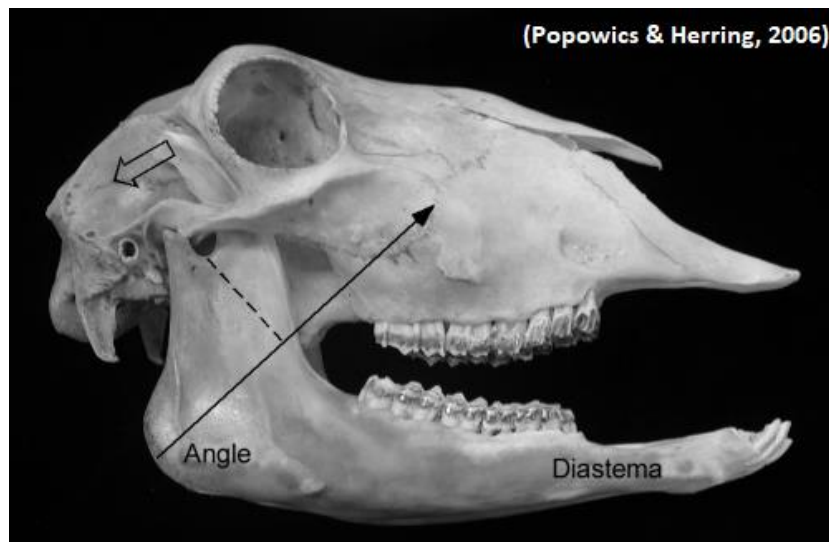


Fig.11. The increased mechanical properties of the masseter muscle as observed in sheep, *Ovis aries*. The solid arrow represents the mechanical advantage of the masseter, while the dashed line is the moment arm. Decreased and more horizontally aligned moment arm of temporalis restricts its function mainly in posterior movements (open arrow). Photo taken by (Popowics and Herring, 2006).

In general, a set of various similar craniodental morphological adaptations can be observed in herbivorous carnivorans, regarding food processing. Cheek teeth have their surface flattened, specialized for grinding (Figueirido et al., 2010; Sacco and Van Valkenburgh, 2004), while the temporomandibular joint (TMJ) is elevated above the toothrow, increasing the mechanical advantage for masseter muscle (Figueirido et al., 2010; Fraser and Rybczynski, 2014). Moreover, attachment areas for masseter have been broadened, as observed in ruminants, highlighting its functional importance (Figueirido et al., 2010; Fraser and Rybczynski, 2014). The rostrum is decreased and the zygomatic arches are expanded, enhancing the mechanical properties of the adductor muscles (decreasing the out lever distance) thus allowing high forces relative to their body sizes exerted during biting or mastication (Christiansen and Wroe, 2007; Figueirido et al., 2010). Herbivorous carnivorans have not developed a specialized digestive system like ungulates, ruminants and other mammalian herbivores (Figueirido et al., 2010), thus feeding on plant material is a challenging process. Efficient mastication is essential, as it breaks down the food bolus and boosts the digestion process (Davis, 2014). A study of the lower molar occlusal surface area revealed a dietary transition in *Nyctereutes* species (Asahara and Takai, 2019, 2017; Bartolini Lucenti, 2019). More precisely smaller ratios of m2/m1 areas are indicative for a more carnivorous diet while bigger ratios suggest a more omnivorous diet (Asahara and Takai, 2017). The more primitive fossil species *N. tingi* and *N. donnezani* present lower scores indicating a more carnivorous diet than the more derived *N. megamastoides* and representatives of *N. sinensis* from the Pliocene to the early Pleistocene (Asahara & Takai, 2017, 2019; Lucenti, 2019). A transition to a more carnivorous diet is indicated from early Pleistocene onwards in Asian *N. sinensis*, however it is not clear yet if later specimens indeed belong to *N. sinensis* and not to *N. procyonoides* (Asahara and Takai, 2019). Major morphological differences between the older and more recent species of *Nyctereutes* are the presence of a pronounced subangular lobe, and broader molars (Asahara and Takai, 2019; Bartolini Lucenti, 2019; Daguinet and Sen, 2019; Lucenti et al., 2018; Monguillon et al., 2004; Tedford and Qiu, 1991). Broader molars increase the occlusal surface area for grinding (Sacco and Van Valkenburgh, 2004; Van Valkenburgh and Koepfli, 1993), while the subangular lobe increases the attachment area for the masseter (Penrose, 2018) and the digastricus muscles (Curtis and Santana, 2018; Scapino, 1976), adaptations that indicate the enhancing of mastication (Berkovitz and Shellis, 2018; Miller and Fowler, 2015).

Mastication is a very important procedure. It is the beginning of food processing produced by the rhythmic breakdown, called chewing, of food particles between the occluding post-canine teeth (Davis, 2014). The grinding of the food particles before the organism swallows them accelerates the duration of digestion (Davis, 2014). For this, the different muscles involved in mastication need to cooperate to move the jaw and finally the teeth. The physical properties of the temporomandibular joint, which is the center of this whole operation, have crucial part during this process. High muscle forces exerted during mastication are less favored by weak temporomandibular joints and may result in dislocation of the jaw (Davis, 2014; Ito and Endo, 2019). Thus, strong mastication muscles and robust jaw joints are essential elements for mastication. The dominant mastication muscles are the temporalis, the masseter and the pterygoids forming the adductor muscles, while the digastricus is the main abductor muscle (Howard and de Lahunta, 2013).



The temporalis is the largest of the mastication muscles (Howard and de Lahunta, 2013; Penrose et al., 2016). More precisely the temporalis is divided into three different layers: the superficial part, the suprazygomatic and the deep temporalis (Penrose, 2018). The lateral surface of the cranium serves as an attachment site (origin) for the temporalis with the combination of parts from the parietal, temporal, frontal and occipital bones (Penrose et al., 2016). The coronoid process of the mandible along with the medial side of the vertical ramus serve as an insertion point for temporalis (Penrose, 2018). The masseter is a complex muscle and is usually described as a multilayered muscle consisted by three layers; superficial, middle and deep (Howard and de Lahunta, 2013; Ito and Endo, 2016). There is a contradiction regarding the middle layer, with many authors supporting that it consists a separate muscle called zygomaticomandibularis (Penrose, 2018). In this case, the masseter is composed of three layers: the superficial, zygomaticomandibularis and the deep masseter (Penrose, 2018). The origin of the masseter is on the ventral aspect of the zygomatic arch and all three layers insert of the caudal-lateral side of the masseteric fossa while the superficial part inserts partially onto the pterygoid by a tendon, on the medial side of the mandible at its ventral part (Penrose, 2018). The main function of the masseter is to close the jaw while it can also cooperate with the pterygoid muscle in specific species in order to move the jaw on the working side (Penrose, 2018). The pterygoid group is composed of two muscles, the medial and lateral pterygoid. The medial pterygoid is much greater in size in respect with the lateral pterygoid, so in most studies, they are considered as a single muscle. The medial pterygoid arise from the medial side of the pterygoid plate on the sphenoid bone and inserts on the lingual surface of the ascending ramus (Wall and Smith, 2001). There is a consensus concerning the function of the medial pterygoid among authors, that of an adductor muscle (Howard and de Lahunta, 2013; Penrose, 2018). It has been proposed that the insertion of the medial pterygoid and masseter on the opposite sides of the jaw, enables the rotation of the mandibular body in different directions around the long axis (Popowics and Herring, 2006). The function of the lateral pterygoid is yet unclear, although is thought to also be an adductor muscle (Howard and de Lahunta, 2013) cooperating with oral's floor muscles the digastric and geniohyoid, by pulling the jaw anteriorly and medially while the latter open the jaw with ventral and caudal movements (Popowics and Herring, 2006). Due to its negligible size the role of medial pterygoid is considered insignificant (Penrose, 2018).

During carnivoran biting, force apply occurs at all tooth points along the jaw. Greaves (2012) tried to illustrate the forces in the carnivoran jaw during bite and described the whole process as a third-class lever, where the two temporomandibular joints (TMJs) and the bite point form a triangle. When the bite point's distance is equal from both TMJs and the forces applied are equal from both TMJs the force vector is placed at half the distance of the fulcrums (TMJs) and the bite point along the midline (Penrose, 2018). However when a more caudal bites occurs the distances between each TMJ and bite point are uneven, the force vector is situated outside the triangle of support, thus the balancing side's forces have to be reduced in order to avoid dislocation of the TMJ (Penrose, 2018) (Fig. 12).

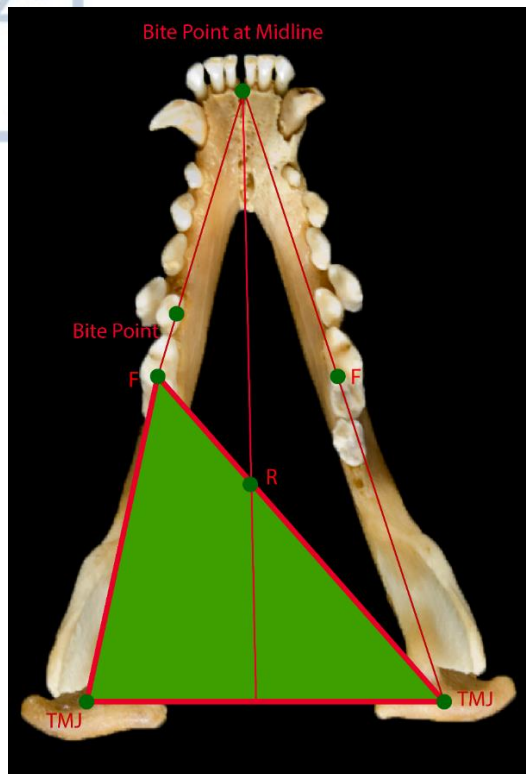


Fig. 12. The jaw as a 3rd class lever. The jaw joints (TMJ) are at the bottom left and right. Muscle force (F) in half the distance from TMJs during bite at midline. Solid green area indicates the triangle of support. Occlusal view of *Nyctereutes* lower jaw. Specimen is stored in Museum of Zoology, University of Michigan-Ann Arbor, picture taken by Phil Myers.

3D simulations verified Greave's (2000) model predictions and showed that the reduction of the forces on the balancing side prevent dislocation of the TMJ and have minor effect on the resulting bite force (Clausen et al., 2008). The further the distance is between the bite point and the TMJ the lesser is the bite force exerted, but on the contrary a wider gape and a faster bite is facilitated.

Considering the importance of the previously mentioned morphological characters specific analyses were selected in order to investigate the functional morphology of *Nyctereutes* skull.

3.3.2 Methods

An analysis regarding the accommodation of the adductor muscles within fossil *Nyctereutes* was attempted. Isometrical scaling of the adductor muscles relative to body mass has been found in different Carnivoran groups (Mustelidae, Felidae) (Hartstone-Rose et al., 2019, 2012) including Canidae (Penrose et al., 2016). That is, as size increases the size of the muscle increases at a similar rate. Surprisingly in Canidae, endocranial volume scales negatively with body size (Penrose, 2018). Considering the above, Penrose (2018) found that the Canidae need to house an isometrically scaling temporalis muscle into a negatively scaling cranium. The external surface of the cranium and the sagittal crest serve as attachment areas for the temporalis muscle. Dissection on various Canidae species witnessed the presence of a sagittal gap dorsally in the midline of the neurocranium and the absence of a sagittal crest in species below 5 Kg, while in species varying from 5-10 Kg there is a weak or absent sagittal crest. Species exceeding the 10 Kg limit displayed a pronounced sagittal

crest. *Nyctereutes procyonoides* possesses a well-developed sagittal crest, while displaying the smallest endocranial volume relative to body mass, leading to the conclusion ultimately that the development of sagittal crest in *Nyctereutes* is controlled by the temporalis requirements (Penrose et al., 2016). Regarding the muscle accommodation issue it has been suggested that if the zygomatic arch width is constant while the endocranial volume decreases, the extra space between the cranium and zygomatic arches can be utilized to accommodate a positively scaling temporalis muscle (Penrose, 2018; Radinsky, 1981).

We hypothesize that the less carnivorous *Nyctereutes* will display less space for the accommodation of temporalis muscle, as temporalis is more tied with carnivory than herbivory. To test the space for the accommodation of the temporalis muscle in *Nyctereutes*, we used the function for the estimation of endocranial volume as given by Finarelli (2006). Endocranial volume may not directly reflect the exterior surface of the cranium utilized for the attachment of temporalis, but it is a reliable estimator. Finarelli (2006) calculated the endocranial volume of extant and fossil species using only external skull measurements and more precisely the height (H), length (L) and width (W) as displayed in Fig. 13.

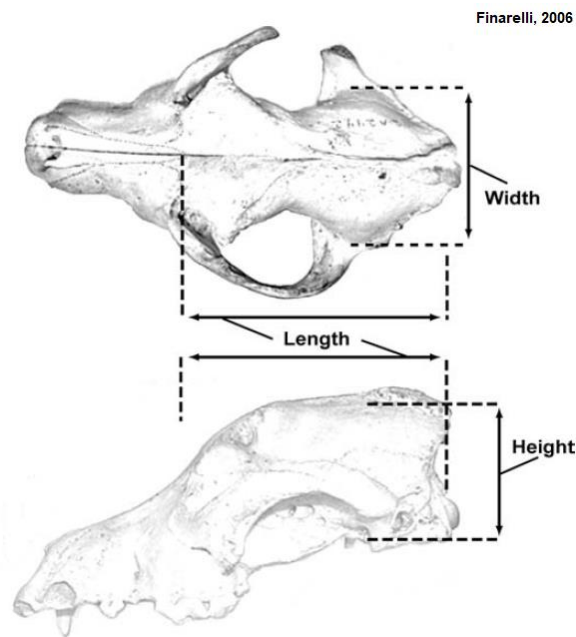


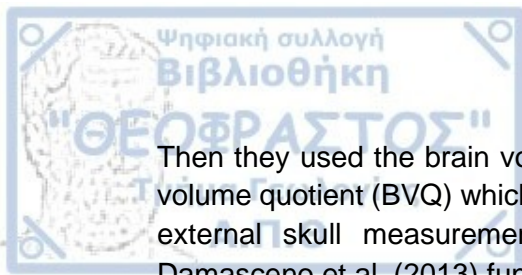
Fig. 13. Measurements used for the computation of endocranial volume, source (Finarelli, 2006).

The previous measurements are used into Finarelli's (2006) function for the calculation of endocranial volume.

Finarelli's (2006) function: $Ln_{(brainvol.)} = -6,23 + 1.06 * \ln(H) + 0.28 * \ln(L) + 1.27 * \ln(W)$ (1)

Damasceno et al. (2013) created a regression function for the estimation of brain volume solely based on skull length.

Brain volume function using skull length as given by Damasceno et al. (2013): $Log_{(brainvol.)} = 1.7501 * log_{(skull length)} - 2.0889$ (2)



Then they used the brain volume estimations based on skull length to create a brain volume quotient (BVQ) which is the ratio of the estimated endocranial volumes through external skull measurements (1) divided with the brain volume estimated via Damasceno et al. (2013) function (2).

$$BVQ \text{ function as given by Damasceno et al. (2013): } BVQ = \frac{Ln(\text{brainvol.})}{Bv_{length}}$$

Penrose et al. (2020), tested the efficiency of Finarelli's (2006) function and found it reliable. The variance of endocranial volume in examined *Nyctereutes* sample was tested using the brain volume quotient, BVQ as given by Damasceno et al. (2013).

To test the distribution of the zygomatic arch width in the studied sample, we used the Miller's index, that is the ratio of the zygomatic arch width divided by the total skull length as follows: $MI = MSW * 100 / SKL$ (Ellis et al., 2009).

Geometric morphometric analysis was conducted to infer the variation of the cranium morphology between *Nyctereutes* species. At least one representative was used for each of the studied species, resulting in equal weighting in the analysis. The software TPS_{DIG} v. 2.31 (Rohlf, 2008) was used for the digitization of the landmarks used in this analysis, inserted into high-resolution digital photographs and into a two-dimensional Cartesian coordinates (x,y) of the studied crania in lateral view. The landmarks used in this study emphasize on cranial structures related to the function of the main adductor muscles, the temporalis and masseter, as pointed out by previous authors (Figueirido et al., 2010; Figueirido & Soibelzon, 2010). An investigation regarding the mechanical advantage of temporalis and masseter muscle is attempted, as carnivorans rely more on vertical oriented forces while herbivores utilize mostly transverse movements. Therefore, the used landmarks are related with the mechanical properties of temporalis and masseter muscle and are located mainly on the sagittal crest (origin of temporalis), the zygomatic arches (insertion area for both temporalis and masseter) and the temporomandibular joint of the studied sample, resembling the in-lever ratios for the previous muscles. The out-lever ratios are reflected by landmarks positioned on the carnassials and canines. The analytical list of landmarks used in this study is given in Table 4). The landmarks used during the exact geometric morphometric analysis are displayed in Fig. 14.

Table 4. Definitions of the Landmarks used in this study.

Landmark	Definition
1 (TMJ)	At the edge of postglenoid process of the temporomandibular joint (TMJ)
2 (Zygomatic)	Perpendicular to the landmark on TMJ at the dorsal edge of zygomatic arch
3 (Mastoid process)	At the margin of the mastoid process with the paraoccipital bone
4 (Temporalis-nuchal crest)	At the most distal part of nuchal crest
5 (Temporalis-sagittal crest)	Perpendicular to the landmark on mastoid at the dorsal margin

6 (Temporalis-sagittal crest)	Perpendicular to the TMJ and zygomatic arch landmarks on the dorsal margin
7 (Postorbital process)	At the edge of the postorbital process
8 (M2)	At the middle of the base of M2
9 (P4)	At the middle of the base of P4
10 (Canine)	At the base of canine
11 (Nasal cavity)	At the dorsal margin of nasal cavity
12 (Zygomatic)	Perpendicular to M2 landmark on the dorsal margin of the zygomatic

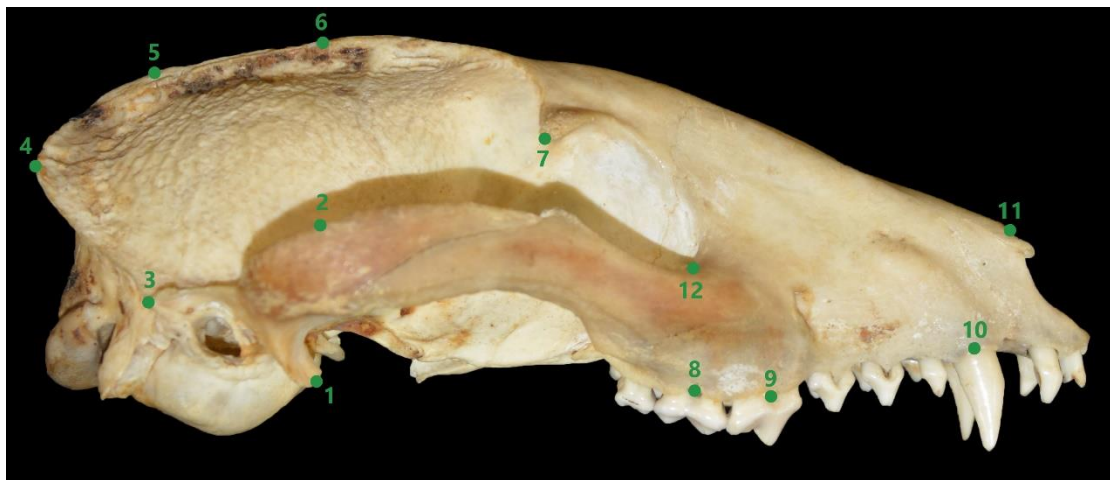
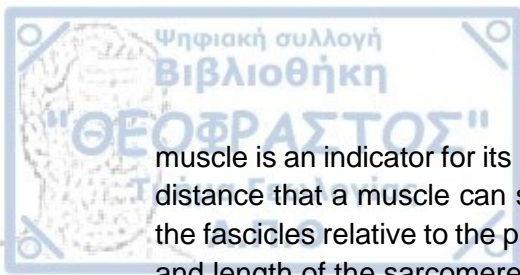


Fig. 14. Lateral view of the skull. Landmarks used during present geometric morphometric analysis of skull morphology.

The three-dimensional coordinates of the produced landmark set were imported into MorphoJ v107.a (Klingenberg, 2011). Generalized least squares Procrustes fit analysis was conducted to align and eliminate the effect of size in the studied specimens and then they were projected to the tangent space. To visualize the distribution of the chosen landmarks within the shape space, scatterplot of the principal component (PC) scores was produced. The visualization of the mean shape variation along each principal component axis was conducted using a wireframe graph produced by the selection of important landmarks.

The estimation of the bite force in fossil and extant *Nyctereutes* crania was conducted as it can prove a defining feature regarding its ecology. It is known that felids can produce greatest bite forces amongst carnivorans (Christiansen and Adolfssen, 2005; Ito and Endo, 2019) as they try to kill their prey with a single lethal bite, targeting the neck or abdomen (Turner and Antón, 1997). In contrast, canids have invested in rapid jaw mobility instead of tremendous bite forces, as they try to sever multiple fatal wounds to their prey until they can overpower them (Van Valkenburgh & Koepfli, 1993). Like their skeletal features, the muscles of the animals also present various morphological differences. The structural elements of the muscles are: the muscle fibers, repetitive layers of myosin and actin protein layers (sarcomeres) which are the muscle contraction site, with the second element being the fascicle which is a structure formed by multiple muscle fibers (Martin et al., 2020). The internal architecture of a



muscle is an indicator for its properties, the maximum force that can be exerted and the distance that a muscle can stretch for example. The number of fascicles, the angle of the fascicles relative to the plane of the force applied (pennation angle) and the number and length of the sarcomeres are the elements that consist the internal architecture of a muscle, the quantification of these features is called Physiological Cross-sectional Area (PCSA) of a muscle (Ito and Endo, 2016; Martin et al., 2020; Penrose, 2018). The calculation type for the PCSA is:

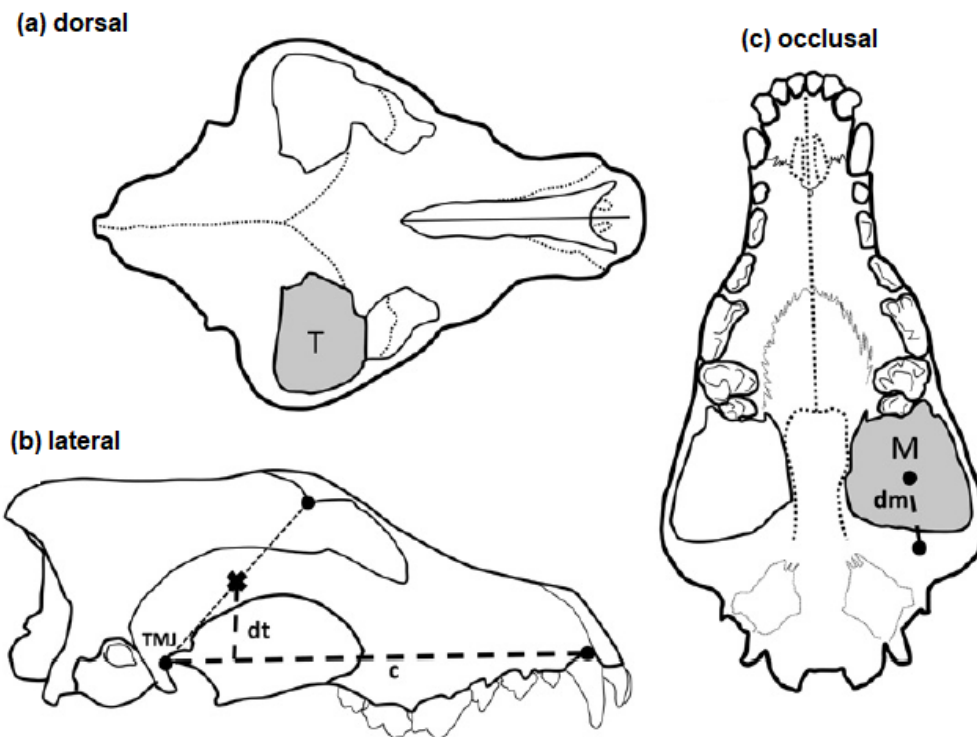
$$PCSA (cm^2) = \frac{Muscle\ mass (g) * (Pennation\ angle\ (\cos\theta))}{Muscle\ density (g\ cm^{-3}) * fascicle\ length (cm)}$$

When the PCSA of a specific muscle is multiplied by the isometric stress produced by the mammalian muscle, results in the maximum muscle force extracted from the muscle (Martin et al., 2020). Until recently the amount of 30 N (or 300 KPa) was applied as an estimator for the isometric stress produced by mammalian muscles (Thomason, 1991). This resulted lower bite forces than expected when tested with actual data from muscle dissections. Hence, the previous value was reviewed and corrected to 37 N (370 KPa) by Christiansen & Wroe (2007).

When dealing with extant animals it is easy to take a specific specimen that interests the researcher, dissect the muscles in the laboratory, and then calculate the PCSA for the specific animal. When dealing with fossils, where no soft tissue is available the estimation of the PCSA is not an option. So, what can be said about fossils in the end? Thomason (1991) managed to construct a method for calculating the bite forces exerted by mammals using only external skull measurements and more precisely by measuring the space (Cross-sectional Area) that the masticatory muscles occupy in the skull. To do that he used photographs of crania from different animals in specific angles and measured the area that the muscle would occupy (Thomason, 1991). Based on Thomason's (1991) beam theory many researchers managed to calculate the biting forces on mammals using only skull measurements (Christiansen and Adolfssen, 2005; Christiansen and Wroe, 2007; Damasceno et al., 2013). In general the dry skull method is simple, with no cost and can be easily applied to fossils (Penrose, 2018). The CSA is estimated via skull photographs with specific angle and the result is multiplied by the maximum isometric force for the mammalian muscles. However, this method includes some disadvantages. The dry skull method does not consider the variation of the extend of the muscle origin or insertion in many mammals. For instance, the origin of the temporalis varies in canids depending on size. In small canids, below 5kg like *Vulpes corsac*, the temporalis originates parasagittally, whereas in larger canids, like *Canis lupus*, it originates from the midline (Penrose, 2018). Moreover, there is overlap between the CSA of temporalis and masseter-pterygoid that may result in miscalculation of the CSA and false estimation of the force (Penrose, 2018). Another issue is the angle of the captured photos which varies depending on the method used and increases the risk for a miscalculation. Lastly, although muscle length seems easy to be counted, e.g. the distance between the origin and insertion of a muscle, there is no clue regarding the internal architecture of the muscle in fossils (fiber length, pennation angle etc.) (Perry and Prufrock, 2018).

For the estimation of bite force, we followed here the method used by Damasceno et al., (2013) because it is simple and easy to apply on fossils. In order to eliminate, as much as possible, the possibility for miscalculation of the CSA area, we preferred to

use Damasceno et al. (2013) method, where the photos captured are at perpendicular angle. For the estimation of the CSA of the temporalis and masseter-pterygoid complex caudal and ventral photographs of the skull were taken at perpendicular angle. When viewing the crania caudally, the area between the zygomatic arches and the frontal bone, excluding the area anterior of the postorbital processes, represents the CSA for the temporalis muscle (Damasceno et al., 2013). Additionally, in ventral view, the area between the zygomatic arches and the palatine-pterygoid bones is considered the CSA for the masseter-pterygoid complex (Damasceno et al., 2013). The specific measurements used for the estimation of bite force are depicted in Fig. 15. Then the CSA for the temporalis was multiplied with the distance between the centroid of the temporalis area (T) with the TMJ (dt). Similarly, the CSA area for the masseter-pterygoid complex was multiplied with the distance between the centroid of the masseter-pterygoid complex with the TMJ (dm). Then both muscle areas were multiplied by 300 KPa (maximum isometric force of mammalian muscles) and then both products were summed together and multiplied by two, representing the force produced by both mandibles. Finally, the previous product was derived by the distance between the TMJ and the bite point representing the out-lever arm.

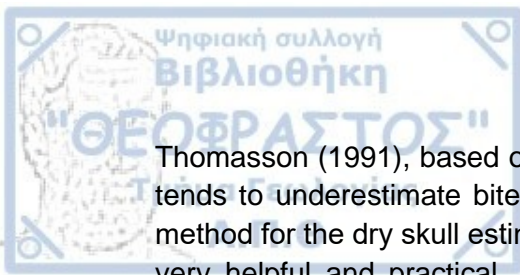


Damasceno et al. (2013)

Fig. 15. Measurements used for the estimation of bite force as given by Damasceno et al. (2013). M: Cross-sectional area for masseter, T: Cross-sectional area for temporalis, dm: distance between the centroid of masseter and temporomandibular joint (TMJ), dt: distance between centroid of temporalis and TMJ, c: distance between TMJ and bite point (canine) after Damasceno et al. (2013).

The previous calculations conclude to this type as given by Damasceno et al., (2013):

$$F = \frac{2*(dm*(M*300KPa)+dt*(T*300KPa))}{c}$$



Thomasson (1991), based on studies on opossums, noticed that the dry skull method tends to underestimate bite forces derived in vivo and thus he created a correction method for the dry skull estimations. Thomasson's (1991) correction method, although very helpful and practical, it was reluctantly used, because its precision on larger specimens than opossums was not clear (Christiansen & Adolfssen, 2005; Wroe et al., 2005; Christiansen & Wroe, 2007). Sakamoto et al. (2010) tested Thomasson's (1991) correction method on a sample of felids, using zygomatic arch width, with size significantly larger than opossums, and verified the application of the correction method to larger carnivorans as it is below:

$$F_{corr} = 10^{(0.859 \cdot \log F + 0.559)}$$

Due to the great size variation in canids, further correction of the bite force was needed. Using skull length as a body mass estimator in canids (Van Valkenburgh, 1990), Damasceno et al. (2013) managed to generate a reliable function that allows the calculation of the bite force based solely on the skull length (F_L) and noted that this function must be used with the actual data:

$$F_L = 10^{(1.95 \cdot \log L - 1.12)}$$

The effect of body size on bite force is evident (Christiansen, 2007; Sakamoto et al., 2010; Wroe et al., 2005), so the introduction of a function without the effect of size was essential for the comparison of the bite force between different species based on their ecology and not size. Damasceno et al. (2013) following Sakamoto's (2010) notes, calculated the bite force quotient (BFQ), which is the corrected bite force value (F_{corr}) derived by the skull-based bite force (F_L), a quotient without the effect of body size. Other authors calculated BFQs with the use of body mass instead of skull length in order to eliminate size (Christiansen and Wroe, 2007). Because the actual body mass of a fossil is not available and has to be estimated using a function, increasing error, the use of Damasceno's (2013) method is considered more secure.

Methods using external skull measurements for the estimation of bite force include many limitations. For instance, it is not very safe to compare the force produced by the temporalis or the masseter individually when estimated by CSA, and, the skull of the studied specimen must be complete in order to estimate the bite force. It is very common in paleontology the fossil material to be incomplete. Many fossil *Nyctereutes* specimens from the studied sample lack the zygomatic arches, thus it is not possible to estimate the bite forces for these specimens via the dry skull method. As it has been previously stated, allometric relations in the Carnivoran guild remain a constant both within the scientific community. Correlation between bite force and body size in Carnivorans has been previously highlighted (Damasceno et al., 2013), but size alone is not the only factor influencing bite force, morphology and ecology play also some role (Christiansen & Adolfssen, 2005; Wroe et al., 2005; Hartstone-Rose et al., 2019). Recent studies about the PCSA of the masticatory muscles in Carnivora noted the relation between body size and the PCSA of the masticatory muscles, where carnivorans of greater sizes possess also larger masticatory muscles (Ito and Endo, 2016). Carnivorans above the 20 kg threshold need to hunt large-sized preys in order to cover their energetical needs (Carbone et al., 1999); thus a need for larger masticatory muscles is evident for killing larger preys, leading to the assumption that the correlation between size and masticatory PCSA value is connected with the feeding

habits of the carnivorans. During their research Ito & Endo (2016) reported that the PCSA highly correlates with jaw length, with $r^2 = 91$, $r^2 = 87$ and $r^2 = 93$ for the whole masseter, temporalis, and medial pterygoid respectively, in their studied sample, highlighting that larger body sizes possess higher PCSA values in Carnivorans. The studied sample of *Nyctereutes* is scarce on complete lower jaws, so the proxy of the lower jaw was not an option. Based on that, we used the skull length as a body size estimator and then used ordinary least squares regression of the skull length against the PCSA values for each adductor muscle individually of each specimen from Ito and Endo's (2016) research. The data used in RMA regression analysis as given by Ito & Endo (2016) can be seen in Table 23 in the Appendix, while the produced functions are presented in Table 5.

Table 5. Produced functions of regression analysis between skull length and PCSA.

Variable	Ordinary LS Slope	y-intercept	R ²
Temporalis	0.2022	-10.381	0.8098
Masseter	0.2009	-13.82	0.7905
Pterygoid	0.0745	-5.2724	0.7977

As it can be noticed there is a reliable correlation between the skull length and the PCSA values in the studied sample, allowing the estimation of the PCSA of the adductor muscles via the skull length and the comparison between the various *Nyctereutes* fossil species.

The mechanical properties of the *Nyctereutes* dentition were tested investigating the development of the Hunter-Schreger Bands pattern. Hunter-Schreger Bands are patterns produced by the folding of the enamel at the outer surface of the tooth. When the tooth is observed under a light microscope, HSB is reflected by a folding pattern of white and black bands (Stefen, 1999; Ferretti, 2007; Koenigswald et al., 2011). More acute angles in the folding of the enamel on the outer surface of the tooth is thought to increase its endurance, thus HSB patterns were related to diet preferences (Stefen, 1999; Ferretti, 2007; Tseng, 2012).

There are three different HSB types observed, depending on how developed the folding of the enamel is (Fig. 16):

- Undulating HSB with angles > 140°
- Acute angled HSB with angles between 140° and 70°
- Zigzag HSB with angles < 90°

Stefen, 1999

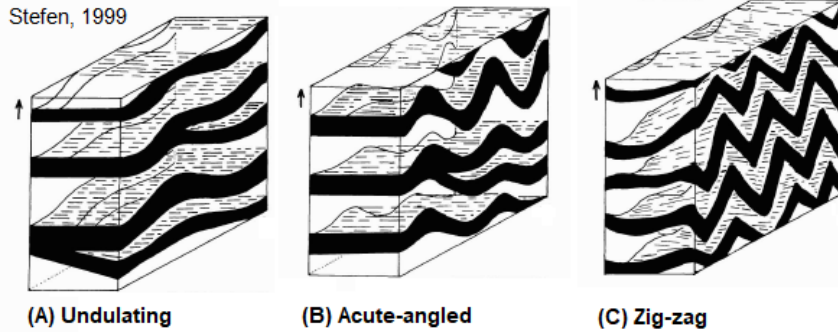


Fig. 16. Schematic drawing of the HSB pattern variation, (A): undulating, (B): acute-angled, (C): zig-zag, (figure modified from Stefen, 1999).

For instance, Hyaenids and borophagine dogs, animals that have become specialized in carcass utilization and bone consumption (Stefen, 1999; Tseng, 2012) show exclusively zig-zag HSB patterns (Koenigswald and Sander, 1997). Less developed angles are found in species that prefer softer diets. Therefore HSB pattern in carnivores has been closely tied with the amount of bone consumption in each species diet (Koenigswald and Sander, 1997). We expect that if any *Nyctereutes* species included more bone in its diet, this would be reflected in its HSB pattern.

For the study of HSB patterns in *Nyctereutes* specimens, a electronical microscope (KONUS Crystal-45) was used that was connected with a digital camera (KONUS #5830), using the software SCMOS. Photos of the surface of the teeth of *Nyctereutes* specimens were taken in three different heights of each tooth, at the base, the middle and at the tip of each cusp wherever the HSB folding was visible. Then the various angles of the HSB folding were measured using the software ImageJ (Schneider et al., 2010).

Due to the established allometric relation between the energetic demands and the body size of an animal, carnivorous predators prefer to specialize on specific prey sizes that provide maximum energetic value while foraging (Schoener, 1969). That is smaller animals spend a lot of time and energy foraging but choose preys that do not require much of energy to capture but on the contrary provide a worthy energy supply such as insects (Balisi et al., 2018). On the other hand larger predators may spend more energy during predation of larger preys but at the same big-sized preys are rich in nutrients (Carbone et al., 1999). The more carnivorous *N. tingi* and *N. donnezani* are thought to be larger than the more omnivorous *N. procyonoides* and *N. megamastoides*. In order to visualize the body size variation within *Nyctereutes* we attempted to estimate the average body weight of *Nyctereutes* fossil species. Despite that skull length is considered a reliable body size estimator (Van Valkenburgh, 1990), complete preserved skulls are scarce in the fossil record thus minimizing the efficiency of the estimation. We estimated the average body weights of *Nyctereutes* species using the function constructed by Flower (2016). The predictive accuracy of estimation methods was tested comparing the standard error of estimate (SEE), the percent of prediction error (%PE) and the percent of standard error of estimate (%SEE). The %SEE indicates the predictive precision of the estimation, highlighting how good the independent variable is at predicting the dependent variable. The %SEE and %PE are computed as follows:

$$\%SEE = 10^{2+SEE} - 100 \text{ and } \%PE = \left[\frac{O_{BM} - P_{BM}}{P_{BM}} * 100 \right],$$

where O_{BM} and P_{BM} correspond to predicted body mass and observed body mass respectively, as calculated by Van Valkenburgh (1990). Lower values of %SEE indicate an equation with higher predictive ability. Van Vankenburgh (1990) notes that m1 length has the least precision between the various skeletal and dental predictors for body mass, however Flower's (2016) function seems to be more accurate (%SEE = 25.75 and %PE = 17.41) against skull length and m1 length (%SEE=31%, %PE=21 and %SEE = 44, %PE = 27) respectively. There is no isometric scaling between m1 length and body mass, with the m1 length growing at a faster rate than the body mass (Flower, 2016), so the predicted values for body mass must be treated with caution as they can be overestimated. Finally, we estimated the body weights of the available fossil specimens, using Van Valkenburgh's (1990) skull length equation and Flower's (2016) m1 length equation and compared the results.

Secondly, the average prey size of the different *Nyctereutes* spp. was estimated using the function provided by Carbone et al. (1999). Carbone et al. (1999), pointed out that mostly all animals above the 21 kg threshold need to feed on prey of similar size or larger than themselves to satisfy their energetic demands, whereas animals below this limit mainly take prey that is about half their size. Carbone et al. (1999), managed to create a function that estimates the maximum prey size for a carnivoran if its body mass is known. This function is considered reliable and it has been used previously to estimate the prey size of fossil canids (Van Valkenburgh et al., 2003).



4 Systematic Paleontology:

Order: **Carnivora** Bowditch, 1821

Suborder: **Caniformia** Kretzoi, 1943

Family: **Canidae** Fischer, 1817

Subfamily: **Caninae** Fischer, 1817

Tribe: **Vulpini** Hemprich and Ehrenberg, 1832

Genus: *Nyctereutes* Temminck, 1838

Nyctereutes megamastoides (Pomel, 1842)

Locality: «Dafnero-3», DFN3, Macedonia, Greece

Age: 2,3 Ma, Middle Villafranchian (Benammi et al., 2020)

Referred material: DNF3-155, DFN3-342

4.1 Descriptions

DFN3-155:

Cranium:

The DFN3-155 cranium is strongly compressed vertically and as a result its total height has been decreased massively (Fig. 17-18). The incisors and canines are not preserved. The right P2-P3 are also missing while the left P4 is damaged with the protocone missing. The cranium presents the vulpine-like look, with lengthened snout and elongated zygomatic arches. The extensive nasal bones form a shallow canal up to the frontal bone in front of the orbits. The postorbital processes are well developed and extend almost half the distance from the top of the orbit to the jugular bone. Moving from the postorbital processes to the sagittal crest a massive V shaped temporal ridge is formed. The fusion of the postorbital processes with the sagittal crest takes place at the middle of the neurocranium. The distal part of the cranium is broken, so the point where the sagittal meets the nuchal crest is missing. The braincase seems to be globular despite the overall deformation of the cranium. The occipital condyles are present although damaged, however the paraoccipital and mastoid processes are missing. The auditory bullae are limited just above the glenoid processes, but this could probably be due to the extensive deformation. The glenoid process seems to be well structured with a medium angle, similar to that of DFN3-154.

Table 6. Skull measurements for DFN3-155.

Character	Measurement (mm)
SKL	147.23
BCL	58.33
BCW	57.01
MSW	82.33
SKH	32.21

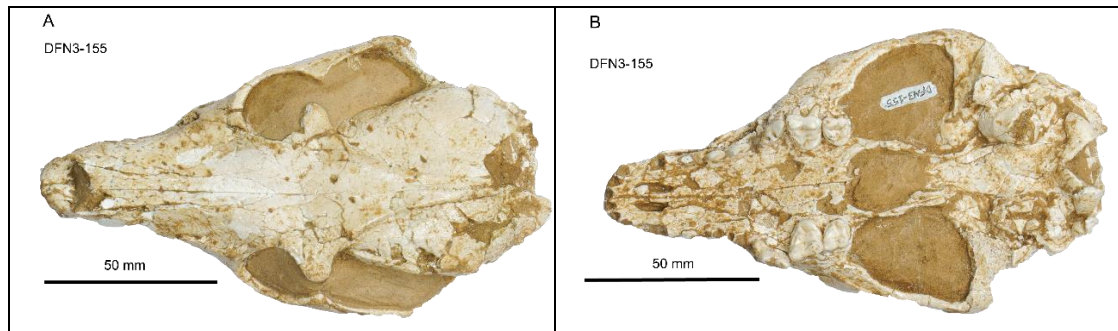


Fig. 17. DFN3-155 skull: A: dorsal view, B: ventral view, LGPUT



Fig. 18. DFN3-155 lateral view, LGPUT.

Upper Teeth:

The P1-P3 are conical shaped while the size of each tooth increases moving from the P1 to P3. No accessory cuspids are noticed on P1. A distal cingulum on P2-P3 forms a cuspid-like structure. Small crista seems to descend from the tip of the protocone to the distal part of the tooth on P3. The left P4 is generally shortened. The protocone is well-developed, prominent, pointy, and it is placed anteriorly and lingually from the mesial border of the tooth. The embayment between the protocone and the paracone is deep and circular, similar to *N. megamastoides* from Perrier (Lucenti, 2017: Fig. 2, Boule, 1889 Pl.VII, Fig.2, F). A strong lingual cingulum is visible while the buccal one is less developed. The metastylar blade is about the same length as the paracone. M1

is roughly quadrangular shaped. The paracone and the metacone are equally large. There is a small crista connecting the paracone with the protocone and a large protoconule expanded at the mesial side. The metaconule is also well-developed but smaller than the protocone. The hypocone is D-shaped and does not present a disto-lingual curve like DFN3-154 or DFN3-8b. The lingual cingulum is robust, both at the distal part where it reaches the limits of the metaconule but also at the mesial side where a cuspid-like structure protrudes towards the P4. M2 is idem to M1 with subquadrate shape and equally large paracone and metacone. The protocone is well-developed. The metaconule is similar in structure with the protocone but far less developed. The hypocone is small and slightly curves disto-lingually. The lingual cingulum is very prominent, expands peripherally at the distal part of the tooth till it joins the metacone. It forms a cuspid-like enlargement on the meso-lingual part of the tooth.

**DFN3-342:
Mandible:**

A left hemi-mandible is preserved almost intact, with all teeth present except for the incisors and the canine (DFN3-342) (Fig. 19-21). The part of the right hemi-mandible DFN3-342 preserves all teeth from p1 to m3 except for p4. At DFN3-342, a well-developed sub-angular lobe can be noticed at the point below the ascending ramus and angular process, posterior to m3. The angle between the mandibular body and the corpus is acute, almost vertical. The mandibular body is thin, and its depth increases slightly from the anterior to the posterior part of ramus. The ventral margin of the mandible is almost straight throughout its total length. The masseteric fossa is deep. A small part of the bone seems to be missing at the base of the angular process.

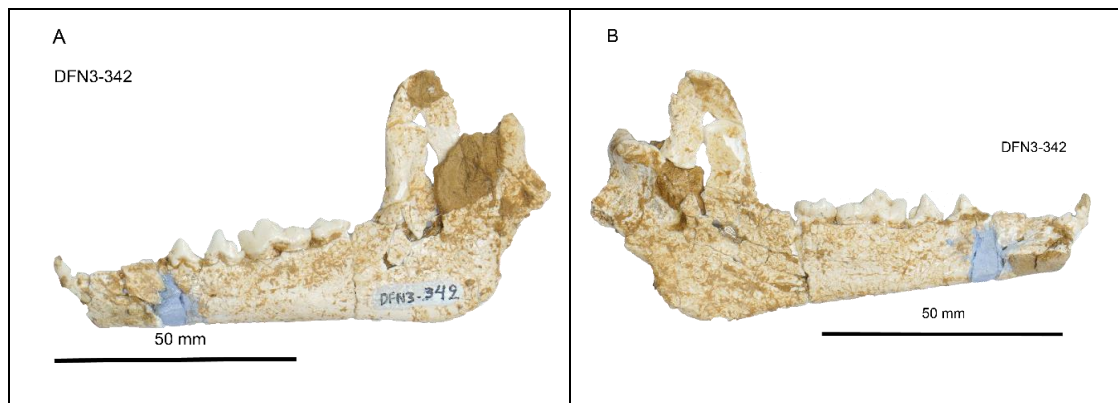


Fig. 19. DFN3-342 left mandible, A: buccal side, B: lingual side, LGPUT.

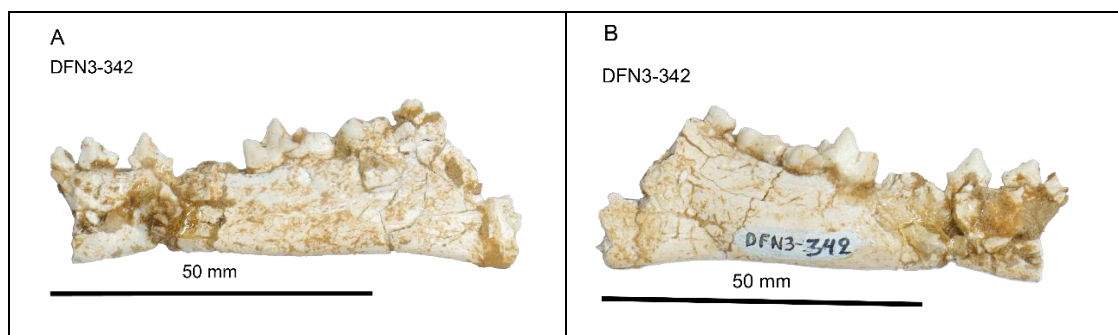


Fig. 20. DFN3-342 right mandible, A: lingual side, B: buccal side, LGPUT.

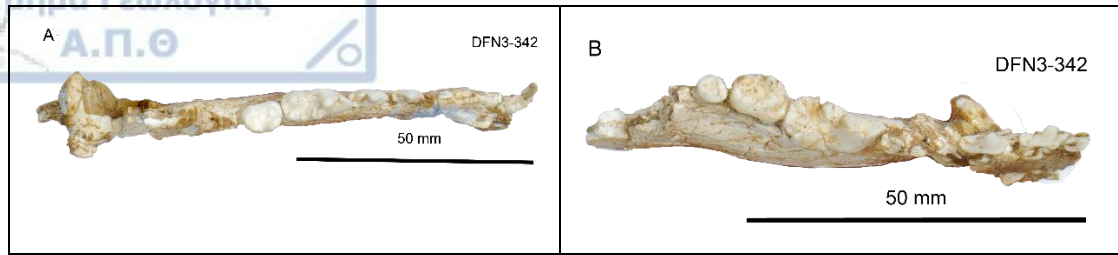


Fig. 21. DFN3-342 occlusal view, A: left mandible, B: right mandible, LGPUT.

Lower Teeth:

All the lower premolars have a conical shape and their length and width is increasing from p1 to p4. The p1 is small with no accessory cuspid (Fig 19-21). The p2 and p3 are similar in morphology, with p3 slightly differentiating in having an anterior cuspid-like cingulum. p4 possess a posterior accessory cuspid. The m1 in general is rather wider than long. The anterior slope of the paraconid is vertical while the posterior one is inclined smoothly backwards. The protoconid exceeds in growth when compared to the rest of the cusps. The posterior slope of the protoconid is steeper than the anterior. The talonid is flat, about the same size of the trigonid if not larger. There is a distinct metaconid that reaches half the height of the protoconid but is not very pointy. The hypoconid is similar in size and height with the entoconid. No accessory conulids are present uniting the hypoconid with the entoconid. m2 is rounded and flat with a talonid equally broadened with the trigonid. There is a strong cingulum anteriorly and buccally. The protoconid and the metaconid are about the same size. The m3 is small and round with at least two visible cusps.

Nyctereutes tingi (Tedford & Qiu, 1991)

DFN3-154:

Cranium:

The cranium DFN3-154 is almost fully preserved with a small posterior segment of the right zygomatic arch missing (Fig. 22-23). Most teeth are present except for the right and left I1, the right I2 and I3 and the left P1. Pressure has been applied laterally to the cranium with direction from the right side to the left, causing some deformation, resulting in a slight dorsoventral compaction. In general, the cranium presents typical vulpine characteristics with narrow and elongated muzzle and strong zygomatic arches. The width of the muzzle is increasing from the prosthion to the palate. When compared with crania of *Nyctereutes* from Megalo Emvolo (*N. tingi*), the palate is wider. The nasal bones are long and they form a relatively deep canal along their fusion line, starting from the nasal cavity to the top of the frontal bone to the point of the postorbital processes. The frontal bone seems inflated at the point of the frontal sinuses, probably because of the deformation. The frontal sinuses seem to invade beneath the diverging limbs of the parasagittal crests. The postorbital processes are pronounced leading to a robust sagittal crest, forming a V shaped temporal ridge. The union of the postorbital ridges with the sagittal crest occurs further caudally than the middle of the braincase.

The nuchal crest is strong and it extends more caudally unlike the DFN-17 and DFN-20 crania, where the nuchal crest is not so pronounced. The mastoid processes of DFN3-154 are flat and project laterally, unlike the rest of the DFN crania where the mastoids are crest-like and positioned in a more vertical stance. The braincase of DFN3-154 is globular, just like the DFN-1 crania.

Table 7. Skull measurements for DFN3-154.

Character	Measurement (mm)
SKL	163.61
BCL	71.21
BCW	55.70
MSW	87.26
SKH	43.34

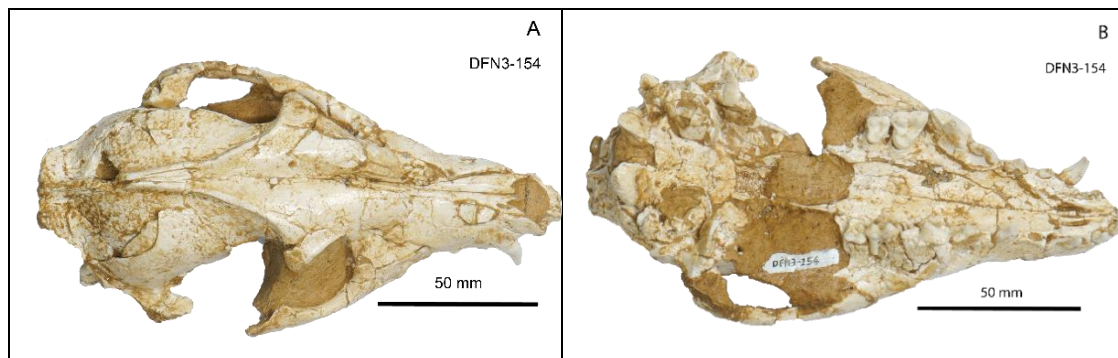


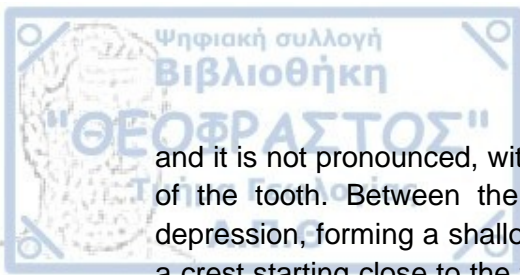
Fig. 22. DFN3-154 skull, A: dorsal view, B: ventral view, LGPUT



Fig. 23. DFN3-154 lateral view, LGPUT.

Upper Teeth:

The teeth of DFN3-154 cranium are preserved in good condition. P4 is large and buccolingually developed. The protocone is positioned mesially and slightly lingually



and it is not pronounced, with the protocone protruding slightly from the mesial border of the tooth. Between the protocone and the paracone there is a mild straight depression, forming a shallow valley. Across the middle part of the paracone, there is a crest starting close to the tip of the paracone and continues vertically to the base of the mesial border of the tooth. The anterior cingulum is not prominent. A moderate lingual cingulum is visible, though not continuous from the protocone to the metastyle blade, while the buccal cingulum appears weak as well. The metastyle blade is short. M1 is larger buccolingually than mesiodistally, being lessened to that direction on the lingual part. The occlusal surface shape of the teeth is close to that of a triangle in contrast to DNF-17 and DNF3-155 where the lingual part of the teeth is wider than that of DNF3-154, giving an overall more quadrangular shape. The paracone is larger than the metacone and slightly taller. The protocone and the metaconule are distinct while there is an evident protoconule. The buccal cingulum is strong. Lingually, both the mesial and distal cingulum are well marked with the former one being more developed and forming a cuspid like projection mesially. M2 is similar to M1, both to its general proportions and its triangular shape. The difference between the size of the paracone and the metacone is not so evident, due to the smaller size of M2 in comparison to M1 but still the paracone excels in growth versus the metacone. The protocone is well developed but the metaconule is strongly reduced. There is a distinct lingual cingulum especially in the mesial side of the tooth, again forming a slight cuspid-like projection. The canines are straight and a mild crest-like structure can be observed on the anterior lingual part of the tooth. I1 is small and straight and no accessory cusps are noticed. It differs from DFN-17 where an extra cusp can be observed on the external side of the tooth. I2 is also straight and a small cuspid can be noticed at the mesial side of the tooth, unlike DFN-17 where two accessory cuspids are present, on the mesial and external side of the tooth, respectively. I3 appears strong and straight. A slight bend is observed at the tip of the tooth. No accessory cusps are noted, while in DFN-17 a small accessory cuspid on the mesial side is apparent.

DFN3-8:

Upper Teeth:

The partial cranium DFN3-8 is badly preserved and highly deformed. It retains a part of the palate with the right canine, P2-M2 right and P2-M1 left (Fig. 24). The canine lacks its upper half, but is robust and does not seem to incline posteriorly. P2 and P3 have a similar conical shape, with the length of the teeth exceling their width. The protocone is high on both teeth and no accessory cuspids are noticed. P4 is elongated with the protocone extending anterior and lingually from the anterior border of the tooth. The valley between the protocone and the paracone is shallow and the border between the two cusps is straight. The protocone is pointy. The paracone is large and inclined slightly backwards. A mild crista is descending from the tip of the paracone at its mesial side. The metastyle is about the same size as the paracone, and sharp as well. A lingual cingulum can be traced at the metastyle but does not proceed to the protocone. M1 has triangular shape, and the width of the tooth is decreasing from the buccal to the lingual side. The hypocone gently curves posteriorly. The paracone is larger than the metacone. The protocone is well formed and a small protoconule on the mesial side is

visible. The metaconule is slightly smaller than the protoconule. The hypocone is present at the lingual side of the tooth and gently curves to the distal part of the tooth. Both the buccal and the lingual cingulum are well developed with the latter being prominent in the mesial side. M2 is alike to M1, triangular shaped with its width decreasing from the buccal to the lingual side. The protocone is well-formed with a tiny protoconule on its mesial side. The paracone is larger than the metacone. The metaconule is small and not particularly developed. The hypocone curves also gently backwards as in M1. There is only a buccal cingulum.

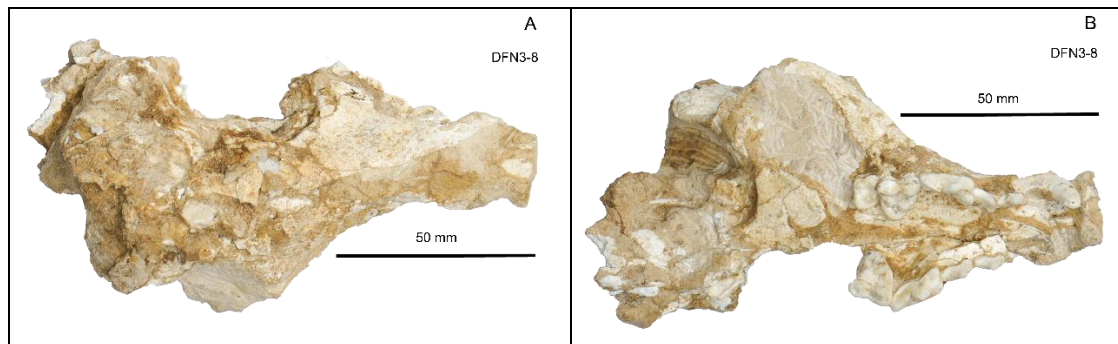


Fig. 24. DFN3-8 skull, A: dorsal view, B: ventral view, LGPUT.

DFN3-8a-b:

Mandible:

DFN3-8b is a part of the right hemimandible with p2 up to m3 still in place (Fig. 25). The ascending ramus of the mandible is totally absent, without the angular process preserved. The mandible is slender in built generally. A presence of a subangular lobe is not evident, with the ventral border of the mandible being slightly curved and not straight as DFN3-342 specimen. The DFN3-8b specimen resembles the primitive condition of the subangular lobe seen in *N. tingi*. DFN3-8a is a small part of the left hemimandible comprising only of the three latter premolars and the first lower molar. m1 is broken with the paraconid and the protoconid only preserved.

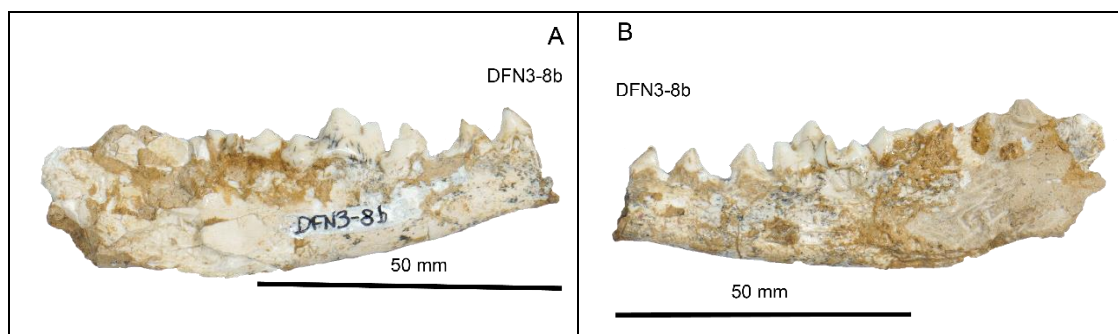


Fig. 25. DFN3-8b right hemimandible, A: buccal view, B: lingual view, LGPUT.

DFN3-b



Fig. 26. DFN3-8b right hemimandible, occlusal view, LGPUT.

Lower Teeth:

p2 and p3 are similar in size with conical shape, small, pointy with no accessory cuspids. pw4 has similar structure with p2, p3 but is larger in size (Fig. 26). The anterior part of the p4 base is broken. An accessory cuspid can be observed at its distal side. The m1 has slender built in general, unlike DFN3-342 specimen, which is more buccolingually expanded, giving a slender appearance to this tooth compared to the DFN3-342 specimen.

The anterior border of the paraconid is almost vertical, while it is flat on top. The protoconid is the largest cusp. It is conical in shape with a pointy tip. The metaconid is strong, larger than in DFN3-342, well-developed and pointy. No accessory cusps are evident between the entoconid and metaconid, instead there is a deep V shaped valley. The entoconid is similar to the metaconid, conical and pointy but shorter. A hypoconulid is distinct in the most distal part of the tooth. The hypocone is not so prominent, less pointy than the entoconid, but larger in area although shorter in height. A crista seems to connect the protoconid with the hypoconid but not the entoconid with the hypoconid. m2 is oval with its length increased than its width. The protoconid is the largest cusp. A strong anterior-buccal cingulum is evident. The protoconid is connected with the hypoconid with a crista. Accessory cuspid posterior to the hypoconid occur. The width of the talonid area is similar to that of the trigonid. m3 is small, circular with a single cusp.

4.2 Metric Data

The PCA of the upper teeth of the studied sample is based on the length and width measurements for the following teeth: P2, P3, P4, M1, and M2. A plot for PC2 against PC1 axis is explaining 89.74% of the total variance. PC3 axis seems also important explaining 5.24% of the studied sample. PC1 axis with 81.676% variance, discriminates

the larger sized taxa from the smaller ones (Fig. 27). The Eigenvalues, %variances and the measurements loadings for the first two PCs are presented in Table 8.

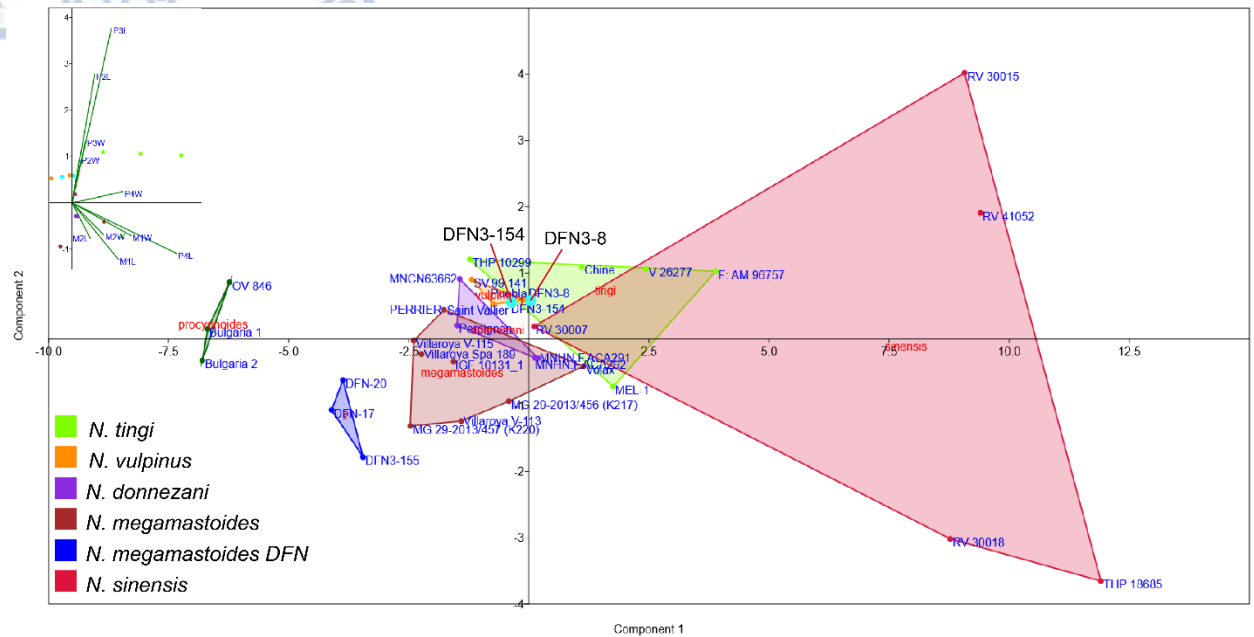
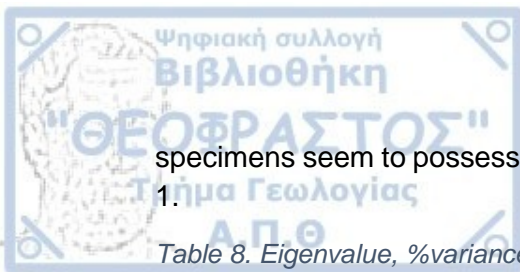


Fig. 27. PCA plot of the upper dental measurements of different *Nyctereutes* samples.

The majority of *N. sinensis* specimens from the Nihewan Basin seem to be distinguished from the rest of the taxa, probably due to their larger size (Farjand et al. 2020). More precisely, *N. sinensis* is mainly characterized by larger carnassials in both proportions (length, width) than the rest of *Nyctereutes* species. A distinct group is apparent in the middle of the plot, including the *N. vulpinus*, *N. tingi* and *N. donnezani* samples, alongside with RV 30007 (*N. sinensis*) which seems to be a smaller individual in comparison with the rest of *N. sinensis* known population from Nihewan Basin and Zhoukoudian. This group displays greater teeth size than *N. megamastoides* and *N. procyonoides* group, which is placed further lower and left on the graph. The DFN3 specimens, DFN3-8b and DFN3-154, are overlapping between the *N. tingi* and *N. vulpinus* groups. The *N. tingi* specimen from Megalo Emvolo (MEL-1) is displaying more similar teeth proportions with the *N. donnezani* specimens from Çalta, but that is more likely because both Çalta specimens and MEL-1 lack P2 and P3, thus creating a bias. As previously stated, *N. megamastoides* is characterized by smaller teeth dimensions from the rest of *Nyctereutes* species except for the extant *N. procyonoides* that possess smaller carnassials but similar in size P2 and P3 lengths. The DFN-1 and DFN3 *N. megamastoides* specimens are placed closer to the *N. megamastoides* group but displaying slightly smaller teeth proportions. The Dafnero specimens (DFN3-154 and DFN3-8b) are placed closer to the *N. vulpinus* specimens from Saint-Vallier and the *N. tingi* specimen THP 10299 from Nihewan Basin. The THP 10299 seems to be smaller than the rest of the *N. tingi* specimens regarding all teeth size measurements except for P3 and P2 lengths. P2L measurement loadings are noteworthy both in PC1 and PC2 while P2W has a considerable impact only in PC2. The fact that DFN3-154 and DFN3-8 are lacking P2 measurements seems to create a bias, resulting in grouping these specimens with the ones from *N. vulpinus* species. Nonetheless, all *N. tingi*



specimens seem to possess larger values of P2L and P3L measurements except MEL-1.

Table 8. Eigenvalue, %variance and loadings of the measurements for the first three PCs of the PCA.

	PC1	PC2	PC3
Eigenvalue	19.4394	1.90559	1.24806
%variance	81.676	8.0065	5.2438
P2L	0.15006	0.5164	0.36435
P2W	0.049459	0.19976	0.086102
P3L	0.2603	0.6998	-0.066415
P3W	0.08908	0.24995	-0.030193
P4L	0.69441	-0.20305	-0.37843
P4W	0.33541	0.044851	-0.29096
M1L	0.30676	-0.22709	0.19395
M1W	0.39026	-0.13113	0.22623
M2L	0.1208	-0.14291	0.4831
M2W	0.20892	-0.12803	0.55178

The *N. megamastoides* group is characterized by well-developed molars regarding their overall body size. The specimens from Kvabebi (MG 29-2013/ (K220)- MG 29-2013/456 (K217)), display a more robust built in comparison with the rest of the *N. megamastoides* specimens, based on their molar measurements. Villaroya specimens are more widespread within the *N. megamastoides* sample, containing both small sized and larger individuals. The Dafnero *N. megamastoides* display smaller teeth proportions, especially in P4 lengths, forming a distinct group placed further on the left of the graph in regard with the rest *N. megamastoides* specimens.

Subsequently, a PCA was conducted on the lower teeth of *Nyctereutes*, using the length and width of p2, p3, p4, m1 and m2. The plot of PC2 against PC1 axis explained 88.46% of total variance and discriminated quite successfully the studied species (Fig. 28). The Eigenvalues, %variance and the measurements loading for the first two PCs are presented in Table 9.

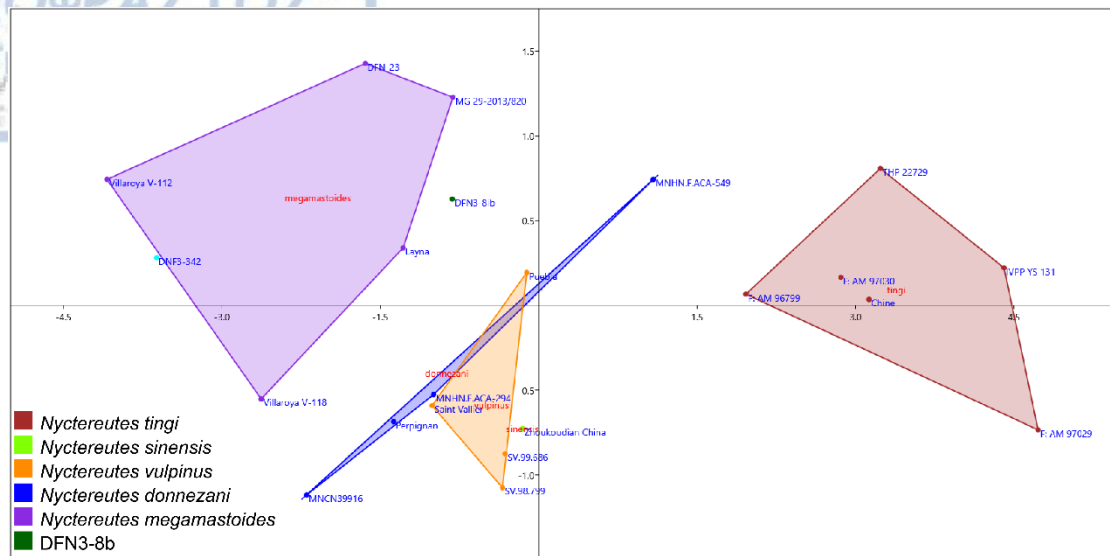


Fig. 28. PCA plot of the lower teeth measurements of the different *Nyctereutes* samples.

Similar to the PCA for the upper dentition, the *N. tingi* group is placed further to the right and it is characterized by greater tooth size, a trait also described previously. The *N. vulpinus* group is positioned at the middle of the plot, presenting intermediate teeth size, between *N. tingi* and *N. megamastoides* group, with lessened molar development and greater premolars growth. Interestingly, DFN3-8b is placed closer to *N. vulpinus* and not to *N. tingi* as was the case in the upper dentition. DFN3-8b is characterized by more modest tooth size than the studied *N. tingi*, similar to those of the *N. vulpinus* group, but with broader molars. The DFN3-342 specimen is placed within the range of *N. megamastoides* group and is quite distinct from the other *Nyctereutes* groups. DFN3-342 displays smaller teeth from the rest of the *N. megamastoides* specimens except from Villaroya V-112.

Table 9. Eigenvalues, %variance and loadings of the lower teeth measurements for the first three PCs of the PCA.

	PC1	PC2	PC3
Eigenvalue	6.02888	0.555715	0.284981
%variance	81.016	7.4677	3.8296
p2L	0.33301	-0.07777	0.27411
p2W	0.16793	0.024177	0.095008
p3L	0.39598	-0.28829	0.20586
p3W	0.18862	0.019781	0.1084
p4L	0.45661	-0.52554	-0.13991
p4W	0.23182	-0.039368	-0.42541
m1L	0.55791	0.28982	-0.091207
m1W	0.22499	0.39954	-0.26314
m2L	0.15497	0.38745	0.69709
m2W	0.14282	0.48824	-0.3125



4.3 Comparison DFN3-155

Cranial features:

The muzzle of DFN3-155 is long but not at the level of *N. donnezani* from Çalta (Daugenet & Sen, 2019: fig. 1. A, fig. 2. A) and Layna (Lucenti et al., 2018: Fig. 2. A). Instead, it is closer to the size/proportions of *N. megamastoides* from Kvabebi (Rook et al., 2017: figure. 1. 1, 5) and Dafnero-1 specimens DFN-17, DFN-20 (Koufos, 1993) where the snout is more massive and shortened. The braincase seems to be globular and spherical similar to that of *N. megamastoides* from Kvabebi (Rook et al., 2017: figure. 1. 1, 5) and the Dafnero-1 specimens (Koufos, 1993), as well as to *N. donnezani* specimen from Çalta, Turkey (Daugenet & Sen, 2019: fig. 1. A, fig. 2. A). The postorbital processes of DFN3-155 are well-developed and dense identical to *N. donnezani*, (MNHN.FACA 291, Çalta Turkey) and *N. megamastoides* from Kvabebi but also to the Dafnero-1 specimens (DFN-17 and DFN-20). The fusion of the postorbital processes with the sagittal crest, occurs in the middle of the braincase in DFN3-155 as in *N. megamastoides* (Kvabebi, Dafnero), and *N. tingi* from Megalo Emvolo (MEL-1, MEL-2; Koufos 1997) and unlike those of *N. donnezani* from Çalta, and Layna where the fusion of the postorbital processes with the sagittal crest is displayed more posteriorly.

Dental features:

According to the morphological traits marked by Sen & Daugenet (2019) and Lucenti (2017) the morphology of P4 varies among the *Nyctereutes* species. In *N. tingi* the protocone is small and placed close to the paracone, limiting the mesial border of the tooth to a straight line (Daugenet and Sen, 2019). Unlike *N. tingi*, in *N. megamastoides* the placement of the protocone is extended more antero-lingually while in *N. donnezani* from Turkey it does not exceed the limit of the anterior side of the paracone (Daugenet and Sen, 2019). The P4 protocone in DFN3-155 is prominent and is placed antero-lingually beyond the anterior border of the paracone, similarly to the protocone of *N. megamastoides* from Perrier (Boule, 1889). Previous authors (Sen & Daugenet 2019, Bartolini Lucenti, 2017), note that the embayment between the protocone and the paracone is moderately deep in *N. donnezani* from Perpignan and Layna but it is placed more lingually in *N. tingi* and *N. megamastoides* from Perrier while in other samples, like in *N. megamastoides* from Montopoli, Dafnero, Sesklo, Kvabebi and *N. sinensis* from Yushe and Nihewan basin, this embayment is decreased, resulting in almost a straight border at the anterior side of P4. In DFN3-155 this embayment is circular and deep and therefore more similar to *N. megamastoides* from Perrier (Lucenti, 2017: Fig. 2. Pl. VII, (F)). The metastyle blade length of *N. donnezani* (Layna, Perpignan) and *N. vulpinus* (Saint-Vallier) is less developed while it is long in *N. megastoides* from Montopoli (Bartolini Lucenti, 2017) and short in the specimens from Kvabebi (Rook et al., 2017). Daugenet & Sen (2019) studied the ratio of the metastyle blade length in regard to the total buccal length (paracone plus metastyle) and did not succeed in discriminating *Nyctereutes* species based on this character. M1 of DNF3-155 tends to be quadrangular in shape. This trait is characteristic for *N. megamastoides*, *N. vulpinus* and *N. sinensis* (Daugenet and Sen, 2019; Lucenti et al., 2018) while in *N. tingi*, *N. donnezani* and the extant *N. procyonoides* it is more triangular (Daugenet and Sen, 2019). The paracone and the metacone of DFN3-155 are equal in size. The paracone

is of the same size with the metacone in *N. megamastoides* (Perrier, Dafnero, Kvabebi) and *N. donnezani* (Çalta, Perpignan) whereas in *N. sinensis*, *N. tingi* and *N. procyonoides* the paracone is more developed in comparison with the metacone (Daguenet and Sen, 2019; Rook et al., 2017). The protoconule is well-developed in the DFN3-155 specimen. This feature agrees with the descriptions for *N. megamastoides* from Villaroya, Kvabebi (Rook et al., 2017) and Dafnero-1 specimen DFN-20, but in DNF-17 (Dafnero-1) and IGF 10131_2 (Montopoli; Lucenti, 2017: Fig. 1C), the teeth are very worn to the point where no conclusions can be drawn. In *N. donnezani* material from Layna (Lucenti et al., 2018: fig. 3. (F)) and Çalta (Daguenet & Sen, 2019: figs 1c, 2c) the protoconule is distinct, especially in MNHN.F.ACA291. In *N. sinensis* the protoconule is reduced or totally absent (Rook et al., 2017; Tedford and Qiu, 1991). The main diagnostic morphological feature of the M2 of *Nyctereutes* is the development of the metaconule. In *N. tingi* metaconule appears to be significantly reduced compared to *N. megamastoides* and *N. donnezani* (Daguenet and Sen, 2019; Rook et al., 2017). The metaconule of DFN3-155 is certainly less developed than the protoconule, but still distinct, whereas in *N. tingi* from Megalo Emvolo (MEL-1) the whole cusp is smaller and the metaconule appears to be more constricted just as the whole tooth. Moreover in *N. sinensis* from Nihewan basin the metaconule appears to be absent (Farjand et al., 2020: fig. 3. (c)) in a similar manner as in *N. vulpinus* specimen from St. Vallier (Monguillon et al., 2004).

Mandible:

As reported in the literature (Daguenet and Sen, 2019; Lucenti et al., 2018; Rook et al., 2017; Tedford and Qiu, 1991), species of *Nyctereutes* are distinguished by the position of the subangular lobe of the mandible. The subangular lobe is rather weak in the primitive forms, like *N. donnezani* and *N. tingi* (Daguenet and Sen, 2019; Lucenti et al., 2018; Rook et al., 2017). In DFN3-342 there is a distinct strong subangular lobe positioned at the posterior part of the mandible posterior to m3. The corpus is high and it is positioned perpendicular to the mandibular body, thus shaping a vertical distal margin of the lobe. The mandible of *N. donnezani* from Layna (Lucenti et al., 2018: Fig. 4. A-C) possesses a weaker subangular lobe, positioned behind m3 but with a curved ventral margin. Additionally, the mandible of *N. donnezani* from Çalta (Daguenet & Sen, 2019: Fig. 3. A-C), has the subangular lobe positioned below m1-m3 and is rather weak, with a curved ventral margin. Based on the description of the mandible of *N. tingi* and the figure provided by Tedford & Qiu (1991) the subangular lobe of this species is more similar to *N. donnezani*, with weak development of the subangular lobe and curved distally below the ascending ramus (Fig. 25). According to the available literature the subangular lobe is strong in *N. megamastoides*, whereas in *N. sinensis* and *N. vulpinus* the development of the subangular lobe is intermediate, stronger than in *N. donnezani* and *N. tingi* but weaker than in *N. megamastoides* (Daguenet and Sen, 2019; Lucenti et al., 2018). The subangular lobe in *N. megamastoides* is stronger and positioned more posteriorly than in *N. sinensis*, whereas the ventral margin of the mandible is straight in *N. megamastoides* instead of curved unevenly in *N. sinensis* (Daguenet and Sen, 2019; Rook et al., 2017). Based on the figure provided by Tedford & Qiu (1991) the subangular lobe of F:AM 97007 *N. tingi* (Tedford & Qiu, 1991: Fig. 1. B) is weaker and has the distal margin slightly curved and not vertical like in DFN3-342. *N. vulpinus* displays an intermediate state of what is considered primitive and evolved character regarding the subangular lobe, with less prominent subangular lobe than *N.*

megamastoides and *N. sinensis* and high angled curvature at the distal margin of the lobe (Daguenet and Sen, 2019; Lucenti et al., 2018). The right hemimandible of *N. vulpinus* from Saint-Vallier (Drome) has an intermediate subangular lobe, reaching its maximum development perpendicular of the coronoid process, with the angle between the lobe and the ascending ramus being high but not so vertical as in *N. megamastoides* from DNF3. The ventral margin of the hemimandible is straight as in DNF3-342. Both the strong development and the vertical distal margin of the subangular lobe of DNF3-342 distinguish it from *N. vulpinus* and suggest stronger similarities with *N. megamastoides*.

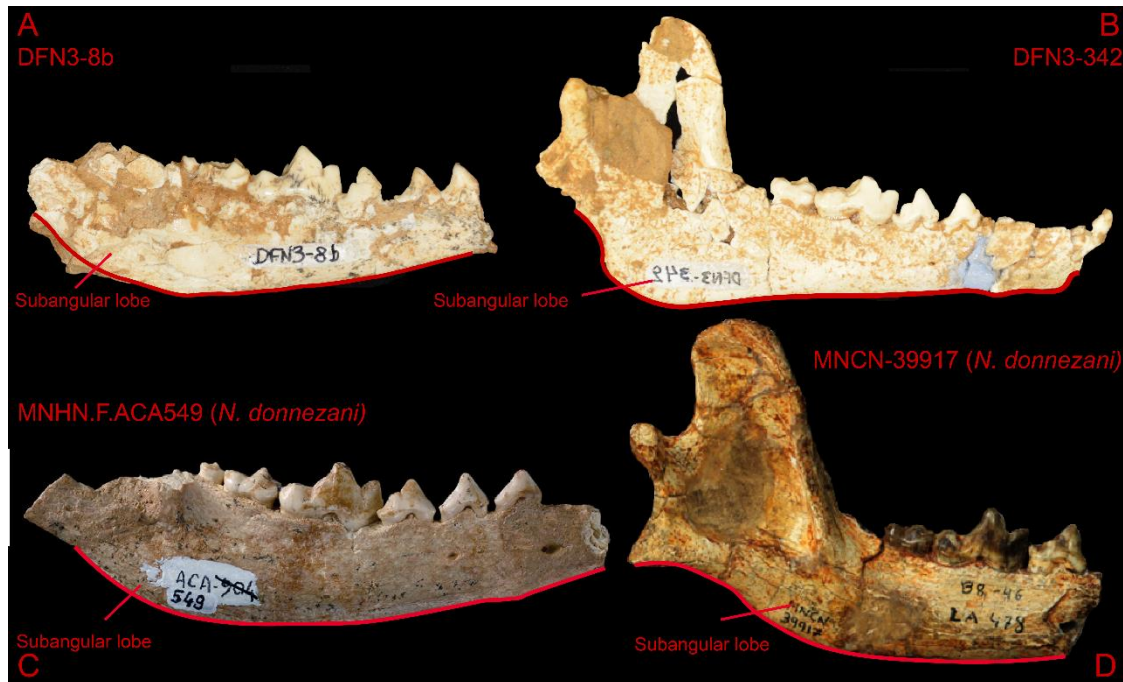
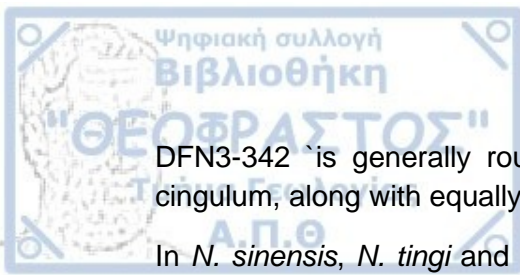


Fig. 29. *Nyctereutes* mandibles. Red lines indicate the lower ventral margin of the mandibles. A: DFN3-8 (Dafnero), B: DFN3-342 (Dafnero), C: MNHN.F. ACA549, *N. donnezani* (Çalta), D: MNCN-39917, *N. donnezani* (Layna).

Lower Dentition

Nyctereutes species are also distinguished by the development of m1. Specifically, the width of the talonid area versus the trigonid is superior in the majority of *Nyctereutes* species, especially in *N. megamastoides*, except in *N. sinensis* and *N. donnezani* from Perpignan (Daguenet and Sen, 2019; Rook et al., 2017). In DFN3-342 the talonid area is wider than the trigonid similarly with the *N. megamastoides* specimen MG 29-2013/592 (K4177) from Kvabebi (Rook et al., 2017: Fig. 2. 4-6) and *N. donnezani* from Çalta and Layna (Daguenet & Sen, 2019: Fig. 3. A, D; Lucenti et al., 2018: Fig. 4. C, F). Similarly with *N. sinensis*, m1 of *N. vulpinus* often displays a narrower talonid in comparison with the trigonid (Monguillon et al., 2004), a trait that differs from that observed in the DFN3-342 specimen. The hypoconid and entoconid of m1 are equal in size in *N. megamastoides* while the hypoconid exceeds in size the entoconid in *N. tingi* and *N. sinensis* (Daguenet and Sen, 2019). The *N. donnezani* specimens from both Layna and Çalta have the hypoconid more developed than the entoconid (Daguenet and Sen, 2019; Lucenti et al., 2018). In contrast with the Layna and Çalta specimens, the DFN3 specimen possesses equally sized hypoconid and entoconid. The m2 of



DFN3-342 is generally rounded with expanded talonid and distinct antero-buccal cingulum, along with equally sized protoconid and metaconid.

In *N. sinensis*, *N. tingi* and *N. donnezani* specimens from Perpignan and Layna, the talonid area is limited compared to DFN3-342. Regarding m3, *N. tingi* displays a single cusped tooth, *N. donnezani* specimens from Çalta are characterized by the presence of two cusps in m3, while in the rest of *Nyctereutes* species, m3 is considered to have at least two or in some cases three evident cusps of variable volumes (Daguenet and Sen, 2019). DFN3-342 exhibits three cusps, as in most *Nyctereutes* species, unlike *N. tingi* and the Çalta specimens.

Briefly, the cranial characteristics of DFN3-155, such as the shortened muzzle, the spherical braincase and the position of the fusion of the postorbital processes with the sagittal crest at the middle of the neurocranium, are characters point to *N. megamastoides*. Regarding its dentition, the morphology of P4 along with the embayment between the protocone and the paracone, the sub-quadrangular shape of the upper molars with equally sized paracone and metacone, but also a distinct protoconule and metaconule, are further clues that support the attribution of DFN3-155 into *N. megamastoides*. The distinctive development of the subangular lobe, the flattened lower molars with no reduced talonids, the similarly sized cusps between the entoconid and hypoconid, support the reference of DFN3-342 to as *N. megamastoides*.

DFN3-154, DFN3-8a-b

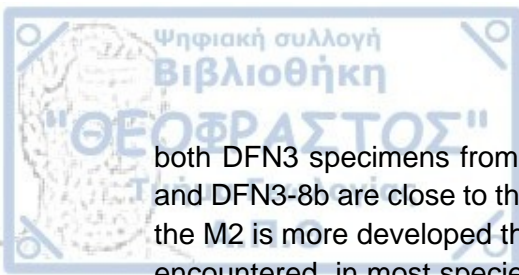
Cranial features:

The cranial size of DFN3-154 is larger than the rest of the Dafnero specimens but also from MNHN.F.ACA-292 of *N. donnezani* from Çalta and *N. megamastoides* from Kvabebi. It is close in proportions to *N. tingi* crania from Megalo Emvolo (MEL-1 and MEL-2) and MNHN.F.ACA-291 of *N. donnezani* from Çalta, but smaller than *N. sinensis* from Nihewan. *Nyctereutes tingi* was originally described as similar in size with *N. sinensis* (Tedford and Qiu, 1991). However, a recent study showed that new *N. sinensis* material from Nihewan is characterized by a larger skull size, more prominent sagittal crest and less developed auditory bullae in comparison with *N. tingi* (Farjand et al., 2020). Although DFN3-154 skull is smaller than *N. sinensis* specimens from Nihewan, it possesses a robust sagittal crest and the auditory bullae do not surpass the level of the post-glenoid process. The frontal sinus in DFN3-154 has a posterior inflation as described in Tedford & Qiu, 1991, beneath the diverging limbs of the parasagittal crests. DFN3-154 differs from Megalo Emvolo crania by having a more robust build in general, where the Megalo Emvolo specimens have more elongated and narrow braincases. The Megalo Emvolo crania possess more elongated and narrow braincases than DFN3-154. Sexual dimorphism has not been studied very thoroughly in fossil *Nyctereutes* yet. Reports on sexual dimorphism in extant *Nyctereutes* state that is not so evident, yet specific differences can be spotted between sexes in cranium and mandible but not in dental characters (Hidaka et al., 1998; Kim et al., 2012). In fossil *Nyctereutes* particularly, Daguenet & Sen (2019), report indications about sexual dimorphism expressed in cranial features and especially in the more pronounced sagittal and nuchal crests, stronger temporal line, broader zygomatic process of the maxillary bone, more elongated braincase and stronger development of the subangular lobe in male individuals. Indeed, the skull characters of DFN3-154 are more

pronounced relative to *N. tingi* specimens from Megalo Emvolo. If sexual dimorphism is present in *Nyctereutes*, then DFN3-154 is probably a male individual while MEL-1 and MEL-2 are presumably females.

Upper dentition:

The P4 of DNF3-154 appears to be robust, while P4 of DFN3-8b seems to have a slenderer built with the length of the tooth being superior to its width. The protocone of DFN3-154 and DFN3-8b is placed mesially and slight lingually with the anterior border being almost straight, similar to DFN-17, the Montopoli specimen IGF 10131_1 and *N. vulpinus* (Lucenti, 2017: Fig. 2. C, D). In comparison with *N. donnezani* specimens from Layna and Çalta, the P4 protocone of the DFN3 specimens is positioned slightly more lingually and protrudes moderately from the mesial margin of the tooth whereas in both the Çalta and Layna samples, the mesial margin of the P4 is straight with the protocone being positioned more mesially than lingually (Daguenet & Sen, 2019: Fig. 1. C, Fig. 2. C; Lucenti et al., 2018: Fig. 3. B, C, D). Both DNF3-154 and DFN3-8 specimens are identical with the specimen V 26277 of *N. tingi* from Nihewan basin (Farjand et al., 2020: Fig. 3., e), in which the protocone is mesio-lingually placed and projecting slightly anteriorly from the mesial margin. The paracone of DFN3-154 is rather mesio-distally expanded with a short metastyle. In DFN3-8b the paracone is about the same size as in DFN3-154, but the metastyle is longer. A mesio-distally developed paracone along with a short metastyle blade are also seen at Layna, Perpignan and Çalta specimens of *N. donnezani* as well as in *N. vulpinus* (Daguenet and Sen, 2019; Lucenti et al., 2018). Unlike *N. donnezani* and *N. vulpinus*, *N. megamastoides* possess a mesio-distally reduced paracone and an elongated metastyle blade (Bartolini Lucenti, 2017). The lingual cingulum of DFN3-154 and DFN3-8b is weak, similar to *N. tingi* and unlike *N. donnezani* from Çalta and Layna and *N. megamastoides* from Kvabebi and Dafnero. The upper molars of DNF3-154 and DFN3-8b are shortened mesio-distally at the lingual part and curve gently backwards giving an overall triangular shape. This feature is reported as characteristic for *N. tingi* and *N. donnezani* and it is considered primitive (Daguenet and Sen, 2019; Rook et al., 2017); it is unlike the more derived sub-quadrangular upper molar shape of *N. megastoides* and *N. sinensis* (Lucenti et al., 2018; Rook et al., 2017). There is a discrepancy about the *N. vulpinus* molar shape. According to Lucenti (2018) *N. vulpinus* has sub-quadrangular molars while Monguillon et al. (2004) noted that *N. vulpinus* from Saint Vallier differs from *N. megamastoides* by having sub-triangular M1. The paracone of the M1 is larger than the metacone in both the DFN3 specimens (DFN3-154 and DFN3-8b) distinguishing them from *N. megamastoides* and *N. donnezani*, which both possess equal sized paracones and metacones (Daguenet and Sen, 2019; Lucenti et al., 2018; Rook et al., 2017). Regarding the size of the paracone and the metacone, Lucenti (2018) mentions that *N. vulpinus* has equally large paracone and metacone, even though the Saint Vallier specimen possess slightly larger paracone than metacone. Both the protocone and the metaconule are well formed on DFN3-154 and DFN3-8b while there is a distinct protoconule, similar to *N. megamastoides*, *N. donnezani* and *N. tingi*. On the contrary *N. sinensis* protoconule is absent or highly reduced (Rook et al., 2017). Both M1 of DFN3-154 and DFN3-8b possess cusp-like cingulum on the mesial side, a feature that is rarely seen in *N. sinensis* or *N. vulpinus* (Lucenti et al., 2018), and thus discriminating



both DFN3 specimens from these species. The triangular shape of M2 in DFN3-154 and DFN3-8b are close to that of *N. donnezani* from Çalta and Layna. The paracone of the M2 is more developed than the metacone in both specimens. This characteristic is encountered in most species like *N. donnezani*, *N. megamastoides*, and both *N. tingi* and *N. sinensis* (Daguenet and Sen, 2019), so it cannot be used to discriminate the studied specimens. Additionally, the decrease of the metaconule relative to the protocone is more pronounced to *N. sinensis* and *N. tingi* compared to *N. donnezani* and *N. megamastoides* (Daguenet and Sen, 2019). Both DFN3-154 and DFN3-8b specimens display a well-developed protoconule while the metaconule is lessened greatly with a weak crista joining the metaconule with the protocone.

Mandible

Despite being broken on the posterior and ventral parts, the DFN3-8b subangular lobe seems to be primitive in condition as in *N. tingi*. It is less developed than the DFN3-342 specimen, thus separating the DFN3-8b from *N. megamastoides*. In DFN3-8b the subangular lobe is positioned posterior to the m3, unlike *N. donnezani* from Layna, where the subangular lobe is further distally positioned than in DFN3-8b and not so highly curved (Lucenti et al., 2018: Fig. 4. A-B). In MNHN.F.ACA549 (*N. donnezani*) specimen from Çalta the subangular lobe has a curved ventral margin but it is placed between the distal half of m1 till the posterior end of m3, as in *N. tingi* from Yushe Basin and *N. donnezani* from Perpignan (Daguenet and Sen, 2019) (Fig. 25). The different position of the mandibular lobe in the specimens of *N. donnezani* from Layna, Çalta, and Perpignan was attributed to sexual dimorphism, with the Layna specimen considered to represent a female individual (Daguenet and Sen, 2019). Additionally, the ventral margin on the mandibular body of the DFN3-8b is curved like in *N. donnezani* from Çalta and Layna and *N. tingi* from Yushe Basin and not straight as in DFN3-342 and *N. megamastoides* from Kvabebi.

Lower dentition

The lower m1 is relatively slender in built with the talonid area being equal with the trigonid in width, like in most *Nyctereutes* species apart from *N. sinensis* and *N. donnezani* from Perpignan, in which the talonid is narrower than the trigonid. The hypoconid is larger in area compared to the entoconid in DFN3-8b but not higher. A larger hypoconid than entoconid is also a feature reported for *N. tingi* and *N. sinensis* while *N. megamastoides* possesses equally sized hypoconid-entoconid (Daguenet and Sen, 2019). The small hypoconulid traced at the distal part of the DFN3 m1, is a character sometimes noticed in *N. sinensis* and *N. megamastoides*. The DFN3 m2 is slender in built with the width being inferior to the length, like in *N. sinensis* and *N. tingi* and not circular like in *N. megamastoides* (Daguenet and Sen, 2019; Rook et al., 2017). The m2 protoconid of DFN3-8b is larger than the metaconid. Rook et al. (2017) noted that in *N. sinensis*, the protoconid is larger than the metaconid, whereas in *N. megamastoides* these cusps are equal in size. On the other hand, Daguenet & Sen (2019) mentioned that on the m2 of the Çalta specimens, the metaconid is superior to the other cusps, a state also reported for *N. sinensis* and *N. megamastoides*. The m3 of DFN3-8b seems to possess a single cusp a characteristic only met in *N. tingi*,

whereas the rest of *Nyctereutes* species possess at least two cusps (Daguenet and Sen, 2019).

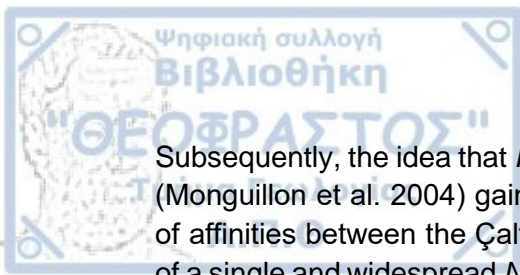
Collectively, regarding the P4 of DFN3-154 and DFN3-8 specimens, the mesio-lingually placed protocone and the shallow embayment between the protocone and paracone, alongside with the triangular shape of the upper molars are primitive characters that place DFN3-154 and DFN3-8 closer to *N. tingi* without however excluding *N. vulpinus*. The larger paracone than metacone and the almost absent metaconule on the M2 are features indicative for *N. tingi* that further support the attribution of DFN3-154 and DFN3-8 to this species and discriminating them from both *N. donnezani* and *N. vulpinus*. The weak development of the subangular lobe along with the curved ventral margin indicate a primitive taxon for DFN3-8b, thus excluding *N. megamastoides*. The m1 talonid of DFN3-8b seems to be equal in size with the trigonid, unlike *N. sinensis* and *N. donnezani* from Perpignan. The m1 hypoconid is larger in area than the entoconid but not higher, a trait observed in *N. tingi* and *N. sinensis* (Daguenet and Sen, 2019). The m2 possess a reduced talonid as seen in *N. tingi* and *N. sinensis* with the protoconid being the largest cusp. Finally, the m3 appears to be single cuspid, a trait marked so far exclusively in *N. tingi*, while the rest of the *Nyctereutes* species display at least two different cuspid. Considering all these traits, DFN3- 154 and DFN3- 8 and DFN3-8b specimens appear to have a variety of characters that are found in the more primitive *N. tingi*.

4.4 Discussion on phylogenetic relationships and evolutionary trends

The Canidae clade originated in North America, with the earliest representatives appearing in the Eocene (Daguenet and Sen, 2019). The Canini tribe emerged around 9 Ma in North America with the genus *Eucyon* including only one widespread representative, *E. davisii* (Tedford et al., 2009). *Nyctereutes* appears to be a rather problematic genus regarding its phylogenetic relationships as it is not yet clear if it should be placed closer to the clade of *Canis* Linnaeus, 1758 or that of *Vulpes* Frisch, 1775. Tedford et al. (2009) suggested possible phylogenetic relations between *Nyctereutes* and *Cerdocyon* Smith, 1839 based on some common features like the developed angular process and the mandibular lobe for the better attachment of the pterygoid muscle and the low crowned canines. Currently *Cerdocyon* is present in South America, but initially, two different fossil species of *Cerdocyon* found in North America, specimen IGM-2903 attributed to *C. avius* of Pliocene age of Mexico and *C. texanus* (AMNH F:AM 62985- AMNHN F:AM 62984) from the Early Pliocene of Texas and New Mexico (Ruiz-Ramoni et al., 2020), indicated that *Cerdocyon* possibly originates from North America (Tedford et al., 2009). More recent phylogenetic studies exclude *C. avius* from the South American fox group *Cerdocyon* and place it within the *Vulpini* tribe (Prevosti, 2010; Ruiz-Ramoni et al., 2020). Ruiz-Ramoni et al. (2020) in their work noted that the extant *N. procyonoides* is basal to the clade of IGM-2903, *M. macconnelli*, *C? texanus*, *N. donnezani*, *N. tingi*, *N. sinensis*, suggesting that *Nyctereutes* is a paraphyletic group, but without enough paleontological evidence to fully confirm this hypothesis. Additional phylogenetic studies (Zrzavý et al., 2018) and DNA analyses (Wayne and Ostrander, 2007), indicate stronger relations of *Nyctereutes* with *Vulpes* and further support the hypothesis that the morphological features shared

between *Nyctereutes* and *Cerdocyon* are homoplastic obtained through convergent evolution under similar ecological adaptations (Lucenti et al., 2018). Hence, a plausible scenario would be that of a fox-like species migrated from North America to Eurasia in late Miocene represents the possible ancestor of *Nyctereutes* (Lucenti et al., 2018). The first appearance of *Nyctereutes* in the fossil record is a specimen from China referred to as *Nyctereutes tingi* (Lucenti et al., 2018; Tedford and Qiu, 1991) and dated to the Early Pliocene (MN 14). The presence of the *N. tingi* in Asia is continuous and from the Late Pliocene on, it shortly co-existed with its successor, *N. sinensis* (Farjand et al., 2020; Tedford & Qiu, 1991; Dagueneit & Sen, 2019). Ultimately, *N. procyonoides* makes its appearance in mid-late Pleistocene, evolving from *N. sinensis*, and making *N. procyonoides* the only surviving member of *Nyctereutes* (Farjand et al., 2020). Soria & Aguirre (1976) were the first to specify the main diagnostic features of *Nyctereutes*: mandibular corpus growth, angle between the ascending ramus and mandibular body, angular region and upper and lower molar morphology. Moreover, they defined the primitive characters (weak subangular lobe, mesio-distal reduced molars on the lingual part, closer to triangular shape) and the derived ones within the genus (stronger subangular lobe, more expanded mesio-distally molars closer to quadrangular shape) (Soria & Aguirre, 1976). The first/earliest European representative of *Nyctereutes* was *N. donnezani* from La Gloria dated at 4.19 Ma (MN 14), hence of an age similar to that of *N. tingi* in Asia (Lucenti et al., 2018). Even though both *N. tingi* and *N. donnezani* are considered primitive taxa, Tedford & Qiu (1991) noted some differences, such as the larger size of the former, the presence of cristids connecting the hypoconid with the entoconid on the lower m1 and the larger paracone than the metacone on the upper molars, whereas in *N. donnezani* both cusps have the same size. The development of the subangular lobe in *N. tingi* differs from that of *N. donnezani*, with the former having a rather thin mandibular body and hook-like angular process, whereas in *N. donnezani*, although still primitive, the subangular lobe is closer to the condition seen in *N. sinensis* and *N. megamastoides* (Lucenti et al., 2018). *N. megamastoides* constitutes the more derived taxon of the European *Nyctereutes* along with *N. vulpinus* and both are the only European species that went through the Pleistocene (Bartolini Lucenti, 2017; Monguillon et al., 2004). The origins of *N. megamastoides* are also debatable. The similarity between *N. megamastoides* and *N. sinensis* on both morphological features and size has led to the idea that these species may consist a single taxon distributed widely (Rook et al., 2017; Tedford and Qiu, 1991). Until recently the first appearance of *N. megamastoides* in Europe was considered to be at 3 Ma (Bartolini Lucenti, 2017), but findings of *N. cf. megamastoides* in the site of Layna (Spain) postponed the arrival of the taxon at around 3.9 Ma (Lucenti et al., 2018). The findings of *N. cf. megamastoides* in Layna, contradict the scenario of a single *N. megamastoides* + *N. sinensis* species and suggests an independent and contemporaneous evolution of *N. megamastoides* in Europe. *Nyctereutes* remains from Çalta, Turkey were originally attributed to *N. donnezani* by Ginsburg (1998), but were later referred to as *Nyctereutes* sp. by Lucenti (2018), who highlighted a sum of both primitive and derived morphological features that do not match neither *N. donnezani* nor *N. tingi*. Additionally, the same author noted similar dental proportions of the Çalta taxon with *N. megamastoides*. Lucenti (2018) suggested that the ancestor of the European *N. megamastoides* originated from a hypothetical taxon in parallel to the lineage of *N. tingi*-*N. donnezani*. Ultimately Dagueneit & Sen (2019) reviewed the remains of *Nyctereutes* from Çalta and contrary to Lucenti (2018), they proposed that the observed differences

are not adequate to distinguish the Çalta specimens from *N. donnezani*. In their view, the possible existence of sexual dimorphism in *Nyctereutes*, like the more posterior position of the subangular lobe on the *N. donnezani* hemimandible from Layna compared to the Çalta specimen, suggests that the former is most likely a female individual (Daguenet and Sen, 2019). Similarly the finding of DFN3-155 specimen from DFN3 fits both the cranio-dental proportions and morphological characteristics of *N. megamastoides* and along with the rest of the DFN1 *N. megamastoides* already described by (Koufos, 1993; specimens: DFN-17, DFN-20, DFN-23) support the presence of this species in the Balkan region at least until the middle Villafranchian (2.3 Ma). Enigmatic is the case of the other Western European derived form of *Nyctereutes*, *N. vulpinus*, described from Saint-Vallier, France by Viret (1954). Viret (1954) and later Martin (1971) and Argant (2004), attributed the *Nyctereutes* material from Saint-Vallier to *N. megamastoides*. Soria & Aguirre (1976) revised the material and noted differences from typical *N. megamastoides* (more elongated upper and lower premolars and lower carnassial and reduced m2) that led them to question the taxonomy of this material and distinguish it as a separate subspecies *N. megamastoides vulpinus*. Following Soria & Aguirre (1976), Monguillon et al. (2004) reviewed once more the Saint-Vallier remains and decided to raise it to the rank of the species. They also suggested the attribution of the La Puebla de Valverde material to *N. vulpinus* (Monguillon et al., 2004). *Nyctereutes vulpinus* displays intermediate characters between the primitive (*N. donnezani*-*N. tingi*) and derived taxa (*N. megamastoides*), similarly with *N. sinensis*. Monguillon et al. (2004) suggested two possible scenarios concerning the origin of *N. vulpinus*. In the first scenario the taxon emerged from a primitive stock of *N. megamastoides* split from the *N. donnezani*-*N. megamastoides* lineage, by adopting a more carnivorous diet reflected as homoplastic reversals of its dental features (triangular shape of upper molars, elongated talonid versus the trigonid) (Monguillon et al., 2004). In the more acceptable scenario, *N. vulpinus* originated from a possible descendant of the European population of *N. tingi* (Lucenti et al., 2018; Monguillon et al., 2004), with the remains of *N. cf. tingi* from Varshets, Bulgaria supporting this hypothesis (Spasov, 2003). The findings of DFN3-154, DFN3-8b, and DFN3-8a in Dafnero are intriguing. Regarding their morphological characteristics these specimens exhibit a sum of primitive features (sub-triangular molars, reduced M2 metaconule, simple structure of m1 with no accessory cusplids, lessened talonid of m1) that recall *N. tingi*. The fact that the upper M1 of both specimens, presents mesial cusp-like cingulum, larger paracone than metacone and a m3 with a single cusp, are in favor of an attribution of these specimens to *N. tingi* instead of *N. vulpinus* or *N. sinensis*. On the other hand, the results from the metric comparison of the lower teeth are not so clear, suggesting a possible relation of DFN3-154 and DFN3-8 specimens with *N. vulpinus*. The Dafnero site has similar age with that of Varshets, so a possible tight relationship between *N. cf. tingi* from Varshets with the Dafnero specimens DFN3-154 and DFN3-8 could be assumed, though this needs to be further supported. The first occurrence of *Nyctereutes* in Asia is documented by the presence of *N. tingi* in Yushe Basin at about 4.4 Ma (Tedford and Qiu, 1991), followed by the appearance of *N. sinensis* in 2.3 Ma and the arrival of the modern *N. procyonoides* in the mid-Pleistocene (Farjand et al., 2020). If the Dafnero and the Bulgarian specimens indeed belong into the *N. tingi* group then a continuous presence of *N. tingi* in the Balkan region would be documented, similar to that in Asia, firstly with the presence of *N. tingi* in Megalo Emvolo (Ruscinian, ~ 4 Ma), and followed by Varshets and Dafnero (Middle Villafranchian).



Subsequently, the idea that *N. vulpinus* originated from the European lineage of *N. tingi* (Monguillon et al. 2004) gains more support. Moreover, if Lucenti's (2018) hypothesis of affinities between the Çalta taxon and *N. megamastoides* is true, then the scenario of a single and widespread *N. megamastoides* + *N. sinensis* taxon (Tedford & Qiu 1991) would be less likely. That would lead to two possible working hypotheses concerning the taxonomy of *N. vulpinus* and *N. sinensis*. Firstly, if the presence of *N. tingi* in Southern Europe is continuous (similarly to Asia) as it is witnessed in the Greek-Bulgarian record, then the Asiatic *N. sinensis* and the European *N. vulpinus* may not consist two different taxa. Their taxonomy probably requires a revision, and they may constitute a single wide-spread taxon, as it was proposed for *N. megamastoides* and *N. sinensis*. On the other hand, *N. vulpinus* could be distinct from *N. sinensis*, sharing similar characteristics.

5 Functional Morphology of fossil *Nyctereutes*

5.1 Geometric Morphometric analysis in *Nyctereutes* crania

The PCA of the covariance matrix produced 5 principal components (PCs). The first three components correspond to about 90% of the total variance. PC1 and PC2 account for 60% and 20% respectively, providing a reliable approximation of the mean shape variation. The graph produced by the PCA is displayed in Fig. 30.

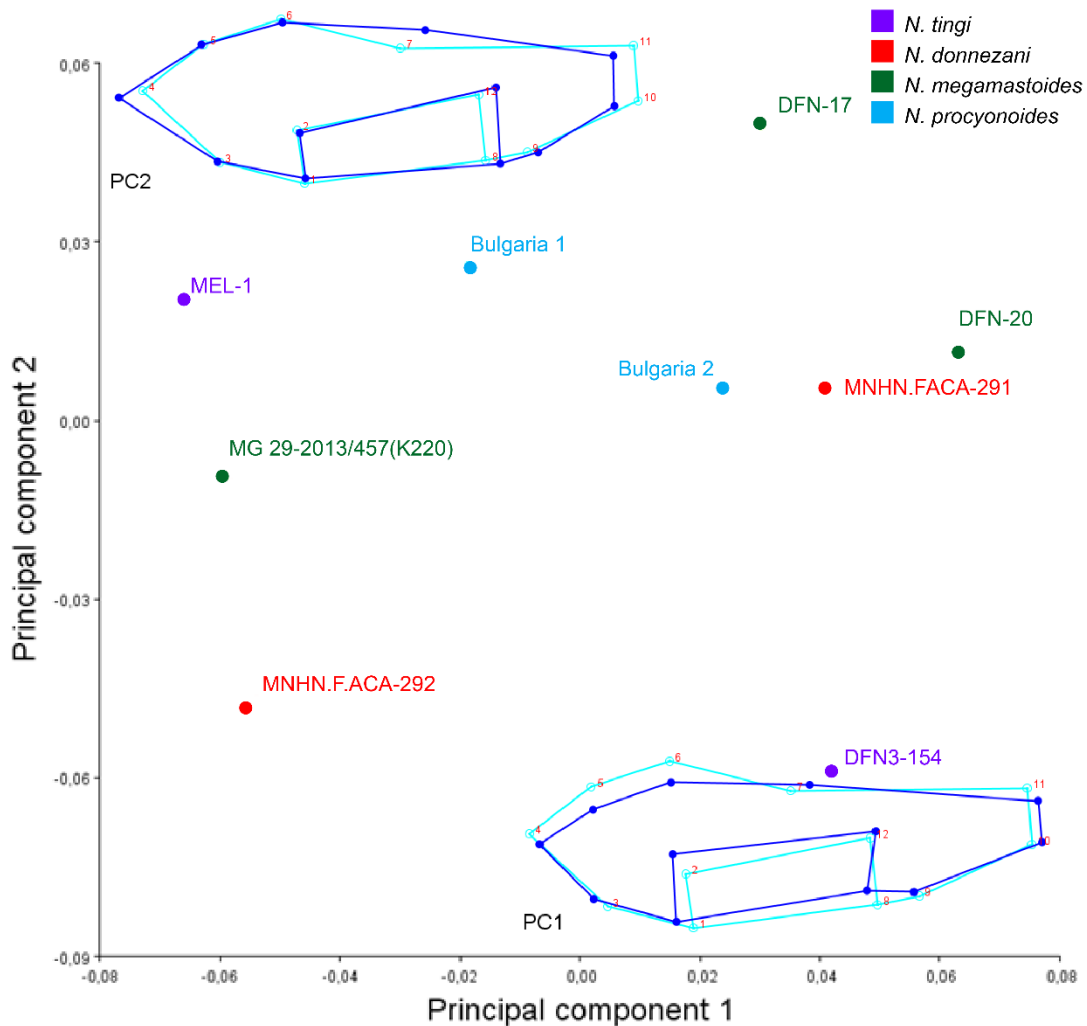


Fig. 30. PCA plot derived from the geometric morphology of *Nyctereutes* crania. Mean shape variation along PC1 and PC2 is indicated by the teal and blue wireframe, respectively. Teal wireframe indicated the mean shape at the origin of PCA plot, while blue wireframe indicates the mean shape at the end of the plot.

Alongside PC1, at the origin of the axes, more robust, vertically oriented crania are encountered (Fig. 26), whereas on the right side of the graph the shape variation designates slenderer, horizontally aligned and dorsoventrally short crania (Fig. 26). Moreover, the position of the temporomandibular joint (TMJ) and that of the zygomatic arches is elevated moving from the origin of the plot to the right (Fig. 26).

On the contrary, more slender crania builds are found at the origin of the PC2, while sturdier crania, with more vertically placed postorbital processes and more protruding nuchal crest caudally are placed on the top of the graph.

The *N. megamastoides* specimens from Dafnero (DFN-17, DFN-20) and *N. procyonoides* (Bulgaria 1, Bulgaria 2) are in the top right part of the graph forming a group. The *N. donnezani* F.ACA-291 specimen from Çalta, is grouped with the previous specimens on the right top of the plot. The DFN3-154 is positioned at the lower right of the graph presenting a slender elongated built, decreased dorsoventrally. Since *N. tingi* and *N. donnezani* are thought to be more carnivorous than *N. megamastoides* and *N. procyonoides*, we expected specimens from *N. tingi* and *N. donnezani* species to be placed on the left side of the graph, possessing more vertically oriented crania. DFN3-154 as reported previously and F.ACA-291 have suffered heavy deformations during fossilization (Daugenet & Sen, 2019), resulting in dorsoventral compaction, thus placing them on the right part of the graph, showing horizontally oriented crania instead of vertically oriented as expected. On the left side of the graph there is a group consisting of MEL-1 (*N. tingi*), K220 (*N. megamastoides*), F.ACA-292 (*N. donnezani*). These three specimens have similar shape, with minor differences such as the more elevated position of the postorbital processes in K220 and MEL-1 and the more protruding caudally nuchal crest in MEL-1. DFN3-154 and MNHN.F.ACA-291 seem to be outliers presenting extreme values and are falsely grouped with *N. procyonoides* and *N. megamastoides*. If we exclude these two specimens from the analysis a clearer discrimination between the studied sample occurs, with the *N. megamastoides* and *N. procyonoides* specimens positioned on the right of the graph and MEL-2 (*N. tingi*) and MNHN.F.ACA-292 (*N. donnezani*) being placed on the left of the plot.

The difference of DFN-20 with the other specimens of *N. procyonoides* and *N. megamastoides* is the slightly higher position of the TMJ and that of the mastoid process. DFN-20 presents a high dorsoventral compression of the cranium. This is probably due to possible deformations during fossilization or because of an expressed sexual dimorphism (see Daguenet & Sen, 2019). DFN-17 and Bulgaria 2 display lower position of the mastoid process and elevated TMJ and zygomatic arches relative to the rest of the *Nyctereutes* specimens. The specimen from Kvabebi (K220) (*N. megamastoides*) is most probably an outlier placed, with MEL-2 and MNHN.F.ACA-292 not grouping with the rest of *N. megamastoides* further to the right. In general a more vertical orientation of the cranium is observed in the *N. tingi*-*N. donnezani* group, while the *N. procyonoides*-*N. megamastoides* group exhibits a more horizontally aligned cranium, except from specimen K220 (*N. megamastoides*) from Kvabebi. Mean shape variation along PC1 axis indicates a decreased moment arm for the temporalis muscle in the more derived species, *N. procyonoides*-*N. megamastoides*.

5.2 Muscle accommodation in *Nyctereutes*

The results of the estimations of endocranial volume ratio and Miller index are presented in Table 10.

Table 10. Results of the estimations for Miller's Index, Brain volume quotient (BVQ) for the studied sample.

Specimens	Species	Miller's Index	BVQ
Bulgaria 1	<i>N. procyonoides</i>	55.62	23.35
Bulgaria 2	<i>N. procyonoides</i>	55.70	23.49
DFN3-154	<i>N. tingi</i>	53.33	22.70
DFN3-155	<i>N. megamastoides</i>	55.92	

MNCN63662	<i>N. donnezani</i>		23.62
MNHN.F.ACA292	<i>N. donnezani</i>		24.21
MNHN.F.ACA291	<i>N. donnezani</i>		22.71
DFN-17	<i>N. megamastoides</i>	57.64	24.53
DFN-20	<i>N. megamastoides</i>	45.74	23.36
MG 29-2013/457 (K220)	<i>N. megamastoides</i>	59.67	26.70
MEL-1	<i>N. tingi</i>		24.16
MEL-2	<i>N. tingi</i>	57.05	
MG 29-2013/581 (K219)	<i>N. megamastoides</i>		24.19

DFN3-155 specimen was excluded from the estimation of the endocranial volume analysis as it presents extreme dorsoventral deformation. The snout of MEL-2 specimen is broken, anteriorly of the canines, so the absolute skull length for this specimen cannot be measured, and thus we could not estimate the absolute endocranial volume ratio relative to skull length for this specimen, which was also excluded from the analysis. The three *N. donnezani* specimens of the studied sample lack the zygomatic arches, so the calculation of Miller index was not possible.

To test whether the differentiation of Miller's index and BVQ are statistically important one way ANOVA analysis was conducted. When tested statistically ANOVA resulted in no significant statistical differences $p = 0.9768$ for Miller's index and $p = 0.414$ for BVQ respectively. To check for any differences of BVQ within *Nyctereutes* species Tukey's pairwise test was conducted Table 11.

Table 11. Tukey's pairwise results of BVQ for the studied sample of *Nyctereutes* (p-values above the diagonal – Tukey's tests results below the diagonal).

	<i>N. procyonoides</i>	<i>N. tingi</i>	<i>N. donnezani</i>	<i>N. megamastoides</i>
<i>N. procyonoides</i>		1.000	0.9997	0.5628
<i>N. tingi</i>	0.0129		0.9998	0.5685
<i>N. donnezani</i>	0.1328	0.1185		0.5262
<i>N. megamastoides</i>	1.912	1.897	2.009	

The constructed boxplot of BVQ shows the variation of endocranial volume in *Nyctereutes* (Fig. 31). *Nyctereutes megamastoides* presents the highest values

followed by *N. procyonoides*. *Nyctereutes donnezani* and *N. tingi* show relatively lower values of endocranial volumes than the previously mentioned *Nyctereutes* species.

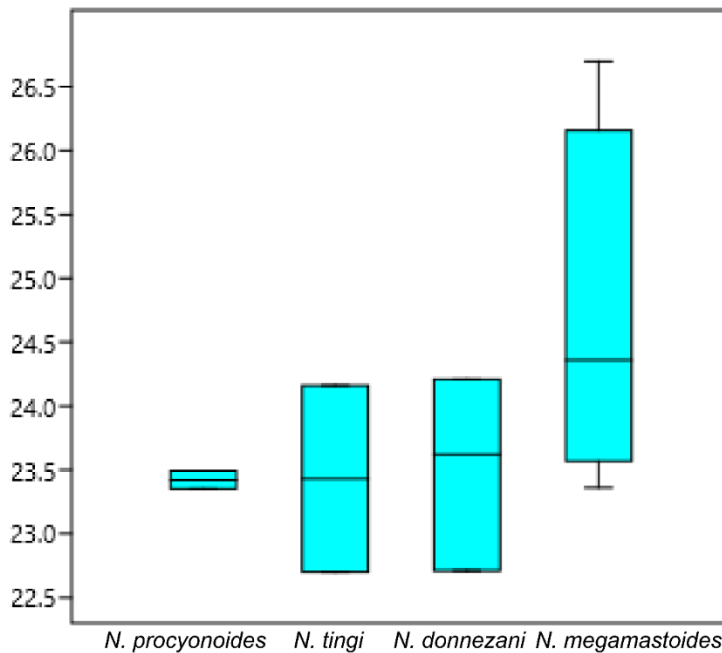


Fig. 31. Boxplot of the BVQ variation in studied *Nyctereutes* sample.

A slight increase in BVQ is observed *N. megamastoides* (Fig. 27), although without any significant statistical differences (Table 13-14). As previously stated, decrease in endocranial volume while the zygomatic arch width relative to body size is constant, creates extra space for housing the temporalis muscle. The specific results speculate that the more primitive *N. tingi* and *N. donnezani* presented more available space to host a larger temporalis. *Nyctereutes procyonoides* most probably resembles an intermediate condition between that of the *N. megamastoides* and *N. tingi* - *N. donnezani* group. A larger sample could possibly support further this hypothesis.

5.3 Hunter-Schreger Bands pattern in *Nyctereutes*

In general, observations with the light microscope of the teeth enamel in the studied sample showed no differences in the HSB folding. All the studied sample is characterized by undulating HSB folding. In some cases, more folded HSB angles were observed in *N. megamastoides* and *N. procyonoides*, but not enough to be characterized as acute angles. The results of the mean HSB angles are presented in Table 12.

Table 12. Average measured HSB angles in the studied *Nyctereutes* sample

Specimen	Species	Tooth	Spot	HSB pattern	Mean Average angle
DFN3-342	<i>N. megamastoides</i>	m1	tip	Undulating	138.25
Bulgaria 2	<i>N. procyonoides</i>	m1	tip	Undulating	139.49
DFN3-8b	<i>N. tingi</i>	m1	tip	Undulating	146.59
DFN3-8b	<i>N. tingi</i>	p4	tip	Undulating	142.42
DFN3-342	<i>N. megamastoides</i>	p4	tip	Undulating	137.88
DFN-23	<i>N. megamastoides</i>	c1	tip	Undulating	138.07
Bulgaria 2	<i>N. procyonoides</i>	c1	tip	Undulating	138.35
DFN3-154	<i>N. tingi</i>	P4	tip	Undulating	131.90
DFN-17	<i>N. megamastoides</i>	P4	tip	Undulating	137.13
DFN3-154	<i>N. tingi</i>	C1	tip	Undulating	146.05
DFN3-8b	<i>N. tingi</i>	C1	tip	Undulating	148.37
DFN-20	<i>N. megamastoides</i>	C1	tip	Undulating	134.50

N. tingi seems to be characterized by slightly more obtuse angles in the examined sample. Despite their metrical differences in measured angles, the HSB folding of all studied species is characterized as undulating. Comparison between the HSB folding of the studied sample is displayed in (Fig. 32).

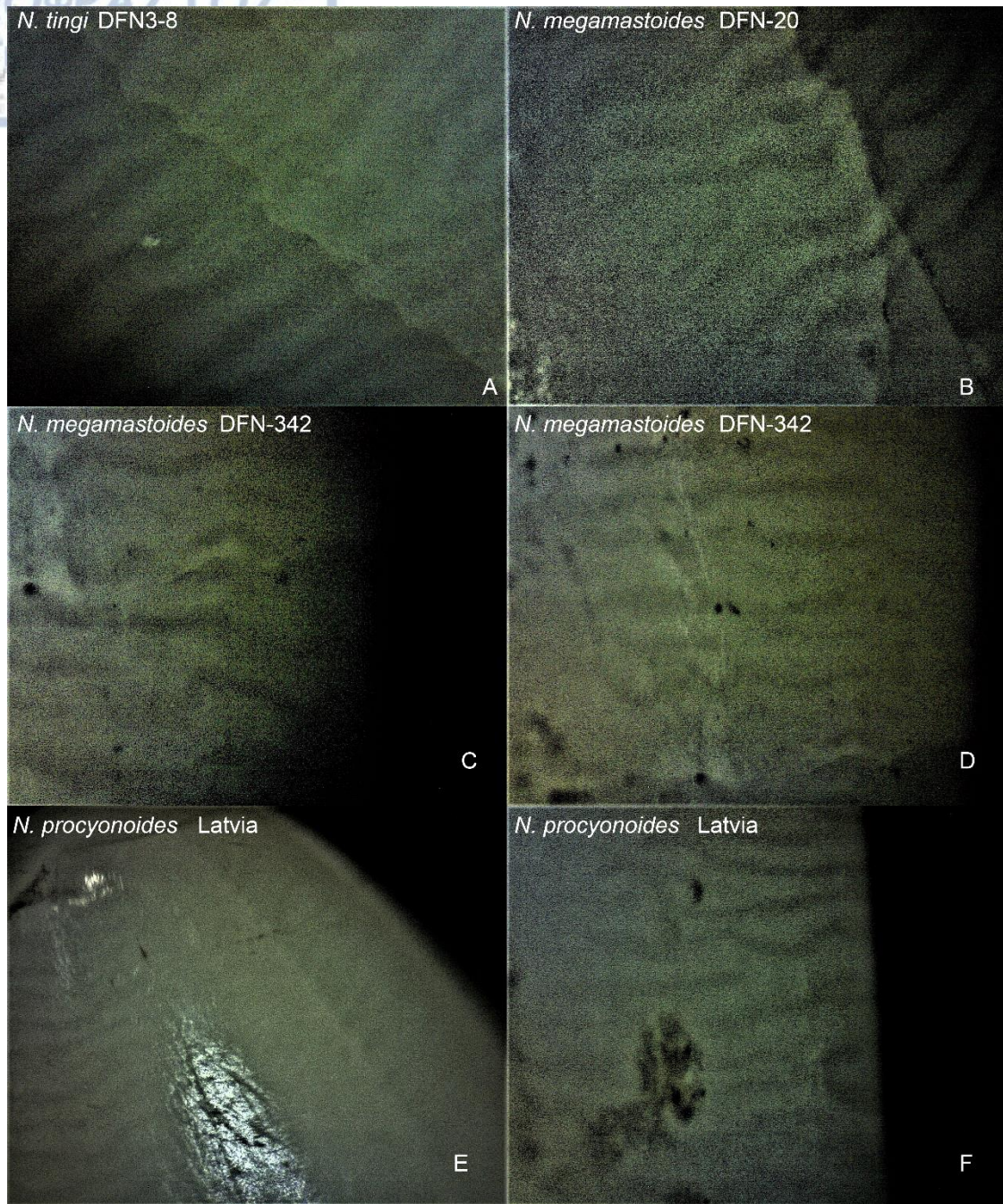
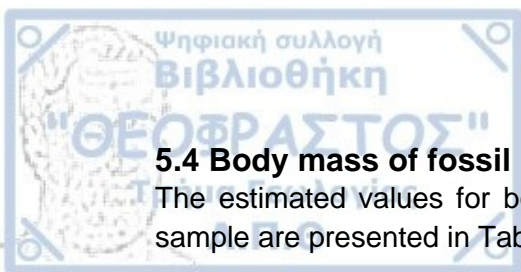


Fig. 32. HSB structure of *Nyctereutes*. A-B: upper C1 of *N. tingi* (DFN3-8) and *N. megamastoides* (DFN-20), C-D: lower c1 of *N. megamastoides* (DFN3-342) (C-D), *N. procyonoides* (Latvia) (E-F)



5.4 Body mass of fossil *Nyctereutes*

The estimated values for body mass using skull length, in the studied *Nyctereutes* sample are presented in Table 13.

Table 13. Predicted body mass values using the skull length as body size estimator.

Specimen	Species	BM (kg)
Bulgaria 1	<i>N. procyonoides</i>	9.20
Bulgaria 2	<i>N. procyonoides</i>	10.02
RV 8003	<i>N. procyonoides</i>	7.84
DFN3-154	<i>N. tingi</i>	21.84
DFN3-155	<i>megamastoides</i>	15.70
MNHN.F.ACA291	<i>N. donnezani</i>	23.17
MNHN.F.ACA292	<i>N. donnezani</i>	16.31
DFN-17	<i>N. megamastoides</i>	12.50
DFN-20	<i>N. megamastoides</i>	14.27
MG 29-2013/457 (K220)	<i>N. megamastoides</i>	12.70
MG 29-2013/581 (K219)	<i>N. megamastoides</i>	10.43
MEL-1	<i>N. tingi</i>	25.24
MEL-2	<i>N. tingi</i>	17.02
MNCN63662	<i>N. donnezani</i>	27.42

The estimated values for body mass using the lower m1 length are given in Table 14.

Table 14. Predicted body mass values using the m1 length as body mass estimator.

Specimen	Species	BM (kg)
DFN3-342	<i>N. megamastoides</i>	6.11
China-1	<i>N. procyonoides</i>	5.11
China-2	<i>N. procyonoides</i>	4.39
Bulgaria 1	<i>N. procyonoides</i>	4.05
Bulgaria 2	<i>N. procyonoides</i>	4.19
DFN3-8b mandible	<i>N. tingi</i>	8.98
Perpignan	<i>N. donnezani</i>	7.73
ACA-903	<i>N. donnezani</i>	7.37
ACA-294	<i>N. donnezani</i>	8.10
ACA-904	<i>N. donnezani</i>	11.14
MNCN39916	<i>N. donnezani</i>	7.61
MNCN39917	<i>N. donnezani</i>	6.68
MNCN39919	<i>N. donnezani</i>	7.73
MNCN62504	<i>N. donnezani</i>	5.42
MNCN62519	<i>N. donnezani</i>	9.41
MNCN71087	<i>N. donnezani</i>	8.10

PERRIER	<i>N. megamastoides</i>	6.13
Villaroya V-118	<i>N. megamastoides</i>	6.46
Villaroya V-112	<i>N. megamastoides</i>	6.35
MNCN39918	<i>N. megamastoides</i>	7.02
MG 29-2013/588 (K221)	<i>N. megamastoides</i>	6.79
MG 29-2013/591 (K214)	<i>N. megamastoides</i>	6.68
MG 29-2013/592 (K4177)	<i>N. megamastoides</i>	6.68
MG 29-2013/820	<i>N. megamastoides</i>	7.97
Chine	<i>N. tingi</i>	11.14
F: AM 97029	<i>N. tingi</i>	12.88
F: AM 97030	<i>N. tingi</i>	10.54
F: AM 96799	<i>N. tingi</i>	10.25
THP 22729	<i>N. tingi</i>	12.07
IVPP YS 131	<i>N. tingi</i>	12.72
Zhoukoudian China	<i>N. sinensis</i>	8.48
SV.99.686	<i>N. vulpinus</i>	7.97
SV.98.799	<i>N. vulpinus</i>	8.10

The average body masses estimated via skull length and m1 length for each species are presented in Table 15. No data for *N. vulpinus* skull length was available so no body mass was estimated using skull length.

Table 15. Estimated body masses for the studied *Nyctereutes* species.

Specimen	Average Body Mass SKL (Kg)	Average Body Mass m1 Length (Kg)
<i>N. procyonoides</i>	9.10	4.43
<i>N. tingi</i>	21.37	11.23
<i>N. megamastoides</i>	13.12	6.69
<i>N. donnezani</i>	22.30	7.93
<i>N. vulpinus</i>		8.04

Van Valkenburgh (1990) notes that both skull length and m1 length for groups sizes between 6-10 Kg share the same prediction error, and Flower's (2016) equation is considered more precise than Van Valkenburgh's (1990). The average body mass predicted for *N. procyonoides* using skull length is 9.10 Kg, while using the m1 length is 4.43 Kg. *Nyctereutes procyonoides* mean body mass is around 4-6 Kg in the summer and 6-10 Kg during winter (Nowak, 2005). The estimated values for body mass using the m1 length as body mass estimator are closer to those predicted using the skull length, therefore the function provided by Flower (2016) is preferred.

5.5 Bite Force Estimation in Fossil *Nyctereutes*

The analytical table of the predicted bite forces for *Nyctereutes* using the dry skull method as in Damasceno et al. (2013) and the estimated PCSA values is displayed in

Table 16. A trend for the overestimation of bite force in *N. procyonoides* is noticeable, as most authors have found lower values (Christiansen and Adolfsen, 2005; Christiansen and Wroe, 2007; Damasceno et al., 2013; Penrose et al., 2020). This may be a result of the variation in size between the different specimens used, or differences in calculation method. However, bite forces estimated here are greater than other values published in the literature, so the possibility of a bias is more likely. It must be noted that, all measurements were taken digitally, hence small differences in the scale of each photo may be present. Body size and muscle size seem to relate with positive allometry (Table 6). The bite forces predicted for *N. procyonoides* using the estimations of the PCSA values for each of the specimens are closer to the published bite forces in the available literature (Damasceno et al., 2013; Penrose et al., 2020), thus they are considered reliable.

Table 16. Estimated bite forces of available *Nyctereutes* sample using the PCSA as bite force estimator and dry skull method as in Damasceno et al. (2013).

Specimens	Species	BF PSCA	BF Dry skull
Bulgaria 1	<i>N. procyonoides</i>	150.35	210.36
Bulgaria 2	<i>N. procyonoides</i>	154.37	199.74
DFN3-154	<i>N. tingi</i>	188.64	212.27
DFN3-155	<i>N. megamastoides</i>	160.41	193.35
MNHN.F.ACA291	<i>N. donnezani</i>	235.92	
MNHN.F.ACA292	<i>N. donnezani</i>	170.02	
DFN-17	<i>N. megamastoides</i>	173.81	200.24
DFN-20	<i>N. megamastoides</i>	185.31	200.26
MG 29-2013/457 (K220)	<i>N. megamastoides</i>	160.40	187.41
MG 29-2013/581 (K219)	<i>N. megamastoides</i>	124.20	
MEL-1	<i>N. tingi</i>	238.17	
MEL-2	<i>N. tingi</i>	170.68	216.68
MNCN-63662	<i>N. donnezani</i>	246.53	

5.6 Prey Size Estimation in Fossil *Nyctereutes*

The estimated average prey sizes for the studied *Nyctereutes* sample are presented in Table 17. Larger prey sizes are observed in the larger species *N. tingi* and *N. donnezani*. *Nyctereutes procyonoides* exhibits the smallest average prey size.

Table 17. Average prey size estimations for the studied *Nyctereutes* sample.

Species	AVR Prey Size (Kg)
<i>N. megamastoides</i>	0.86
<i>N. procyonoides</i>	0.34
<i>N. tingi</i>	2.88
<i>N. donnezani</i>	1.33
<i>N. vulpinus</i>	1.30

5.7 Cranial muscle accommodation in *Nyctereutes*

The temporalis is the primary adductor muscle in most carnivorans (Van Valkenburgh, 2007) but in canids especially, is contributing at about 60% of the total adductor muscle mass and it possess the largest attachment surface (Penrose et al., 2016). The significance of temporalis in carnivorans is unquestionable, as it is the main muscle force producer (Christiansen and Adolfssen, 2005; Ito and Endo, 2016; Penrose, 2018), allowing the infliction of a successive lethal bite (Davis, 2014). Small bodied canids display a sagittal gap, resulting in less surface available for the attachment of temporalis (Penrose et al., 2016). Regardless of being an undersized canid, the temporalis attachment area in *Nyctereutes* scales at a similar rate with that of other canids, implying that sagittal crest growth in *Nyctereutes* varies according to the needs of the temporalis (Penrose et al., 2016). In fossil *Nyctereutes* the sagittal crest is well developed in all species. However, specific specimens, such as MNHN.F.ACA-291 (*N. donnezani*) and DFN3-154 (*N. tingi*) display a more pronounced sagittal crest. Yet, sexual dimorphism is not well explained in *Nyctereutes*, with authors suggesting that it is present in fossil *Nyctereutes*, with males presenting more pronounced cranial characters, including the sagittal crest (Daguenet and Sen, 2019). Moreover, the variation of the available space for housing the temporalis muscle was examined in *Nyctereutes*. Lower endocranial volumes relative to body size were expected in the more carnivorous *Nyctereutes* species, as the temporalis is the primary muscle in carnivoran diet. Former studies show a reduction of endocranial volume in the more derived *Nyctereutes* species (Kargopoulos, 2019). In the current study, differences were found with the more primitive species (*N. donnezani*, *N. tingi*) displaying slightly lower endocranial volume relative to their size compared to *N. megamastoides*, while the ratio of zygomatic arch width against body size remains constant. Surprisingly, *N. procyonoides* endocranial volume development is more similar to that of *N. tingi* and *N. donnezani* and not to *N. megamastoides*. Studies regarding the variation of m2/m1 scores in *Nyctereutes* revealed a more omnivorous diet for *N. megamastoides* and *N. sinensis*, while the extant *N. procyonoides* presents similar or lower values than the primitive *N. tingi* and *N. donnezani* (Lucenti, 2019). Even though, both the ANOVA analysis and Tukey's pairwise comparison for the variation of BVQ in *Nyctereutes*, displayed no significant differences amongst species, the minor variance in endocranial volume ratio observed (Fig. 24) could be indicative for the more omnivorous species showing a preference in favoring the masseter muscle instead of temporalis. A larger study sample could possibly provide further support in the future.

5.8 Cranial shape variation in *Nyctereutes*

The geometric morphometric analysis revealed a grouping between *N. procyonoides* and *N. megamastoides*, as well as between *N. tingi* and *N. donnezani*. A sum of common functional important morphological features seems to characterize the derived species, *N. procyonoides*-*N. megamastoides*, such as the slightly elevated TMJ and zygomatic arches and a horizontal orientation of the cranium. On the other hand, the *N. tingi*-*N. donnezani* group is characterized by more vaulted braincases, with vertical orientation. When the neurocranium is horizontally oriented, the temporalis fascicles tend to align horizontally. It has been suggested that the more horizontally aligned temporalis fascicles enable swift snapping shut of the mandible by pulling the coronoid process caudally (Penrose, 2018). On the other hand a more vertically oriented neurocranium with more vertically aligned temporalis fascicles provides a stable

maintenance of the output force in expense of velocity (Penrose, 2018). A vertically oriented cranium also limits the distribution of stresses in a more dorsoventral plane, limiting the effectiveness of torsional forces and amplifying that of compressive stresses (Tseng and Flynn, 2015). The mammalian cortical bone is better suited to endure compression than torsion (Tseng and Flynn, 2015). Increased stresses are expected if hunting more challenging preys, that comes in an agreement with the hypothesis that *N. tingi* and *N. donnezani* were more carnivorous than *N. megamastoides*. The horizontal alignment of the neurocranium with the simultaneous elevation of the TMJ and zygomatic arches, probably results in decreased moment arm for the temporalis muscle, while it enhances the function properties of the masseter muscle by increasing the in-lever distance for this muscle. The masseter muscle is favored in herbivores, as the dominant muscle among the adductors (Turnbull, 1970). Regarding the specimens from Dafnero, both DFN-17 and DFN-20 (*N. megamastoides*) show a relatively more elongated shape than *N. procyonoides* specimens. This probably reflects the more omnivorous character of *N. megamastoides* as it has been highlighted previously by the m2/m1 area scores, but also a cranium more capable to utilize rapid chewing. The *N. procyonoides* (Bulgaria 1, Bulgaria 2) sample reflects an intermediate condition between the more carnivorous *N. tingi* - *N. donnezani* group and that of *N. megamastoides*. MEL-1 (*N. tingi*) and MNHN.F.ACA-292 (*N. donnezani*) specimens present a vaulted cranium with a slightly shortened muzzle and relatively more ventrally placed TMJ and zygomatic arches. All these elements facilitate the operation of temporalis muscle during prey capture where mostly dorsoventral forces are applied as they increase the in-lever arm in a more vertical position. The vertical orientation of the temporalis muscle is even more pronounced in MEL-1 specimen presenting a moderately more elevated placement of the postorbital processes, a bony structure that is related to the temporalis muscle size (Radinsky, 1981). Bizarre is the position in the morphospace of MG 29-2013/457(K220) of Kvabebi *N. megamastoides* between that of MEL-1 and MNHN.F.ACA-292 (*N. donnezani*). The Kvabebi specimen presents similar cranial geometric characteristics with the more carnivorous species. Variation of skull and tooth morphometrics has been observed in the extant subspecies of raccoon dogs (Kauhala et al., 1998). More precisely the Finnish raccoon dog (*N. procyonoides ussuriensis*) presents more pronounced cranial features, thus a different cranial shape in comparison with its Asiatic relative *N. procyonoides viverrinus*, which is smaller in size and has a less robust built. Kauhala et al. (1998) suggest that the Finnish raccoon dog has adapted to a larger size, because it is preferable in colder climates for thermoregulation (Bergmann's rule), while the more pronounced cranial characteristics reflect its relatively more carnivorous diet. On the other hand, *N. p. viverrinus* has adapted to milder climates and a more omnivorous diet, hence the larger size of the grinding surface areas in the lower molars (Kauhala et al., 1998). During their investigation Kauhala et al. (1988) note that there is no evident sexual dimorphism between these subspecies, thus the scenario of Kvabebi specimen representing a robust male individual with more pronounced cranial characteristics would not be the preferable one. Considering the previous statements, we could assume that the differences between the specimens from Kvabebi and Dafnero are related with the different geographic positions and possibly climates between Kvabebi and Dafnero sites.

5.9 The effect of the subangular lobe

The subangular lobe is one of the main diagnostic features of *Nyctereutes*, discriminating the different species based on its development (Daguenet and Sen, 2019; Lucenti et al., 2018; Tedford and Qiu, 1991). The subangular lobe is lessened in the more primitive species while it is more pronounced in the more derived species of *Nyctereutes* (Tedford and Qiu, 1991; Rook et al., 2017; Lucenti et al., 2018; Daguenet and Sen, 2019). Despite its systematic value, the subangular lobe is very important functionally as it serves as an insertion area for the digastricus and masseter muscle (Penrose, 2018).

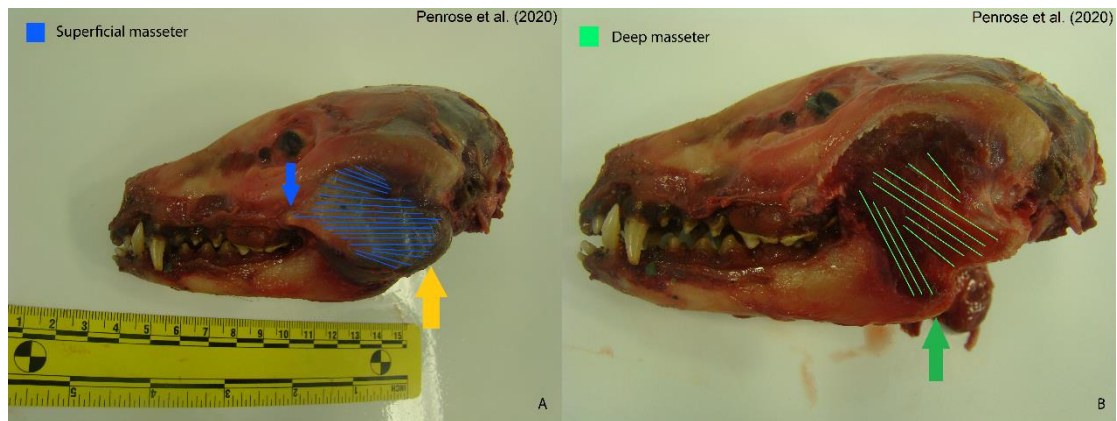
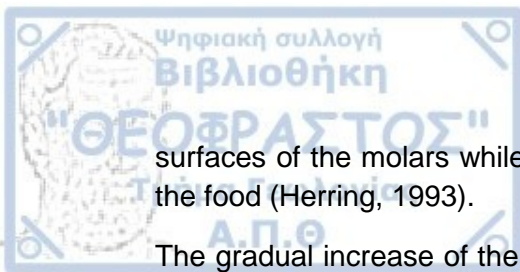


Fig. 33. Lateral view of the skull of *N. procyonoides*. A: Blue arrow indicates the tendinous origin for superficial masseter, yellow arrow indicates its insertion on the mandible. Blue lines represent the orientation of the muscle's fascicles. B: Green arrow indicates the insertion of deep temporalis onto the subangular lobe, green lines indicate the orientation of deep temporalis fascicles. Photos were provided by Dr. Fay Penrose (Penrose et al. 2020).

The masseter is divided into three layers (superficial, zygomaticomandibularis and deep) with the superficial and deep being more distinct (Penrose, 2018). The origin of the superficial layer of the masseter is a stout tendon origin located in a small bony prominence on the maxilla, dorsally of the upper M2 (Penrose, 2018). Masseter is more or less horizontally aligned and runs through the ramus. The muscle inserts partially on the mandible laterally and caudally, on the height of the angular process, while a great amount of fascicles continue around the ventral margins of the mandible. Masseter finally inserts on the ventromedial side of the caudal surface of the mandible and onto the pterygoids (Penrose, 2018) (Fig. 33).

The presence of the subangular lobe enlarges the available insertion surface area for the masseter as a complex including the superficial layer, increasing the moment arm for this muscle layer. The zygomaticomandibularis cannot be easily distinguished between the superficial and the deep part and we will not investigate it further during this study. The deep masseter is the third layer of the masseter. Its insertion is located in the ventral margin of the zygomatic arches and inserts on the lateral and caudal part of the mandible (Penrose, 2018) (Fig. 28). This layer has vertical direction generally. Interestingly on *Nyctereutes procyonoides* the deep masseter fascicles insert onto the subangular lobe, resulting in a more vertical position of the deep masseter fascicles while simultaneously increasing the fascicle length, and thus the mechanical advantage of this muscle (Fig. 28) (Penrose, 2018). During mastication, herbivores use high vertical forces that keep the jaw shut, maintaining the food bolus among the occlusal



surfaces of the molars while transverse movements of the jaw enable the grinding of the food (Herring, 1993).

The gradual increase of the subangular lobe in *Nyctereutes* could be associated with increased grinding ability. Dissection on the adductor muscles of various Canidae revealed different percentages of the deep masseter layers relative to the whole masseter complex mass (Penrose, 2018) (Table 18). Hypercarnivores and generalists display higher percentages of the deep masseter layer than small prey specialists.

Table 18. Deep masseter as a percentage of whole masseter muscle. Deep masseter percentage values were taken by Penrose et al. (2018) (Table 2.5). If *Speothos venaticus* is excluded then both hypercarnivores and generalists display relatively bigger deep masseter percentages than small prey specialists.

Species	Diet	Deep masseter %
<i>Alopex lagopus</i>	Small prey specialist	16.4
<i>Canis lupus</i>	Hypercarnivore	31.2
<i>Canis mesomelas</i>	Small prey specialist	21.2
<i>Chrysocyon brachyurus</i>	Small prey specialist	13.9
<i>Cuon alpinus</i>	Hypercarnivore	36.4
<i>Lycaon pictus</i>	Hypercarnivore	31.5
<i>Nyctereutes procyonoides</i>	Generalist	33.1
<i>Otocyon megalotis</i>	Generalist	21.5
<i>Speothos venaticus</i>	Hypercarnivore	12.2
<i>Vulpes corsac</i>	Small prey specialist	25.3
<i>Vulpes vulpes</i>	Small prey specialist	17.4
<i>Vulpes zerda</i>	Generalist	29.1

Speothos venaticus is a small sized hypercarnivore canid and presents the lowest percentage of deep masseter muscle in the former mentioned analyses. If *Speothos venaticus* is excluded from the analysis, then the variation of deep masseter percentage relative to whole masseter is more pronounced between the hypercarnivores and small prey specialists. This may be due to larger prey sizes selection of the larger hypercarnivores. During prey capture mainly rotational movements of the jaw are applied (Popowics and Herring, 2006). Smaller prey probably presents less resistance during capture, and that is possibly reflected in the percentage of the deep masseter muscle, which is a vertically oriented muscle, probably responsible for keeping the jaw shut. Moreover, the increased development of the deep masseter in specific herbivores is thought to assist in maintaining the occluding premolars in contact during the process of the food bolus (Crompton, 2011). Despite being statistically insignificant, these percentage differences of the deep masseter layer could indicate that hypercarnivores and generalists require larger amounts of vertical forces, e.g. hypercarnivores for the infliction of a successive lethal bite and maintaining the prey under a grip, while generalists for the grinding of their food. Thus, the more omnivorous species of *Nyctereutes* may have required a larger masseter muscle for the grinding of their food. A need for a larger deep masseter is not reflected in the structure of the more carnivorous *Nyctereutes* species most probably because they preyed on animals, half their own size at best. Further studies are needed to support the previous assumption.

The digastricus is the main jaw abductor muscle in mammals and its function is to open the jaw (Curtis and Santana, 2018). When it comes to a successful bite despite the bite force exerted, both fast opening and closing of the jaw are required. Variation of the digastric muscle size and position has been studied in the carnivorans and was associated with killing (Scapino, 1976). For instance, a strong digastric muscle has been observed in aquatic otters, as they have to oppose high stresses to open their mouth due to the water resistance when hunting underwater (Scapino, 1976). A typical example is the different insertion point of the digastric muscle in felids and canids. The insertion is more anteriorly placed in felids than in canids, where it lies ventral to the masseteric fossa (Scapino, 1976) (Fig. 34).

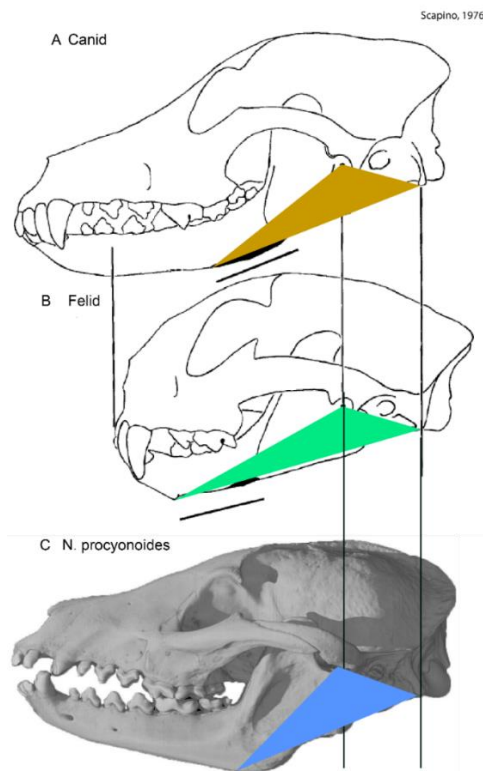


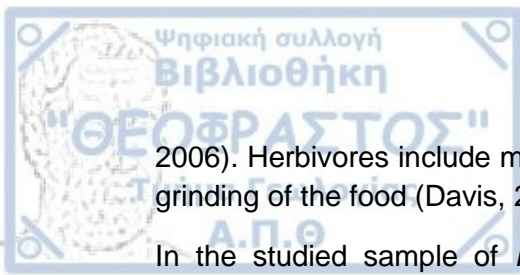
Fig. 34. Schematic presentation of the different insertion position of the digastric muscle in (A) canids and (B) felids and (C) *N. procyonoides*. The black bar indicates the insertion area for the digastric muscle. All skulls are centered on the TMJ and the origin of digastricus. The more posterior position of the digastric muscle insertion in canids and especially in *N. procyonoides* increases the angle between digastric and TMJ. Solid areas correspond to angles between digastricus and TMJ in each sample respectively. Figure modified by Scapino, 1976. The digital model of the skull of *N. procyonoides* was provided by the digital library of the University of Texas, www.DigiMorph.org.

This difference is associated with their different hunting strategies. In specific genera of canids (*Urocyon*, *Otocyon*, *Cerdocyon* and *Nyctereutes*) the posterior part of the dentary has been widened forming a bony projection called subangular lobe serving as an insertion point for the digastricus (Miller and Fowler, 2015). The presence of the subangular lobe has the effect of increasing the angle between the insertion point of digastric and the TMJ, as displayed in (Fig. 30) (Curtis and Santana, 2018). Increased angles of insertion have been linked with high in lever/out lever ratios for digastric muscle in bats (Curtis and Santana, 2018). Increasing the in lever/out lever ratio increases the mechanical advantage for the specific muscle. The increased

development of the subangular lobe allows the more posterior position for the insertion of the digastric muscle in *Nyctereutes*, indicating a gradual increase of the digastricus muscle capability. Increased mechanical advantage of the digastricus in canids has been associated with rapid chewing ability (Ewer, 1973; Miller & Fowler, 2015; Lucenti et al., 2018) and more precisely with the consumption of insects (Curtis and Santana, 2018), as observed in the extant *Otocyon megalotis*, which also possesses sharp cusped teeth and uses fast and repetitive chewing to crush the hard shell of its prey (Berkovitz and Shellis, 2018). Despite the similarities between *Otocyon megalotis* and *Nyctereutes procyonoides*, the former possesses multi-cusped teeth with more pronounced cusps highlighting the "chopping" ability of this animal, as its main food source are insects (Ewer, 1973). *Nyctereutes* do not possess an extra upper molar nor that many cusps in its teeth, indicating a less specialized skull morphology towards insect consumption. *Nyctereutes* follow the skull structure of small prey specialists and generalists, with a slender jaw built, elongated rostrum or mild development of zygomatic arches (Meachen-Samuels and van Valkenburgh, 2009). Shortening of the muzzle is associated in slower opening of the jaw, as the required time for the teeth to disengage is increased (Curtis and Santana, 2018). Geometric morphometric analysis did not present any significance differences in muzzle length of *Nyctereutes*, with the more omnivorous species possessing a slightly more elongated rostrum. This speculates that the development of the subangular lobe aims to further enhance the chewing ability of *Nyctereutes* (bigger gape, faster opening) and not just to compensate for a potential decrease of rostrum length. Small amphibians, reptiles and fish often consist prey for *N. procyonoides* (Ward and Wurster-Hill, 1990). All the previous mentioned animals are very agile and can easily escape in a small space. So *Nyctereutes* has the need for a swift bite in order to catch his fast-moving prey, especially when *Nyctereutes* itself is not suitable for running.

5.10 Pre-postglenoid process and bite force

Ito & Endo (2019) examined the variations of the pre-postglenoid interval between different carnivoran species in accordance with the participation percentage of each of the masticatory muscles (temporalis, masseter, pterygoids). The general concept is that when the pre-postglenoid interval is small (big preglenoid and small postglenoid angles), then the temporomandibular joint structure is sturdy and locks the mandibular condyle inside the fossa without permitting dislocation of the jaw (Ito and Endo, 2019). Development of the temporalis muscle leads to the decrease of the postglenoid angle, or in other words to a more protruding postglenoid process (Ito and Endo, 2019). On the other hand, enhanced masseter muscle has the opposite effects on the postglenoid angle, with a decreased postglenoid process (Ito and Endo, 2019). In Canidae, a wide pre-postglenoid interval is noticed, resulting in a weak TMJ not capable of restricting the mandibular condyle sufficiently in the mandibular fossa. However, the muscle arrangement of canids allows the collaboration of the temporalis, masseter and pterygoids in order to compensate the lack of a sturdy TMJ structure and prevent dislocation of the jaw while exerting remarkable bite forces (Davis, 1955; Turnbull, 1970). A small pre-postglenoid interval prevents the jaw from moving on a sagittal plane and restricts its movements mostly on a vertical plane Popowics & Herring, 2006; Ito & Endo, 2019). A more flattened pre-postglenoid process facilitates anteroposterior movements (Popowics and Herring, 2006). Carnivorans mostly utilize rotational (dorsoventral) jaw movements, especially during prey capture (Popowics and Herring,



2006). Herbivores include more translational (anteroposterior) jaw movements, during grinding of the food (Davis, 2014).

In the studied sample of *Nyctereutes*, when comparing the structure of the pre-postglenoid of the various species a slightly more protruding postglenoid process is observed in the primitive species *N. tingi*-*N. donnezani* group and especially in the MNHN.F.ACA-291 specimens of *N. donnezani* from Çalta. A less developed postglenoid process is observed in the more derived species such as *N. megamastoides* and *N. procyonoides*. The developed postglenoid process is indicative for a stronger temporalis muscle relative to masseter as noted by previous authors (Davis, 1955; Turnbull, 1970; Ito & Endo, 2019). Unfortunately, a precise measurement of the pre-postglenoid processes and pre-postglenoid angle was not possible during this study for many technical reasons. Stronger temporalis muscles have been associated with carnivory as this is a functionally important muscle for vertical jaw movements allowing the produce of high bite forces during hunting (Davis, 2014). This morphological adaptation provides additional support of the carnivorous dietary preferences of the more primitive *Nyctereutes* species, *N. tingi* and *N. donnezani* as it has been previously indicated by their dental adaptations (Bartolini Lucenti, 2019). Further research is needed to be done concerning this topic, with a 3D modeling of various *Nyctereutes* crania in order to measure the exact angle differences of the pre-postglenoid interval between the various *Nyctereutes* species.

5.11 Bite Force, Prey Size Variation in *Nyctereutes*

During this study the bite forces of the smaller sized species, *N. procyonoides* and *N. megamastoides*, are observed to be higher than those of the larger ones *N. tingi* (Table 16). On the other hand, bite forces predicted using regression analyses, are higher at the larger sized species *N. tingi* and *N. donnezani* (see Table 16). The bite force of *Nyctereutes* material from Greece has been studied previously, showing a trend towards reduction in the more derived species (Kargopoulos, 2019). The bite forces of the *Nyctereutes* material studied here are relatively lower than those estimated from Kargopoulos (2019).

Previous studies regarding the bite force variation in carnivorans, support that higher bite force values are observed as the size of prey increases (Christiansen and Wroe, 2007; Slater et al., 2009; Wroe et al., 2005). Hypercarnivores display the highest bite forces amongst carnivorans and that is due to their large prey (e.g., ungulates twice their size) (Van Valkenburgh, 2007), demanding bigger bite forces to subdue their prey (Christiansen and Wroe, 2007; Slater et al., 2009). Specific herbivorous carnivorans present similar bite forces with hypercarnivores, as plant material is very demanding to process it and requires vast force production (Christiansen and Wroe, 2007). Medium-sized prey consumers display intermediate bite force, while omnivores possess the lowest bite forces, relative to their size (Christiansen and Wroe, 2007). Structural adaptations for increasing the bite force in carnivorans leads to specialization in hunting large prey or consuming tough plant material (Christiansen and Adolfssen, 2005). *Nyctereutes* may be a generalist, but its diet does not include demanding plant food such as bamboo, so no structural adaptations related to bite force enhancement, like the widening of the zygomatic arches are visible. Instead small prey specialists prefer to be agile in the expense of brute strength (Slater et al., 2009), as smaller prey are faster than large sized ungulates. The dry skull method revealed minor differences

between the larger *N. tingi* and *N. procyonoides* regarding bite force, while *N. megamasotides* presents the lowest values among the three species but without any significant deviation. *Cerdocyon thous* is another small sized canid of South America, with comparable morphology (developed subangular lobe) and ecology to *Nyctereutes procyonoides* (Lucenti, 2019; Rocha et al., 2008). *Cerdocyon thous* shows a variety of food preferences such as fruits, reptiles, amphibians, arthropods, small vertebrates such as rodents and a small portion of birds that inhabit the ground surface (Rocha et al., 2008). On the other hand another South American canid, the similarly sized hypercarnivore *Speothos venaticus* (Nowak, 2005; Van Valkenburgh, 2007). *Speothos venaticus* is very social and hunts in groups to take down prey greater than its size (Beisiegel and Ades, 2002; Nowak, 2005). In contrast, *C. thous* is solitary, usually living in pairs (Rocha et al., 2008), as *Nyctereutes procyonoides* (Nowak, 2005; Ward and Wurster-Hill, 1990). Even though *Nyctereutes procyonoides* has been observed to forage as a small group before no pack hunting has been recorded (Ward and Wurster-Hill, 1990). Previous studies show that *S. venaticus* exerts significantly higher bite forces compared to both *N. procyonoides* and *C. thous* (Christiansen and Adolfssen, 2005; Damasceno et al., 2013; Penrose et al., 2020; Wroe et al., 2005). Regardless being comparable in size with *N. procyonoides* and *C. thous*, *S. venaticus* presents a set of morphological adaptations related to hypercarnivory (Van Valkenburgh, 2007), allowing this canid to exert high bite forces. Even though previously no specialized morphologies regarding bite force enhancement have been reported in *Nyctereutes*, in this study we observed specific differences in skull morphology related to muscle accommodation (temporalis size) and muscle mechanical leverage. These differences most probably are associated with the bite force variation observed among *Nyctereutes* species taking into account the larger size of *N. tingi* and *N. donnezani* too.

Concerning the maximum prey size (Table 17), apparently the solitary hunting behavior of *C. thous* and *N. procyonoides* along with the unspecialized morphology for killing sets some boundaries to the maximum prey size. Recent re-examination of *Nyctereutes* material from China shows a shift towards larger sizes for raccoon dog after Late Pliocene in the Asiatic region (Farjand et al., 2020). Studies regarding the dietary preferences of *Nyctereutes* mark an increased carnivory in the more derived representatives of *N. sinensis* prior to *N. procyonoides* from Late Pliocene to Pleistocene in Asia (Lucenti, 2019; Farjand et al., 2020). This increase in size could possibly justify the increased meat consumption, as larger sized predators can subdue larger preys. Collectively, *Nyctereutes* does not present any specialized morphological adaptations towards extreme bite force production, resulting in minor differences in bite force between the various species. The fact that no pack hunting has been recorded in *Nyctereutes*, leads to the assumption that the more robust *N. tingi* and *N. donnezani* were able to hunt larger preys than the smaller *N. megamasotides* and *N. procyonoides*, mainly due to their larger size and secondly to the morphological adaptations reported here.

6 CONCLUSIONS

As in the DFN1 site (Koufos 1992), the present study confirmed the presence of *N. megamastoides* in the DFN3 fossil site based on both morphological observations and metric data of the cranium DFN3-155. Additionally, morphological observations of the studied new sample from DFN3 site suggested that some specimens (DFN3-154, DFN3-8), representing two individuals, belong to another species of *Nyctereutes*, most likely *N. tingi*. However, the analysis of the lower dentition also suggests metrical similarities of DFN3-154 and DFN3-8 specimens with *N. vulpinus*. The possibility for *N. vulpinus* originating from a European lineage of *N. tingi* has been previously suggested (Monguillon et al., 2004). The new findings from Dafnero are remarkable. Primarily, because they further support the presence of *N. tingi* in the Middle Villafranchian (2.3 Ma) of Europe (Spassov, 2003), in a similar manner as to Asia. Secondly, because they identify the contemporaneous presence of two *Nyctereutes* species, one primitive (*N. tingi*) and one more derived (*N. megamastoides*) at the same site. Such a coexistence has been previously described in Asia with *N. tingi* and its possible successor *N. sinensis*. The simultaneous occurrence of two different species of *Nyctereutes* at the same habitat (Farjand et al., 2020; Tedford and Qiu, 1991) is probably a result of the extreme dietary plasticity of the genus (Asahara and Takai, 2017; Drygala et al., 2014; Kowalczyk and Zalewski, 2011). A similar ecological scenario is evident in Dafnero site. The more primitive *N. tingi* co-exists with *N. megamastoides*, which is considered the European counterpart of the Asiatic *N. sinensis* (Rook et al., 2017; Tedford and Qiu, 1991). It is curious that *Nyctereutes* did not survive in Europe. In the mid-late Pleistocene the evolution of *N. sinensis* led to the appearance of *N. procyonoides* in Asia which managed to survive through the Ice Age (Farjand et al., 2020). Extant *Nyctereutes* is characterized by its opportunistic behavior. Fossil evidence from South America marks that dietary specialization in canids leads to decreased survival odds (Balisi et al., 2018). Currently, the main competitor of *Nyctereutes* is the similar-sized red fox, *Vulpes vulpes* (Drygala et al., 2014). However, the more opportunistic behavior of *Nyctereutes*, including a wide variety of food sources and the more carnivorous diet of the red fox allow these animals to coexist without a problem (Baltrūnaitė, 2002; Drygala et al., 2014; Elmeros et al., 2018; Sutor et al., 2010). A dietary overlap between the more carnivorous species of *Nyctereutes*, *N. tingi* and *N. donnezani* and the contemporaneous similar-sized canids would have been possible. The appearance of the more derived *Nyctereutes* species is estimated at 3.9 Ma in Europe with *N. megamastoides*-like raccoon dog (Lucenti et al., 2018) and around 2.3 Ma for *N. sinensis* in Asia, respectively (Farjand et al., 2020). We could hypothesize that a more omnivorous diet in the more derived *Nyctereutes* species is preferred in order to avoid competition with other canids. However, the earlier appearance of *N. megamastoides* in Europe marks this dietary transition in *Nyctereutes* prior to the dispersal of wolf-like canids in Europe (Late Pliocene, ~3.0 Ma; Sardella and Palombo, 2007; Sotnikova and Rook, 2010)). The recent invasion of the golden jackal in East Africa has resulted in sympatry among three different similar sized jackal species, that of *Canis aureus*, *Canis mesomelas* and *Canis adustus* (Van Valkenburgh and Wayne, 1994). The intermediate dietary preferences of *Canis aureus* along with the abundance of prey in the plains of Eastern Africa makes this co-existence feasible, despite the simultaneous presence of various smaller and larger carnivore predators (Van Valkenburgh and Wayne, 1994). Size divergence is not noticeable, in order to avoid competition between the

intermediate sized jackals with the smaller or larger carnivore species in Eastern Africa (Van Valkenburgh and Wayne, 1994). The authors report that sympatric carnivores like jackals, should be separated not based on prey choice, but according to the relative ratio of vertebrate and non vertebrate prey in their diet. Size divergence is a character reported in *Nyctereutes* with the more primitive *N. tingi* and *N. donnezani* being relatively larger than the more derived *N. megamastoides* and *N. procyonoides*. Spatially Europe is more restricted, especially in the Balkan peninsula, than the vast plain fields observed in Asia. It is possible that the dispersal of the wolf-like canids in Europe such as *Canis arnensis*, *Canis etruscus* resulted in increased competition. A gradual decrease in size is reported in *Nyctereutes*, with the only exception the recent findings of *N. sinensis* in Asia. Dietary shift is marked in *Nyctereutes* prior the appearance of the wolf-like canids in Europe. We hypothesize that the more restricted area of Europe, resulted in decrease of prey availability but also in an increase of the competition among the carnivores present at the time, including *Nyctereutes tingi*. It is also possible that the gradual reduction in size in *Nyctereutes*, amplified the competition of *Nyctereutes* with the smaller sized carnivores such as badgers, skunks and foxes.

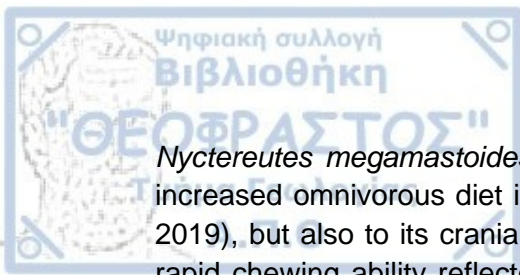
A general trend in *Nyctereutes* diet towards omnivory has been highlighted by previous authors, mainly by dental morphological observations (Lucenti, 2019; Monguillon et al., 2004). Many researchers however have speculated that the presence of the subangular lobe in the more derived *Nyctereutes* is related with a more rapid and successive mastication ability (Lucenti, 2019; Curtis and Santana, 2018; Dagueneet and Sen, 2019; Miller and Fowler, 2015), not managing however to fully reconstruct the ecology of the genus. During our study, a grouping of *N. procyonoides* with *N. megamastoides* and that of *N. tingi* with *N. donnezani* has been observed sharing a sum of common morphological features. The analysis of muscle accommodation in *Nyctereutes* revealed that the more omnivorous *N. megamastoides* invests in the development of the masseter muscle in expense of the temporalis, while *N. procyonoides* along with *N. tingi* and *N. donnezani* retain a stronger temporalis muscle. However, the enrichment of the studied sample is essential to fully confirm this hypothesis. The geometric morphometric analysis in *Nyctereutes* crania also revealed different functional properties between the derived *N. procyonoides* and *N. megamastoides* and the more primitive *N. tingi* and *N. donnezani*. *Nyctereutes procyonoides* and *N. megamastoides* are characterized by more horizontally aligned crania and elevation of the TMJ. The horizontally aligned crania assists the temporalis muscle into faster retrieving of the coronoid process, resulting in swift snapping shut of the lower jaw (Penrose, 2018). On the contrary *N. tingi* and *N. donnezani* show a more vertically structured cranium. A more vertically oriented cranium is believed to provide a more sustainable bite in expense of velocity (Penrose, 2018). Furthermore the vertical orientation of the cranium limits the torsion forces exerted during hunting (Tseng and Flynn, 2015). The elevation of the TMJ provides a better mechanical advantage for the masseter muscle (Figueirido et al., 2010), with the masseter being a functionally important muscle in herbivores, related with the grinding of the food (Allouch, 2018; Herring, 1993; Popowics and Herring, 2006). The presence of the subangular lobe has not only systematic value as a discriminating feature between the different *Nyctereutes* species but also performs multiple functionally important roles. It serves as an additional insertion area for the masseter and pterygoid muscle. Increasing the available surface area results in increased mechanical advantage for these muscles simultaneously. Moreover, the

insertion of deep masseter fascicles into the subangular lobe reorients this muscle's fascicles in a more vertical position, suggesting enhanced grinding ability. The main function of medial pterygoid is to aid in closing the jaw, where the task of the lateral pterygoid is yet unclear (Penrose, 2018). It is thought though that because the medial pterygoid inserts on the opposite sides of the mandible, it participates in rotating the mandibular body around its long axis at opposite directions (Popowics and Herring, 2006). Due to its insignificant size, the lateral pterygoid has not been studied properly yet (Hartstone-Rose et al., 2012; Penrose, 2018; Turnbull, 1970). Lastly the digastric muscle is also enhanced by the presence of the subangular lobe, offering a more posterior insertion position for digastric and increasing its functional properties. The Canidae exhibit a more posterior insertion position for the digastric muscle relative to felids, highlighting the importance for a faster occlusion in canids and for a wider gape in felids (Scapino, 1976). Thus the further posterior insertion position of digastricus in *Nyctereutes* is assumed to allow rapid chewing ability (Ewer, 1973; Miller and Fowler, 2015). Similar HSB patterns were observed in all *Nyctereutes* species examined, suggesting that there is not an apparent dental morphological adaptation for the consumption of tough food material. The examination of bite force in *Nyctereutes* via dry skull method resulted in variation between species, showing higher bite force values in the smaller *N. procyonoides* and *N. megamastoides*. The bite force estimations showed similar bite force values relative to body size, indicating that *N. tingi* and *N. donnezani* possess stronger bite only due to their larger size. The estimation of prey size in *Nyctereutes* revealed that the larger *N. tingi* and *N. donnezani* could probably capture larger preys than *N. megamastoides* and *N. procyonoides*, as expected. Presumably, the largest prey of *Nyctereutes* should be animals such as hares or some sizeable birds and rodents. The fact that the extant *N. procyonoides* is not a pack hunter limits the potential prey size. Most likely the same solitary behavior was also true for the fossil species of *Nyctereutes*.

Our observations in general agree with previous assumptions about the ecology of *Nyctereutes*. *Nyctereutes megamastoides* and *N. procyonoides* present a variety of cranial morphological features towards a more omnivorous diet, while the more primitive *N. tingi* and *N. donnezani* retain some characteristics indicative of carnivory. These characteristics are summarized in Table 19.

Table 19. The various adaptations of *Nyctereutes* reported in this study.

	<i>Nyctereutes</i>			
	<i>tingi</i>	<i>donnezani</i>	<i>megamastoides</i>	<i>procyonoides</i>
<i>Temporalis Extra Space</i>	Present	Present	Absent	Absent
<i>Masseter Extra Space</i>	Absent	Absent	Present	Present
<i>Vertical Cranium</i>	Present	Present	Absent	Absent
<i>Horizontal Cranium</i>	Absent	Absent	Present	Present
<i>Strong Digastricus</i>	Absent	Absent	Present	Present
<i>Strong Bite</i>	Present	Present	Absent	Absent
<i>Rapid chewing</i>	Less Capable	Less Capable	Capable	Capable



Nyctereutes megamastoides is probably the more omnivorous among the rest. His increased omnivorous diet is not only reflected in the higher $m2/m1$ scores (Lucenti, 2019), but also to its cranial development. This species is probably characterized by rapid chewing ability reflected in the horizontally aligned cranium and the increased mechanical properties of digastric muscle with the more insertion position. Presumably, its ecology would be similar with the extant *N. procyonoides*, showing a wide spectrum of diet preferences but probably with higher percentages of plant food. The marked decrease of the temporalis strength, which is the main bite force producer, in *N. megamastoides* should probably affect its capability for preying. Its fast repetitive chewing is probably utilized to catch small and agile prey and not to process demanding tough plant material. The average prey size was estimated around 0,8 Kg for *N. megamastoides*. Most usual prey would be small animals that were easy to catch such as lizards, amphibians and arthropods. Occasionally small rodents like mice could be fallen prey to it, as it has been observed in the extant *Cerdocyon thous*.

Nyctereutes tingi and *N. donnezani* are considered the most carnivorous species compared to the rest of fossil *Nyctereutes*. Their carnivorous behavior is marked by specific modifications that aim to enhance the temporalis. A stronger temporalis muscle is assumed regarding the endocranial volume in comparison with the other fossil *Nyctereutes*. The more vertical structure of the cranium offers stability and endurance during biting and decreases the torsion forces exerted. Furthermore, *N. tingi* and *N. donnezani* possess stronger bite forces due to their larger size overall. Collectively, the previous traits allow both *N. tingi* and *N. donnezani* to catch larger preys than *N. megamastoides* and the extant *N. procyonoides*. The diet of *N. tingi* and *N. donnezani*, would be closer to that of *Vulpes vulpes* (red fox), with frequent hunting of prey such as rodents, hares, birds but also smaller animals like insects and amphibians when prey availability is scarce. Finally, plant material would complete its diet. The average prey size for *N. tingi* and *N. donnezani* is estimated around 1-3 kg. No group hunting has been recorded in extant *N. procyonoides*. Assuming that the same applies to the fossil taxa, *N. tingi* and *N. donnezani* would not have been able to hunt prey larger than themselves.

Fossil *Nyctereutes* has co-existed with similar or larger sized carnivores in the majority of Greek but also in some European fossil sites (e.g., St. Vallier- La Puebla). We could assume that the dietary plasticity of *Nyctereutes* allowed it to co-exist with larger and similar sized carnivores in the same way as the extant *N. procyonoides*. The bovids present in these sites were probably the primary target of the big-sized hypercarnivores, while the smaller canids like foxes and mustelids including *Nyctereutes* selected much easier preys like arthropods, lizards and insects or small rodents and lagomorphs. For instance, the fossil fauna assemblage of Megalo Emvolo is characterized by the presence of *Trischizolagus dumitrescuae*, *Trischizolagus* cf. *maritsae*, *Oryctolagus* cf. *laynensis* and *Microspalax odessanus*. *Trischizolagus* and *Oryctolagus* are similar to extant *Lepus* (hare). Both *Trischizolagus* and *Oryctolagus* are characterized by enhanced fossorial ability (Averianov, 1995). Moreover, *Trischizolagus* seems to be less adapted to cursorial habits than the extant *Lepus* (Averianov, 1995). *Microspalax odessanus* is a mole rat, which is mainly fossorial living in burrows (Genelly, 1965). All the above-mentioned fossil species consist ideal prey for *Nyctereutes* as they lack agility or robustness.

- Abe, G., Ikeda, T., Tatsuzawa, S., 2006. Differences in habitat use of the native raccoon dog (*Nyctereutes procyonoides albus*) and the invasive alien raccoon (*Procyon lotor*) in the Nopporo Natural Forest Park, Hokkaido, Japan. *Assess. Control Biol. Invasion Risks* 116–121.
- Allouch, M.G., 2018. Functional anatomy of the masticatory mechanism: A comparative study of physical characteristics of jaw- closing and jaw- opening muscles in sheep. *Int. J. Vet. Sci.* 2, 38–44.
- Amaike, Y., Oishi, T., Uruguchi, K., Abramov, A. V., Masuda, R., 2015. Geographical variation in skull morphology in the hokkaido population of the red fox, *vulpes vulpes*. *Mammal Study* 40, 245–256. <https://doi.org/10.3106/041.040.0405>
- Asahara, M., Chang, C.H., Kimura, J., Son, N.T., Takai, M., 2015. Re-examination of the fossil raccoon dog (*Nyctereutes procyonoides*) from the Penghu channel, Taiwan, and an age estimation of the Penghu fauna. *Anthropol. Sci.* 123, 177–184. <https://doi.org/10.1537/ase.150710>
- Asahara, M., Takai, M., 2019. Dietary transition in the *Nyctereutes sinensis* and *Nyctereutes procyonoides* lineage during the Pleistocene. *Acta Zool.* 100, 216–217. <https://doi.org/10.1111/azo.12233>
- Asahara, M., Takai, M., 2017. Estimation of diet in extinct raccoon dog species by the molar ratio method. *Acta Zool.* 98, 292–299. <https://doi.org/10.1111/azo.12179>
- Athanassiou, A., 2002. Neogene and Quaternary mammal faunas of Thessaly. *Ann. Géologiques des Pays Helléniques* 39, 279–293.
- Athanassiou, A., 1996. CONTRIBUTION TO THE STUDY OF THE FOSSIL MAMMALS OF THESSALY. National and Kapodistrian University of Athens.
- Averianov, A., 1995. Osteology and adaptations of the early pliocene rabbit *Trischizolagus Dumitrescuae* (lagomorpha: Leporidae). *J. Vertebr. Paleontol.* 15, 375–386. <https://doi.org/10.1080/02724634.1995.10011236>
- Balisi, M., Casey, C., van Valkenburgh, B., 2018. Dietary specialization is linked to reduced species durations in North American fossil canids. *R. Soc. Open Sci.* 5, 1-15. <https://doi.org/10.1098/rsos.171861>
- Baltrūnaitė, L., 2002. Diet Composition of the Red Fox (*Vulpes Vulpes* L.), Pine Marten (*Martes Martes* L.) and Raccoon Dog (*Nyctereutes Procyonoides* Gray) in Clay Plain Landscape, Lithuania . *Acta Zool. Litu.* 12, 362–368. <https://doi.org/10.1080/13921657.2002.10512525>
- Bartolini Lucenti, S., 2019. “Measure my teeth and you’ll know what I ate”: The molar ratio method and an updated interpretation of the diet of *Nyctereutes sinensis* (Carnivora, Canidae). *Acta Zool.* 100, 211–215. <https://doi.org/10.1111/azo.12232>
- Bartolini Lucenti, S., 2017. *Nyctereutes megamastoides* (Canidae, Mammalia) from the early and Middle villafranchian (Late pliocene and early pleistocene) of the Lower Valdarno (Firenze and Pisa, Tuscany, Italy). *Riv. Ital. di Paleontol. e Stratigr.* 123, 211–218. <https://doi.org/10.13130/2039-4942/8327>
- Beisiegel, B.D.M., Ades, C., 2002. The behavior of the bush dog (*Speothos venticus* Lund, 1842) in the field: Review. *Rev. Etol.* 4, 17–23.



- Benammi, M., Aidona, E., Merceron, G., Koufos, G.D., Kostopoulos, D.S., 2020. Magnetostratigraphy and Chronology of the Lower Pleistocene Primate Bearing Dafnero Fossil Site, N. Greece. *Quaternary* 3, 22. <https://doi.org/10.3390/quat3030022>
- Berkovitz, B., Shellis, P., 2018. The teeth of mammalian vertebrates, *The Teeth of Mammalian Vertebrates*. <https://doi.org/10.1016/C2014-0-02212-5>
- Berlioz, É., Kostopoulos, D.S., Blondel, C., Merceron, G., 2018. Feeding ecology of *Eucladoceros tcnoides* as a proxy to track regional environmental variations in Europe during the early Pleistocene. *Comptes Rendus - Palevol* 17, 320–332. <https://doi.org/10.1016/j.crpv.2017.07.002>
- Boev, Z., Koufos, G., 2000. Presence of *Pavo bravardi* (Gervais, 1849) (Aves, Phasianidae) in the Ruscinian locality of Megalo Emvolon, Macedonia, Greece. *Geol. Balc.* 30, 69–74.
- Carbone, C., Mace, G.M., Roberts, S.C., Macdonald, D.W., 1999. Energetic constraints on the diet of terrestrial carnivores. *Nature* 402, 286–288. <https://doi.org/10.1038/46266>
- Castelló, J.R., 2018. *Canids of the World: Wolves, Wild Dogs, Foxes, Jackals, Coyotes and their Relatives*, Reference Reviews. Princeton University Press. <https://doi.org/10.1108/rr-08-2018-0126>
- Christiansen, P., 2007. Comparative bite forces and canine bending strength in feline and sabretooth felids: Implications for predatory ecology. *Zool. J. Linn. Soc.* 151, 423–437. <https://doi.org/10.1111/j.1096-3642.2007.00321.x>
- Christiansen, P., Adolfssen, J.S., 2005. Bite forces, canine strength and skull allometry in carnivores (Mammalia, Carnivora). *J. Zool.* 266, 133–151. <https://doi.org/10.1017/S0952836905006643>
- Christiansen, P., Wroe, S., 2007. Bite Forces and Evolutionary Adaptations to Feeding Ecology in Carnivores Author (s): Per Christiansen and Stephen Wroe Published by : Ecological Society of America content in a trusted digital archive . We use information technology and tools to increa. *Ecol. Soc. Am.* 88, 347–358.
- Clausen, P., Wroe, S., McHenry, C., Moreno, K., Bourke, J., 2008. The vector of jaw muscle force as determined by computer-generated three dimensional simulation: A test of Greaves' model. *J. Biomech.* 41, 3184–3188. <https://doi.org/10.1016/j.jbiomech.2008.08.019>
- Crompton, A.W., 2011. Masticatory motor programs in australian herbivorous mammals: Diprotodontia. *Integr. Comp. Biol.* 51, 271–281. <https://doi.org/10.1093/icb/icr028>
- Curtis, A.A., Santana, S.E., 2018. Jaw-Dropping: Functional Variation in the Digastric Muscle in Bats. *Anat. Rec.* 301, 279–290. <https://doi.org/10.1002/ar.23720>
- Daguenet, T., Sen, S., 2019. Phylogenetic Relationships of *Nyctereutes Temminck*, 1838 (Canidae, Carnivora, Mammalia) from early Pliocene of Calta Turkey. *Geodiversitas* 41, 662–677.
- Damasceno, E.M., Hingst-Zaher, E., Astúa, D., 2013. Bite force and encephalization in the Canidae (Mammalia: Carnivora). *J. Zool.* 290, 246–254. <https://doi.org/10.1111/jzo.12030>
- Davis, D., 1955. Masticatory Apparatus in the Spectacled Bear, *Tremarctos ornatus*. *Fieldiana Zool.* 37, 25–46.

- Davis, J.S., 2014. Functional Morphology of Mastication in Musteloid Carnivorans.
- de Vos, J., Van der Made, J., Athanassiou, A., Lyras, G. a., Sondaar, P.Y., Dermitzakis, M.D., 2002. Preliminary note on the late Pliocene fauna from Vatera (Lesvos, Greece). *Ann. Géologiques des Pays Helléniques* 39, 37–70.
- Drygala, F., Werner, U., Zoller, H., 2014. Diet composition of the invasive raccoon dog (*Nyctereutes procyonoides*) and the native red fox (*Vulpes vulpes*) in north-east Germany. *Hystrix* 24, 190–194. <https://doi.org/10.4404/hystrix-24.2-8867>
- Drygala, F., Zoller, H., Stier, N., Roth, M., 2010. Dispersal of the raccoon dog *Nyctereutes procyonoides* into a newly invaded area in Central Europe. *Wildlife Biol.* 16, 150–161. <https://doi.org/10.2981/08-076>
- Ellis, J.L., Thomason, J., Kebreab, E., Zubair, K., France, J., 2009. Cranial dimensions and forces of biting in the domestic dog. *J. Anat.* 214, 362–373. <https://doi.org/10.1111/j.1469-7580.2008.01042.x>
- Elmeros, M., Mikkelsen, D.M.G., Nørgaard, L.S., Pertoldi, C., Jensen, T.H., Chriél, M., 2018. The diet of feral raccoon dog (*Nyctereutes procyonoides*) and native badger (*Meles meles*) and red fox (*Vulpes vulpes*) in Denmark. *Mammal Res.* 63, 405–413. <https://doi.org/10.1007/s13364-018-0372-2>
- Ewer, R.F., 1973. *The carnivores*. Cornell University Press, Ithaca. <https://doi.org/10.1016/b978-0-08-028002-8.50019-8>
- Farjand, A., Zhang, Z.-Q., Liu, W.-H., Jiao, C.-H., Wang, L.-H., 2020. The evolution of *Nyctereutes* (Carnivora: Canidae) in the Nihewan Basin, Hebei, northern China, *Palaeoworld*. Elsevier B.V. <https://doi.org/10.1016/j.palwor.2020.07.002>
- Ferretti, M.P., 2007. Evolution of bone-cracking adaptations in hyaenids (Mammalia, Carnivora). *Swiss J. Geosci.* 100, 41–52. <https://doi.org/10.1007/s00015-007-1212-6>
- Figueirido, B., Serrano-Alarcón, F.J., Slater, G.J., Palmqvist, P., 2010. Shape at the cross-roads: Homoplasy and history in the evolution of the carnivoran skull towards herbivory. *J. Evol. Biol.* 23, 2579–2594. <https://doi.org/10.1111/j.1420-9101.2010.02117.x>
- Figueirido, B., Soibelzon, L.H., 2010. Inferring palaeoecology in extinct tremarctine bears (Carnivora, Ursidae) using geometric morphometrics. *Lethaia* 43, 209–222. <https://doi.org/10.1111/j.1502-3931.2009.00184.x>
- Finarelli, J.A., 2006. Estimation of Endocranial Volume Through the Use of External Skull Measures in the Carnivora (Mammalia). *J. Mammal.* 87, 1027–1036. <https://doi.org/10.1644/05-mamm-a-430r1.1>
- Flower, L.O.H., 2016. New body mass estimates of British Pleistocene wolves: Palaeoenvironmental implications and competitive interactions. *Quat. Sci. Rev.* 149, 230–247. <https://doi.org/10.1016/j.quascirev.2016.07.023>
- Fountoulis, I., Markopoulou-Diakantoni, A., Mpakopoulou, A., Moraiti, E., Mirkou, M., Saroglou, X., 2001. The presence of marine Pliocene sediments in the Mesohellenic Trough (Pramoritsa banks, Grevena, Greece). *Bull. Geol. Soc. Greece* 2, 603–612.
- Fraser, D., Rybczynski, N., 2014. Complexity of ruminant masticatory evolution. *J. Morphol.* 275, 1093–1102. <https://doi.org/10.1002/jmor.20284>
- Genelly, R.E., 1965. Ecology of The Common Mole-Rat (*Cryptomys hottentotus*) In

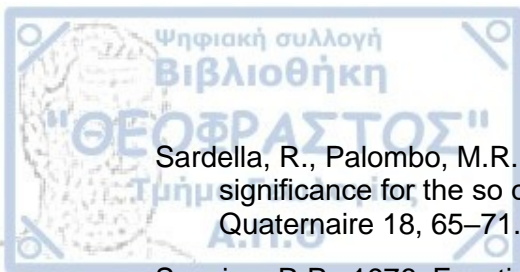
- Rhodesia. *J. Mammal.* 46, 647–665. <https://doi.org/10.2307/1377935>
- Hammer, Ø., Harper, D.A.T., Ryan, P.D., 2001. PAST : Paleontological Statistics Software Package for Education and Data Analysis PAST : PALEONTOLOGICAL STATISTICS SOFTWARE PACKAGE FOR EDUCATION AND DATA ANALYSIS Even a cursory glance at the recent paleontological literature should convince anyone tha. *Palaeontol. Electron.* 4, 1–9.
- Hartstone-Rose, A., Hertzig, I., Dickinson, E., 2019. Bite Force and Masticatory Muscle Architecture Adaptations in the Dietarily Diverse Musteloidea (Carnivora). *Anat. Rec.* 302, 2287–2299. <https://doi.org/10.1002/ar.24233>
- Hartstone-Rose, A., Perry, J.M.G., Morrow, C.J., 2012. Bite Force Estimation and the Fiber Architecture of Felid Masticatory Muscles. *Anat. Rec.* 295, 1336–1351. <https://doi.org/10.1002/ar.22518>
- Hermier, R., Merceron, G., Kostopoulos, D.S., 2020. The emblematic Eurasian Villafranchian antelope *Gazellospira* (Mammalia: Bovidae): New insights from the Lower Pleistocene Dafnero fossil sites (Northern Greece). *Geobios* 61, 11–29. <https://doi.org/10.1016/j.geobios.2020.06.006>
- Herring, S.W., 1993. Functional morphology of mammalian mastication. *Integr. Comp. Biol.* 33, 289–299. <https://doi.org/10.1093/icb/33.3.289>
- Hidaka, S., Matsumoto, M., Hiji, H., Ohsako, S., Nishinakagawa, H., 1998. Morphology and Morphometry of Skulls of Raccoon Dogs, *Nyctereutes procyonoides* and Badgers, *Meles meles*. *J. Vet. Med. Sci.* 60, 161–167. <https://doi.org/10.1292/jvms.60.161>
- Hirasawa, M., Kanda, E., Takatsuki, S., 2006. Seasonal food habits of the raccoon dog at a western suburb of Tokyo. *Mammal Study* 31, 9–14. [https://doi.org/10.3106/1348-6160\(2006\)31\[9:sfhotr\]2.0.co;2](https://doi.org/10.3106/1348-6160(2006)31[9:sfhotr]2.0.co;2)
- Howard, E., de Lahunta, A., 2013. *Miller's Anatomy of the Dog*, 4th ed. Elsevier.
- Ito, K., Endo, H., 2019. The effect of the masticatory muscle physiological cross-sectional area on the structure of the temporomandibular joint in Carnivora. *J. Vet. Med. Sci.* 81, 389–396. <https://doi.org/10.1292/jvms.18-0611>
- Ito, K., Endo, H., 2016. Comparative Study of Physiological Cross-Sectional Area of Masticatory Muscles among Species of Carnivora. *Mammal Study* 41, 181–190. <https://doi.org/10.3106/041.041.0403>
- Kargopoulos, N., 2019. Carnivoran Dietary Adaptations A Multiproxy Study on the Feeding Ecology of the Fossil Carnivorans of Greece. Master Thesis, Department of Geology and Geoenvironment, National and Kapodistrian University of Athens, 214 pp.
- Kauhala, Kaarina, Kowalczyk, R., 2012. The raccoon dog (*Nyctereutes procyonoides*) in the community of medium-sized carnivores in Europe: Its adaptations, impact on native fauna management of the population, Carnivores: Species, conservation, and management. Nova Publishers.
- Kauhala, K., Kowalczyk, R., 2011. Invasion of the raccoon dog *Nyctereutes procyonoides* in Europe: History of colonization, features behind its success, and threats to native fauna. *Curr. Zool.* 57, 584–598. <https://doi.org/10.1093/czoolo/57.5.584>
- Kauhala, K., Viranta, S., Kishimoto, M., Helle, E., Obara, I., 1998. Skull and tooth morphology of Finnish and Japanese raccoon dogs. *Ann. Zool. Fennici* 35, 1–16.



- Kim, S.I., Suzuki, S., Oh, I., Koyabu, D., Oshida, T., Lee, H., Min, M.S., Kimura, J., 2012. Sexual dimorphism of craniodental morphology in the raccoon dog *Nyctereutes procyonoides* from South Korea. *J. Vet. Med. Sci.* 74, 1609–1616. <https://doi.org/10.1292/jvms.12-0281>
- Klingenberg, C.P., 2011. MorphoJ: An integrated software package for geometric morphometrics. *Mol. Ecol. Resour.* 11, 353–357. <https://doi.org/10.1111/j.1755-0998.2010.02924.x>
- Koenigswald, W. Von, Holbrook, L.T., Rose, K.D., 2011. Diversity and evolution of hunter-schreger band configuration in tooth enamel of perissodactyl mammals. *Acta Palaeontol. Pol.* 56, 11–32. <https://doi.org/10.4202/app.2010.0021>
- Koenigswald, W. Von, Sander, P.M., 1997. Tooth enamel microstructure, Tooth enamel microstructure. CRC Press.
- Kostopoulos, D.S., Aidona, E., Benammi, M., Gkeme, A., 2019. The Lower Pleistocene Primate-Bearing Fossil Site of Dafnero (W . Macedonia , Greece): New Data from classic and Innovative Approaches.
- Kostopoulos, D.S., Guy, F., Kynigopoulou, Z., Koufos, G.D., Valentin, X., Merceron, G., 2018. A 2Ma old baboon-like monkey from Northern Greece and new evidence to support the *Paradolichopithecus* – *Procynocephalus* synonymy (Primates: Cercopithecidae). *J. Hum. Evol.* 121, 178–192. <https://doi.org/10.1016/j.jhevol.2018.02.012>
- Koufos, G.D., 2013. Neogene Mammal Biostratigraphy and Chronology of Greece, in: Wang, X., Flynn, L.J., Fortelius, M. (Eds.), *Fossil Mammals of Asia*. Columbia University Press, pp. 595–626. <https://doi.org/10.7312/columbia/9780231150125.003.0028>
- Koufos, G.D., 1997. The canids *Eucyon* and *Nyctereutes* from the Ruscinian of Macedonia, Greece. *Paleontol. i Evol.* 30–31, 39–48.
- Koufos, G.D., 1993. Late Pliocene carnivores from western Macedonia (Greece). *Paläontologische Zeitschrift* 67, 357–376. <https://doi.org/10.1007/BF02990288>
- Koufos, G.D., Kostopoulos, D.S., 1997. Biochronology and succession of the Plio-Pleistocene macromammalian localities of Greece. *Proc. Biochrom* 97, Mém. Trav. E.P.H.E., Inst. Montpellier 21, 619–634.
- Koufos, G. D., Kostopoulos, D.S., Koliadimou, K.K., 1991. Un nouveau gisement de mammiferes dans le Villafranchien de Macedoine occidentale (Grece). *Comptes Rendus - Acad. des Sci. Ser. II* 313, 831–836.
- Koufos, G.D., Kostopoulos, D.S., Merceron, G., 2020. The saber-toothed cat *Homotherium latidens* (Owen, 1846) from the lower pleistocene locality Dafnero, western Macedonia, Greece. *Geodiversitas* 42, 139–149. <https://doi.org/10.5252/geodiversitas2020v42a10>
- Koufos, George D., Syrides, G.E., Koliadimou, K.K., 1991. A pliocene primate from Macedonia (Greece). *J. Hum. Evol.* 21, 283–294. [https://doi.org/10.1016/0047-2484\(91\)90109-9](https://doi.org/10.1016/0047-2484(91)90109-9)
- Kowalczyk, R., Zalewski, A., 2011. Adaptation to cold and predation — shelter use by invasive raccoon dogs *Nyctereutes procyonoides* in Bia ł owie ż a Primeval Forest (Poland) 57, 133–142. <https://doi.org/10.1007/s10344-010-0406-9>
- Kowalczyk, R., Zalewski, A., Jędrzejewska, B., Ansorge, H., Bunevich, A.N., 2009. Reproduction and mortality of invasive raccoon dogs (*Nyctereutes procyonoides*)

- in the Biatowieża Primeval Forest (eastern Poland). *Ann. Zool. Fennici* 46, 291–301. <https://doi.org/10.5735/086.046.0406>
- Lucenti, S.B., 2018. *Nyctereutes Temminck, 1838 (Mammalia, Canidae): a revision of the genus across the Old World during Plio-Pleistocene times*. *Foss. - Reports Palaeontol.* 1838, 7–10. <https://doi.org/10.32774/fosreppal.20.1810.010710>
- Lucenti, S.B., 2017. *Nyctereutes megamastoides (Canidae, Mammalia) from the early and Middle villafranchian (Late pliocene and early pleistocene) of the Lower Valdarno (Firenze and Pisa, Tuscany, Italy)*. *Riv. Ital. di Paleontol. e Stratigr.* 123, 211–218. <https://doi.org/10.13130/2039-4942/8327>
- Lucenti, S.B., Rook, L., Morales, J., 2018. *Nyctereutes (Mammalia, carnivora, canidae) from layna and the eurasian raccoon-dogs: An updated revision*. *Riv. Ital. di Paleontol. e Stratigr.* 124, 597–616. <https://doi.org/10.13130/2039-4942/10739>
- Lyras, G. a., van der Geer, A. a. E., 2007. *The Late Pliocene vertebrate fauna of Vatera (Lesvos Island, Greece)*. *Cranium* 24, 11–24.
- Martin, M.L., Travouillon, K.J., Fleming, P.A., Warburton, N.M., 2020. *Review of the methods used for calculating physiological cross-sectional area (PCSA) for ecological questions*. *J. Morphol.* 281, 778–789. <https://doi.org/10.1002/jmor.21139>
- Matsuo, R., Ochiai, K., 2009. *Dietary overlap among two introduced and One native sympatric carnivore species, the raccoon, the masked palm civet, and the raccoon dog, in chiba prefecture, Japan*. *Mammal Study* 34, 187–194. <https://doi.org/10.3106/041.034.0402>
- Meachen-Samuels, J., van Valkenburgh, B., 2009. *Craniodental indicators of prey size preference in the Felidae*. *Biol. J. Linn. Soc.* 96, 784–799. <https://doi.org/10.1002/jmor.10712>
- Meloro, C., 2011. *Locomotor adaptations in plio-pleistocene large carnivores from the italian peninsula: Palaeoecological implications*. *Curr. Zool.* 57, 269–283. <https://doi.org/10.1093/czoolo/57.3.269>
- Meloro, C., 2008. *Plio-Pleistocene large carnivores from the Italian peninsula: functional morphology and macroecology*.
- Miller, E., Fowler, M., 2015. *Fowler's Zoo and Wildl Animal Medicine*.
- Monguillon, A., Spassov, N., Argant, A., Kauhala, K., Viranta, S., 2004. *Nyctereutes vulpinus comb. et stat. nov. (Mammalia, Carnivora, Canidae) du Pliocène terminal de Saint-Vallier (Drôme, France)*. *Geobios* 37, S183–S188. [https://doi.org/10.1016/S0016-6995\(04\)80014-7](https://doi.org/10.1016/S0016-6995(04)80014-7)
- Mulder, J., 2012. *A review of the ecology of the raccoon dog (Nyctereutes procyonoides) in Europe*. *Lutra* 55, 101–127.
- Naderi, M., Çoban, E., Kusak, J., Kemahli Aytekin, M.Ç., Chynoweth, M., Ağirkaya, İ.K., Güven, N., Çoban, A., Şekercioğlu, Ç.H., 2020. *The first record of raccoon dog (Nyctereutes procyonoides) in Turkey*. *Turkish J. Zool.* 44, 209–213. <https://doi.org/10.3906/zoo-1910-29>
- Natchev, N., 2016. *Newly registered tracks of Raccoon dogs (Nyctereutes procyonoides) indicate the presence of resident population in the region of Bolata dere (NE Bulgaria)*. *ZooNotes* 3, 1–3.

- Nowak, R.M., 2005. Walker's Carnivores of the World. John Hopkins University Press.
- Palmqvist, P., Arribas, A., Martínez-Navarro, B., 2007. Ecomorphological study of large canids from the lower Pleistocene of southeastern Spain. *Lethaia* 32, 75–88. <https://doi.org/10.1111/j.1502-3931.1999.tb00583.x>
- Penrose, F., 2018. Cranial morphology and masticatory biomechanics in the Canidae. University of Liverpool 372 pp.
- Penrose, F., Cox, P., Kemp, G., Jeffery, N., 2020. Functional morphology of the jaw adductor muscles in the Canidae. *Anat. Rec.* 303, 2878–2903. <https://doi.org/10.1002/ar.24391>
- Penrose, F., Kemp, G.J., Jeffery, N., 2016. Scaling and Accommodation of Jaw Adductor Muscles in Canidae. *Anat. Rec.* 299, 951–966. <https://doi.org/10.1002/ar.23355>
- Perry, J.M.G., Prufrock, K.A., 2018. Muscle Functional Morphology in Paleobiology: The Past, Present, and Future of "Paleomyology." *Anat. Rec.* 301, 538–555. <https://doi.org/10.1002/ar.23772>
- Popowics, T.E., Herring, S.W., 2006. Teeth, jaws and muscles in mammalian mastication. *Feed. Domest. Vertebr.* 61–83. <https://doi.org/10.1079/9781845930639.0061>
- Prevosti, F.J., 2010. Phylogeny of the large extinct South American Canids (Mammalia, Carnivora, Canidae) using a "total evidence" approach. *Cladistics* 26, 456–481. <https://doi.org/10.1111/j.1096-0031.2009.00298.x>
- Price, S.A., Hopkins, S.S.B., Smith, K.K., Roth, V.L., 2012. Tempo of trophic evolution and its impact on mammalian diversification. *Proc. Natl. Acad. Sci. U. S. A.* 109, 7008–7012. <https://doi.org/10.1073/pnas.1117133109>
- Radinsky, L.B., 1981. Evolution of skull shape in carnivores: 2. Additional modern carnivores. *Biol. J. Linn. Soc.* 16, 337–355. <https://doi.org/10.1111/j.1095-8312.1981.tb01657.x>
- Rocha, V.J., Aguiar, L.M., Silva-Pereira, J.E., Moro-Rios, R.F., Passos, F.C., 2008. Feeding habits of the crab-eating fox, *Cerdocyon thous* (Carnivora: Canidae), in a mosaic area with native and exotic vegetation in Southern Brazil. *Rev. Bras. Zool.* 25, 594–600. <https://doi.org/10.1590/s0101-81752008000400003>
- Rook, L., Lucenti, S.B., Bukhsianidze, M., Lordkipanidze, D., 2017. The Kvabebi Canidae record revisited (late Pliocene, Sighnaghi, eastern Georgia). *J. Paleontol.* 91, 1258–1271. <https://doi.org/10.1017/jpa.2017.73>
- Ruiz-Ramoni, D., Juan Prevosti, F., Lucenti, S.B., Montellano-Ballesteros, M., Carreño, A.L., 2020. The Pliocene canid *Cerdocyon avius* was not the type of fox that we thought. *J. Vertebr. Paleontol.* 40, 1–9. <https://doi.org/10.1080/02724634.2020.1774889>
- Sacco, T., Van Valkenburgh, B., 2004. Ecomorphological indicators of feeding behaviour in the bears (Carnivora: Ursidae). *J. Zool.* 263, 41–54. <https://doi.org/10.1017/S0952836904004856>
- Sakamoto, M., Lloyd, G.T., Benton, M.J., 2010. Phylogenetically structured variance in felid bite force: The role of phylogeny in the evolution of biting performance. *J. Evol. Biol.* 23, 463–478. <https://doi.org/10.1111/j.1420-9101.2009.01922.x>



- Sardella, R., Palombo, M.R., 2007. The Pliocene-Pleistocene boundary: Which significance for the so called "Wolf Event"? Evidences from Western Europe. *Quaternaire* 18, 65–71. <https://doi.org/10.4000/quaternaire.969>
- Scapino, R.P., 1976. Function of the digastric muscle in carnivores. *J. Morphol.* 150, 843–859. <https://doi.org/10.1002/jmor.1051500405>
- Schneider, C.A., Rasband, W.S., Eliceiri, K., 2010. NIH Image to ImageJ: 25 years of Image Analysis. *Fundam. Digit. Imaging Med.* 9, 671–675. https://doi.org/10.1007/978-1-84882-087-6_9
- Schoener, T., 1969. Models of Optimal Size for Solitary Predators. *Am. Nat.* 103, 277–313.
- Sheldon, W.J., 1992. *WILD DOGS The Natural History of the Nondomestic Canidae*, ACADEMIC PRESS, INC. <https://doi.org/10.2307/40222782>
- Slater, G.J., Dumont, E.R., Van Valkenburgh, B., 2009. Implications of predatory specialization for cranial form and function in canids. *J. Zool.* 278, 181–188. <https://doi.org/10.1111/j.1469-7998.2009.00567.x>
- Sotnikova, M., Rook, L., 2010. Dispersal of the Canini (Mammalia, Canidae: Caninae) across Eurasia during the Late Miocene to Early Pleistocene. *Quat. Int.* 212, 86–97. <https://doi.org/10.1016/j.quaint.2009.06.008>
- Spassov, N., 2003. The Plio-Pleistocene vertebrate fauna in South-Eastern Europe and the megafaunal migratory waves from the east to Europe. *Rev. paléobiologie* 22, 197–229.
- Spassov, N., 1997. VILAFRANCHIAN SUCCESSION OF MAMMALIAN MEGAFANAS FROM BULGARIA AND THE BIOZONATION OF SOUTH-EAST EUROPE.
- Stefen, C., 1999. Enamel microstructure of Recent and fossil Canidae (Carnivora: Mammalia). *J. Vertebr. Paleontol.* 19, 576–587. <https://doi.org/10.1080/02724634.1999.10011166>
- Sutor, A., Kauhala, K., Ansorge, H., 2010. Diet of the raccoon dog *Nyctereutes procyonoides* -A canid with an opportunistic foraging strategy. *Acta Theriol. (Warsz)*. 55, 165–176. <https://doi.org/10.4098/j.at.0001-7051.035.2009>
- Sutor, A., Schwarz, S., Conraths, F.J., 2014. The biological potential of the raccoon dog (*Nyctereutes procyonoides*, Gray 1834) as an invasive species in Europe- new risks for disease spread? *Acta Theriol. (Warsz)*. 59, 49–59. <https://doi.org/10.1007/s13364-013-0138-9>
- Tedford, R.H., Qiu, Z., 1991. Pliocene *Nyctereutes* (Carnivora : Canidae) from Yushe, Shanxi, with comments on chinese fossil racoon-dogs. *Vertebr. Palasiat.* 29, 176-189.
- Tedford, R.H., Wang, X., Taylor, B.E., 2009. Phylogenetic Systematics of the North American Fossil Caninae (Carnivora: Canidae). *Bull. Am. Museum Nat. Hist.* 325, 1–218. <https://doi.org/10.1206/574.1>
- Thomason, J.J., 1991. Cranial strength in relation to estimated biting forces in some mammals. *Can. J. Zool.* 69, 2326–2333. <https://doi.org/10.1139/z91-327>
- Tseng, Z.J., 2012. Connecting Hunter-Schreger Band microstructure to enamel microwear features: New insights from durophagous carnivores. *Acta Palaeontol. Pol.* 57, 473–484. <https://doi.org/10.4202/app.2011.0027>



- Tseng, Z.J., Flynn, J.J., 2015. Are cranial biomechanical simulation data linked to known diets in extant taxa? A method for applying diet-biomechanics linkage models to infer feeding capability of extinct species. *PLoS One* 10, e0124020. <https://doi.org/10.1371/journal.pone.0124020>
- Turnbull, D.W., 1970. Mammalian masticatory apparatus. *Fieldiana Geol.* 18, 149–356.
- Turner, A., Antón, M., 1997. The Big Cats and Their Fossil Relatives: An Illustrated Guide to Their Evolution and Natural History, in: *BioScience*. Columbia University Press, pp. 614–616. <https://doi.org/10.2307/1313168>
- Van Valkenburgh, B., 2007. Déjà vu: The evolution of feeding morphologies in the Carnivora. *Integr. Comp. Biol.* 47, 147–163. <https://doi.org/10.1093/icb/icm016>
- Van Valkenburgh, B., Koepfli, K.-P., 1993. Cranial and dental adaptations to predation in canids. *Symp. Zool. Soc. London* 65, 15–37.
- Van Valkenburgh, B., Sacco, T., Wang, X., 2003. Pack hunting in Miocene borophagine dogs: Evidence from craniodental morphology and body size. *Bull. Am. Museum Nat. Hist.* 279, 147–162. [https://doi.org/10.1206/0003-0090\(2003\)279<0147:C>2.0.CO;2](https://doi.org/10.1206/0003-0090(2003)279<0147:C>2.0.CO;2)
- Van Valkenburgh, B., Wayne, R.K., 1994. Shape divergence associated with size convergence in sympatric East African jackals. *Ecology* 75, 1567–1581. <https://doi.org/10.2307/1939618>
- Wall, C.E., Smith, K.K., 2001. Ingestion in Mammals. *Encycl. Life Sci.*, London Macmillan Publisher, 1-6. <https://doi.org/10.1038/npg.els.0001837>
- Ward, G. Oscar, W.-H.D.H., 1959. ECOLOGICAL STUDIES OF JAPANESE RACON DOGS, NYCTEREUTES PROCYONOIDES VIVERRINUS. *J. Mammal.* 40, 521–531.
- Ward, O.G., Wurster-Hill, D.H., 1990. *Nyctereutes procyonoides*. *Mamm. Species* 1–5. <https://doi.org/10.2307/3504213>
- Wayne, R.K., Ostrander, E.A., 2007. Lessons learned from the dog genome. *Trends Genet.* 23, 557–567. <https://doi.org/10.1016/j.tig.2007.08.013>
- Wroe, S., McHenry, C., Thomason, J., 2005. Bite club: Comparative bite force in big biting mammals and the prediction of predatory behaviour in fossil taxa. *Proc. R. Soc. B Biol. Sci.* 272, 619–625. <https://doi.org/10.1098/rspb.2004.2986>
- Zrzavý, J., Duda, P., Robovský, J., Okřinová, I., Pavelková Řičánková, V., 2018. Phylogeny of the Caninae (Carnivora): Combining morphology, behaviour, genes and fossils. *Zool. Scr.* 47, 373–389. <https://doi.org/10.1111/zsc.12293>

Table 20. Raw data of skull Measurements of *Nyctereutes*. All measurements were taken digitally using ImageJ.

CBL	RL	NH	NW	POC	IOD	PL	PW	RWC	RWM	MW	MSW	ZL	ZH	ZFW	ZFL	CB	OD	SKH	
109.74	49.93	11.39	11.80	22.06	30.69	57.10	35.41	23.83	36.23	31.97	69.03	3.61	55.05	9.89	24.14	32.79	34.04	17.69	45.48
112.61	51.87	11.30	10.41	19.20	28.23	64.53	29.49	22.72	33.92	33.80	71.05	2.92	49.77	11.22	22.07	32.34	37.57	17.50	40.02
110.74						59.51	24.81	23.65	31.53			3.65	38.00		21.19	29.28			
142.02	67.70	15.15	14.16	35.75	55.00	79.80	42.49	24.91	40.38	44.80	87.26	7.14	44.46	10.63	19.86	59.05	49.15	17.47	43.34
125.67	62.09	13.66	8.47	34.46	51.45	71.95	40.98	23.11	41.67	39.63	82.33	4.96	59.88	11.44	27.76	31.99	29.70	17.68	32.21
	77.43			33.88	39.17	89.27		25.41										20.96	46.02
143.19	56.05			24.09	27.75	73.39	36.84	20.29	36.23			6.90	44.58	9.25	21.26	39.63	28.46	18.51	55.19
	64.18			32.69	31.01	83.19	23.74	18.36	42.86	50.21								20.79	46.05
133.69	58.68			34.35	44.25	66.35	47.26	21.37	41.64	36.61	78.91	6.34	52.45	12.17	20.69	34.83	26.75	17.12	43.35
139.87	56.44			29.95	35.41	70.69	25.98	21.39	37.68	46.06	65.32		50.00	10.12	25.33	33.11	27.26	17.96	37.43
																			35.20
129.70	57.33			31.48	45.81	64.90	23.20	17.11	35.91		82.10	6.51	49.90	9.88	28.45	23.13			42.50
																	23.30		43.00
				31.86		67.40	16.80												36.60
160.2	54.5		12.4	29.98	46.6	64.7		21.4	37.2	37.4							27.4	24.3	54.9
145.9				33.91	47.6					37.6	86.2		53.1	11	27.8	34.6	25.8	20	53.4
143.20										52.20	77.60						29.80		

	Genus	Species	Author	SKL	BCL	BCW
Bulgaria -1	Nyctereutes	procyonoides	MNHS (Bulgaria)	124.11	147.50	42.65
Bulgaria -2	Nyctereutes	procyonoides	MNHS (Bulgaria)	127.56	48.82	43.65
RV 8003	Nyctereutes	procyonoides	Farjand et al.. 2020	117.94		
DFN3-154	Nyctereutes		LGPU	163.61	71.21	55.70
DFN3-155	Nyctereutes		LGPU	147.23	58.33	57.01
MNCN63662	Nyctereutes	donnezani	Bartolini-Lucenti. 2018	175.94	61.80	59.42
MNH.N.F.ACA292	Nyctereutes	donnezani	Daguinet T. & Sen S..	149.04	42.04	47.72
MNH.N.F.ACA291	Nyctereutes	donnezani	Daguinet T. & Sen S..	166.16	69.15	53.99
DFN-17	Nyctereutes	megamastoides	Koufos. 1993	136.89	55.54	52.50
DFN-20	Nyctereutes	megamastoides	Koufos. 1993	142.80	57.93	50.94
MG 29-2013/455	Nyctereutes	megamastoides	Rook et al.. 2017			42.20
MG 29-2013/457	Nyctereutes	megamastoides	Rook et al.. 2017	137.60	63.60	62.90
MG 29-2013/567	Nyctereutes	megamastoides	Rook et al.. 2017		66.30	46.90
MG 29-2013/581	Nyctereutes	megamastoides	Rook et al.. 2017	129.20	58.00	49.10
MEL-1	Nyctereutes	tingi	Koufos. 1993	171.4	66.3	52.7
MEL-2	Nyctereutes	tingi	Koufos. 1993	151.1	62.8	54.3
DIK-31-1	Nyctereutes	lockwoodi	Geraads et al.. 2010			

Table 21. Raw measurements of Nyctereutes upper dentition. All measurements were taken digitally using ImageJ.

DIK-31-1	
Nyctereutes	
lockwoodi	
Geraads et al.. 2010	
4.00	
2.70	
6.70	
2.80	
7.50	
3.50	
13.60	
6.00	
9.20	
13.10	

THP 18685	RV 41052	C/C. 1275	SV.96.185	SV.99.1144	SV.99.141	Puebla	Saint Vallier
Nyctereutes sinensis	Nyctereutes sinensis	Nyctereutes sinensis	Nyctereutes vulpinus	Nyctereutes vulpinus	Nyctereutes vulpinus	Nyctereutes vulpinus	Nyctereutes vulpinus
Farjand et al.. 2020	Farjand et al.. 2020	Farjand et al.. 2020	Argant. 2004	Argant. 2004	Argant. 2004	Koufos. 1993	Monguillon et al.. 2004
						7.40	6.10
						4.30	4.10
						4.60	4.10
							2.70
					7.90	7.50	7.30
					3.10	3.00	2.90
	13.40					8.80	8.50
	5.50					3.30	3.20
24.10	21.40	14.20			13.20	13.63	14.80
12.00	10.50	7.30			6.50	6.90	6.60
14.90	12.60	10.20	11.00	10.50	10.30	10.77	10.60
17.60	16.00	11.70	13.20	13.20		13.85	11.70
8.60	6.40	6.90	6.80	6.80		6.70	6.60
10.60	10.50	8.40	8.00	8.00		9.52	7.90

V 26277	F: AM 96757	THP 10299	MEL-1	MEL-2	RV 30007	RV 30015	RV 30018
Nyctereutes tingi	Nyctereutes tingi	Nyctereutes tingi	Nyctereutes tingi	Nyctereutes tingi	Nyctereutes sinensis	Nyctereutes sinensis	Nyctereutes sinensis
Farjand et al.. 2020	Farjand et al.. 2020	Tedford & Qiu. 1991	Koufos. 1993	Koufos. 1993	Farjand et al.. 2020	Farjand et al.. 2020	Farjand et al.. 2020
8.60	8.60	6.60	6.58	6.58	6.30	6.30	
5.50	5.50	4.30	3.60	3.60	4.20	4.20	
4.80	4.70	4.60	7.71	7.71			
3.10	3.00	2.60	2.60	2.60			
8.90	8.70	7.00			10.90	10.90	
3.50	3.60	3.40			4.40	4.40	
9.20	10.00	8.90			8.60	13.20	
4.20	3.90	3.90			3.70	5.00	
15.60	16.50	13.30	15.11		14.80	19.90	21.30
7.50	7.90	7.10	7.63		7.00	10.70	9.80
12.10	12.40	9.80	11.70	10.90	10.70	13.30	15.00
13.80	14.70	12.50	14.22	13.45	12.40	15.60	16.30
8.00	8.40	6.80	7.86	6.61	7.50	7.50	8.10
9.50	9.70	8.60	10.35	9.35	9.20	10.00	11.00

MG 29-2013/457 (K220)	MG 29-2013/567 (K4173)	MG 29-2013/581 (K219)	MG 29-2013/456 (K217)	MG 29-2013/573 (K233)	Chine
Nyctereutes	Nyctereutes	Nyctereutes	Nyctereutes	Nyctereutes	Nyctereutes
megamastoides	megamastoides	megamastoides	megamastoides	megamastoides	tingji
Rook et al.. 2017	Rook et al.. 2017	Rook et al.. 2017	Rook et al.. 2017	Rook et al.. 2017	Monguillon et al.. 2004
5.40			5.70	6.10	7.50
3.70			3.70		4.90
			4.70	4.50	4.70
			2.50		2.80
			6.90	7.20	7.90
			2.70		3.40
			7.50	8.10	9.30
			3.10		3.90
			14.00		14.60
			6.80		7.50
			11.10	10.90	10.90
			12.90		13.70
			7.70	7.70	7.50
			9.80		9.40

DFN-17	DFN-20	IGF 10131_2	IGF 10131_1	MNCN39921	MG 29-2013/455 (K234)
Nyctereutes	Nyctereutes	Nyctereutes	Nyctereutes	Nyctereutes	Nyctereutes
megamastoides	megamastoides	megamastoides	megamastoides	cf. megamastoides	megamastoides
Koufos. 1993	Koufos. 1993	Bartolini-Lucenti. 2018	Bartolini-Lucenti. 2018	Bartolini-Lucenti. 2018	Rook et al.. 2017
5.00	5.63				
3.50	3.47				
4.20	4.23				
2.40	2.85				
5.90	5.98		6.90		
2.50	2.54		3.00		
6.70	7.00		7.50		
3.00	3.00		3.60		
11.50	11.85		12.90	12.10	11.90
5.40	5.69		6.40	6.20	6.30
10.30	9.81	10.60		10.60	11.00
11.40	12.06	12.30		11.90	12.10
7.50	6.89				7.00
8.60	7.50				8.00

Layna	Volax	Villaroya Spa 189	Villaroya V-113	Villaroya V-115	Villaroya i	Villaroya d
Nyctereutes	Nyctereutes	Nyctereutes	Nyctereutes	Nyctereutes	Nyctereutes	Nyctereutes
megamastoides	megamastoides	megamastoides	megamastoides	megamastoides	megamastoides	megamastoides
Koufos. 1993	Koufos. 1993	Soria & Aguirre. 1976				
			5.80			
			4.00			
	4.00		3.90			
	3.20		2.40			
	7.00		6.40	6.60		
	3.30		2.50	2.70		
	8.50	7.45	7.10	7.90		
	3.50	3.20	3.00	3.30		
13.03	15.40	13.35	13.50	13.00	13.40	13.30
6.96	6.60	5.60	6.40	5.70	6.30	6.10
10.50	11.70	10.60		10.40	9.40	9.30
13.63	13.50	11.60		11.80	11.30	11.30
7.75	7.50	6.90		6.70	6.50	6.90
10.10	9.40	8.70		8.70	7.90	7.90

MNCN62493	MNCN39920	MNCN63662	MNH.F.ACA292	MNH.F.ACA291	PERRIER
Nyctereutes donnezani	Nyctereutes donnezani	Nyctereutes donnezani	Nyctereutes donnezani	Nyctereutes donnezani	Nyctereutes megamastoides
Bartolini-Lucenti. 2018	Bartolini-Lucenti. 2018	Bartolini-Lucenti. 2018	Daguenet T. & Sen S.. 2019	Daguenet T. & Sen S.. 2019	Ginsburg. 1998
		7.20			
		4.60			
		3.80			
		2.50			
		7.80			6.80
		2.80			3.00
					8.60
					3.30
		13.30	14.15	14.37	12.80
			6.94	6.68	6.40
	9.70	10.70	11.34	11.57	10.90
	11.20	11.20	12.45	12.67	11.90
6.80	6.40	7.10	7.84	7.36	7.50
8.10	8.30	9.00	10.73	10.22	8.80

MNCN62482	MNCN62478	MNCN62479	MNCN62481	MNCN62491	MNCN62492
Nyctereutes donnezani	Nyctereutes donnezani	Nyctereutes donnezani	Nyctereutes donnezani	Nyctereutes donnezani	Nyctereutes donnezani
Bartolini-Lucenti. 2018	Bartolini-Lucenti. 2018	Bartolini-Lucenti. 2018	Bartolini-Lucenti. 2018	Bartolini-Lucenti. 2018	Bartolini-Lucenti. 2018
6.50					
2.90					
	12.80		12.80		
	7.40	6.10	7.00		
				9.70	9.95
					10.50

Bulgaria 2	RV 8003	OV 846	DFN3-154	DFN3-155	DFN3-8	Perpignan	MNCN62494
Nyctereutes	Nyctereutes	Nyctereutes	Nyctereutes	Nyctereutes	Nyctereutes	Nyctereutes	Nyctereutes
procyonoïdes	procyonoïdes	procyonoïdes				donnezani	donnezani
MNHS (Bulgaria)	Farjand et al.. 2020	Farjand et al.. 2020	LGPU T	LGPU T	LGPU T	Monguillon et al.. 2004	Bartolini-Lucenti. 2018
5.33	6.90	7.16			6.50	6.40	
3.97	3.70	4.25			3.90	4.30	
	3.50				4.50		
	2.70				2.70		
5.38	6.20		3.94		7.41		
2.19	2.90		2.43		2.89		
6.30	7.00	8.85	7.19		8.83		
2.87	3.10	3.23	2.88		3.50		
10.60	11.30	14.90	12.81		14.65		
5.32	6.20	7.10	6.12		6.90		
8.80	8.10	10.85	10.08		11.40		
9.90	9.00	11.70	11.20		12.63		
4.77	5.40	6.86	6.70		6.87		
6.42	6.30	7.83	8.25		7.95		

Specimen	Bulgaria 1
Genus	Nyctereutes
Species	procyonoides
Author	MNHS (Bulgaria)
C1L	5.48
C1W	4.03
P1L	
P1W	
P2L	5.74
P2W	2.95
P3L	6.38
P3W	3.12
P4L	9.98
P4W	6.05
M1L	8.27
M1W	9.87
M2L	5.36
M2W	7.69

Table 22. Raw measurements of Nyctereutes lower dentition. All measurements were taken digitally using ImageJ.

Zhoukoudian China	SV.99.686	SV.98.799	Puebla	Saint Vallier
Nyctereutes sinensis	Nyctereutes vulpinus	Nyctereutes vulpinus	Nyctereutes vulpinus	Nyctereutes vulpinus
Jin et al.. 1984	Argant. 2004	Argant. 2004	Koufos. 1993	Monguillon et al.. 2004
				6.1
				4.2
	7.5	7.4	7.4	6.9
		3	3	3
	9.1	9.2		8.5
	3.4	3.4		3.3
10	10	10.1	9.7	9.7
5	4.3	4.1	4.3	4.2
16.3	15.9	16		15.9
7	6.5	6.4		6.4
7.9	8.4	8.6	8.4	8.4
5.8	6	5.6	6.8	5.9

Chine	F: AM 97029	F: AM 97030	F: AM 96799	THP 22729	IVPP YS 131
Nyctereutes	Nyctereutes	Nyctereutes	Nyctereutes	Nyctereutes	Nyctereutes
tingi	tingi	tingi	tingi	tingi	tingi
Monguillon et al., 2004	Tedford & Qiu, 1991				
8.8	9.6	8.7	8	8.7	8
5.7	6	5.7	5.6	5.3	3.9
8.7	9.2	8.2	8.5	8.3	10.5
3.8	4.1	3.8	3.6	3.9	4.3
9.8	10.6	9.6	9.4	9.5	12
4.1	4.3	3.9	3.8	4.2	5.5
11.2	12.1	11.5	10.5	10.8	19.2
5.2	5.6	5.2	4.9	5.2	7.9
18.2	19.3	17.8	17.6	18.8	
7.6	7.9	7.6	7.3	8.2	
9.3		9.6	9.1	10	9.7
6.8		7.2	6.6	6.3	7.2

MNCN39918	MG 29-2013/588 (K221)	MG 29-2013/591 (K214)	MG 29-2013/592 (K4177)	MG 29-2013/820	MG 29-2013/606
Nyctereutes	Nyctereutes	Nyctereutes	Nyctereutes	Nyctereutes	Nyctereutes
cf. megamastoides	megamastoides	megamastoides	megamastoides	megamastoides	megamastoides
Bartolini-Lucenti. 2018	Rook et al.. 2017	Rook et al.. 2017	Rook et al.. 2017	Rook et al.. 2017	Rook et al.. 2017
	4.5				7.1
	3.6				4
				7.2	
				3	
				8.1	
				3.1	
				9.1	
				4.2	
15.1	14.9	14.8	14.8	15.9	
6.4	5.8	6.7	6.6	7.7	
		9.5	8.4	9.2	
8.9	7.9			8.7	
6.3	5.8			7.5	

MNCN70007	PERRIER	Layna	Villaroya V-118	Villaroya V-112	DFN-23
Nyctereutes	Nyctereutes	Nyctereutes	Nyctereutes	Nyctereutes	Nyctereutes
donnezani	megamastoides	megamastoides	megamastoides	megamastoides	megamastoides
Bartolini-Lucenti. 2018	Ginsburrig. 1998	Koufos. 1993	Soria & Aguirre. 1976	Soria & Aguirre. 1976	Koufos. 1997
					5.1
					3.5
	6.5	6.8	6.7	6	6.4
	2.8	2.9	3	2.7	3
	7.8	7.5	7.6	7.2	7.4
	2.9	3	3.1	3	3.2
	9.1	9.26	9.1	7	8.3
	3.7	3.9	3.8	3.9	4
	14.3		14.6	14.5	
	5.8		6.3	6	
	8.9	8.16	8.4	8.5	8.7
	5	6.06	5.6	5.9	6.7

MNCN62504	MNCN62495	MNCN62497	MNCN62651	MNCN70008	MNCN70009
Nyctereutes donnezani	Nyctereutes donnezani	Nyctereutes donnezani	Nyctereutes donnezani	Nyctereutes donnezani	Nyctereutes donnezani
Bartolini-Lucenti. 2018	Bartolini-Lucenti. 2018	Bartolini-Lucenti. 2018	Bartolini-Lucenti. 2018	Bartolini-Lucenti. 2018	Bartolini-Lucenti. 2018
6.8	6.8	6.8	6.7	6.6	6.1
4.3	4.3	4.3	4.5	4.49	4.4
9					
3.5					
13.6					
5.2					

ACA-299	ACA-903	ACA-294	ACA-904	MNCN39916	MNCN39917	MNCN39919
Nyctereutes	Nyctereutes	Nyctereutes	Nyctereutes	Nyctereutes	Nyctereutes	Nyctereutes
donnezani	donnezani	donnezani	donnezani	donnezani	donnezani	donnezani
Ginsburgg. 1998	Ginsburgg. 1998	Ginsburgg. 1998	Ginsburgg. 1998	Bartolini-Lucenti. 2018	Bartolini-Lucenti. 2018	Bartolini-Lucenti. 2018
7.9						
5.4			8.55	6.1		
			3.5	2.5		
			9	7.5		
			3.6	2.7		
	10		10.3		9.1	9.1
	4.2		4.5		3.9	
15.4	16		18.2	15.6	14.8	15.7
7.1	6.6		7.5	5.9	6.2	
	9.4		10.4	7.8	8	8.4
	6.15		7.2	5.4	5.245	6.7

Jilin Fossil China	DNF3-342	Allatini dex	Allatini sin	DFN3-155	DFN3-8	Perpignan	ACA-295
Nyctereutes	Nyctereutes	Nyctereutes	Nyctereutes	Nyctereutes	Nyctereutes	Nyctereutes	Nyctereutes
procyonoides		donnezani	donnezani			donnezani	donnezani
Jin et al.. 1984	LGPU	Koufos. 1993	Koufos. 1993	LGPU	LGPU	Monguillon et al.. 2004	Ginsburrig. 1998
	4.918	5.1	5.2			6.4	8.5
	4.192					4.1	4.95
	6.2	8.4	8.8		6.85	7.2	
	2.8	3.2	3.1		2.95	3	3.6
	6.932	9.9			8.33	8.1	8.8
	2.638	3.3			3.22	3	3.6
7.7	8.35	10.3	10.3		8.94	9.7	
3.8	3.548	4.2	4.2		3.93	3.83	
11	14.282				16.68	15.7	
5	6.668				7.03	6.3	
	5.588				5.89		
	9.64				10.9		
5.5	8.686	9.2	9		9.58	8.4	
4.6	5.69	6.1	6.4		5.54	5.7	
	3.578				4.41		

Specimen	China-1	China-2	Bulgaria 1	Bulgaria 2
Genus	Nyctereutes	Nyctereutes	Nyctereutes	Nyctereutes
Species	procyonoides	procyonoides	procyonoides	procyonoides
Author	Φώτο	Φώτο	MNHS (Bulgaria)	MNHS (Bulgaria)
c1L	4.76	4.639	5.84	5.09
c1W	2.825	2.436	5.84	4.434
p2L	5.06	4.937	5.718	5.192
p2W	2.488	2.136	2.926	2.528
p3L	5.726	5.887	6.072	6.62
p3W	2.542	2.33	2.998	2.92
p4L	7.271	6.695	7.38	6.372
p4W	3.273	3.24	3.66	3.218
m1L	13.287	12.492	12.09	12.26
m1W	5.5	4.429	5.08	5.278
m1Ltal	4.367	4.05	4.114	4.132
m1Ltrig	8.693	8.835	7.96	7.998
m2L	6.194	7.683	6.888	5.958
m2W	4.344	4.414	4.428	4.264
m2Ltal	2.931	3.865	3.194	0

Table 23. Raw data used for RMA regression analysis in this study as given by (Ito and Endo, 2016).

<i>Nyctereutes procyonoides</i>	<i>Vulpes vulpes japonica</i>
	4
111.02	141.01
16.16	43.63
1.7	3.01
9.04	13.78
0.19	0.29
2.48	4.94
0.84	1.46
2.8	3.2
7.01	16.28
0.91	1.4
7.32	11.15

					Procyonidae					Phocidae	Canidae
<i>Mustela itatsi</i>											
	<i>Martes melampus</i>										
		1.3	3.4								
55.48		85.65	101.56		126.85	117.57	80.23				135.02
3.51		7.7	23.18		40.37	46.98	5.44		73.45		36.63
0.95		1.83	1.54		3.23	2.59	1.3		4.09		3.03
3.42		4	14.63		11.87	17.18	3.96		17.01		11.44
0.02		0.11	0.19		0.33	0.35	0.03		3.03		0.54
0.24			0.59				0.48				
0.03			0.3				0.06				
0.2		0.77	1.39		3.76	5.29	0.54		9.65		4.73
0.47		0.83	0.83		1.22	1.05	0.9		2.03		1.08
0.43		0.88	1.59		2.92	4.67	0.57		4.51		4.13
0.53		2.84	4.82		9.46	15.59	2.1		25.51		10.28
0.53		0.67	0.92		1.39	1.29	1.11		2.12		1.8
1.16		4.01	5.28		6.91	12.6	1.89		11.73		6.2

Felidae	<i>Felis catus</i>	<i>Panthera uncia</i>	Viverridae	Mustelidae	<i>Aonyx cinerea</i>	<i>Enhydra lutris</i>	<i>Neovision vison</i>
<i>Puma concolor</i>			<i>Paguma larvata</i>	<i>Aonyx capensis</i>			
192.8	85.33	171.14	106.47	123.16	81.04	136.48	70.52
148.89	11.17	104.75	16.54	54.48	17.03	79.34	6.72
5.06	1.88	3.56	1.54	3.53	2.04	3.04	1.62
27.94	5.28	27.91	10.46	14.63	7.9	24.71	3.92
0.53	0.06	1.08	0.06	0.28	0.14	0.38	0.09
	0.24	0.81				0.6	0.59
	0.06	1.26				0.6	0.13
26,5	1.76	13	2.56	2.1	1.35	3.18	0.45
2,12	1.24	1.41	0.92	0.89	0.64	1.11	0.76
11,86	1.38	8.75	2.66	2.27	2.05	2.75	0.56
87,93	6.51	53.54	8.43	10.1	3.32	12.09	1.53
2,82	1.13	2.31	0.95	1.45	0.74	1.37	0.95
32,17	5.77	24.71	8.63	6.46	4.6	10.62	1.56

Family	Species	BW (Kg)	SKL (mm)	Mass (g)	FL (cm)	PCSA (cm ²)	Mass (g)	FL (cm)	PCSA (cm ²)	Mass (g)	FL (cm)	PCSA (cm ²)	Mass (g)	FL (cm)	PCSA (cm ²)
						Temporalis									
									Lateral pterygoid						
									Medial pterygoid						
									Whole masseter						

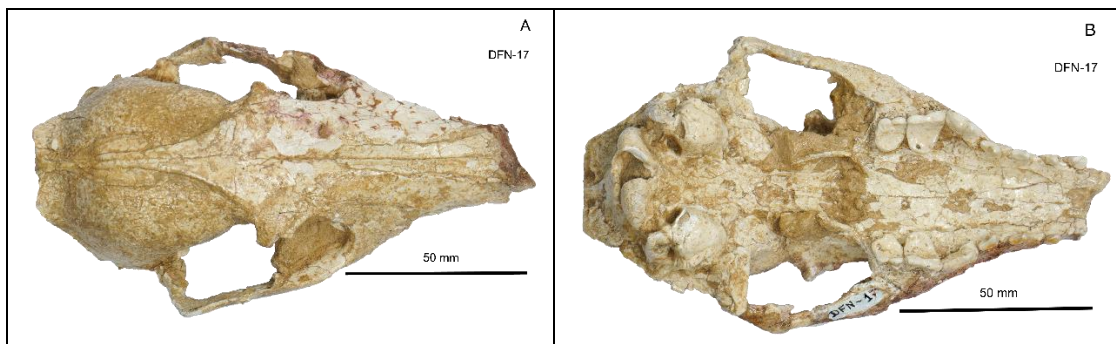


Fig. 35. DFN-17 (*N. megamastoides*), A: dorsal view, B: ventral view, LGPUT.

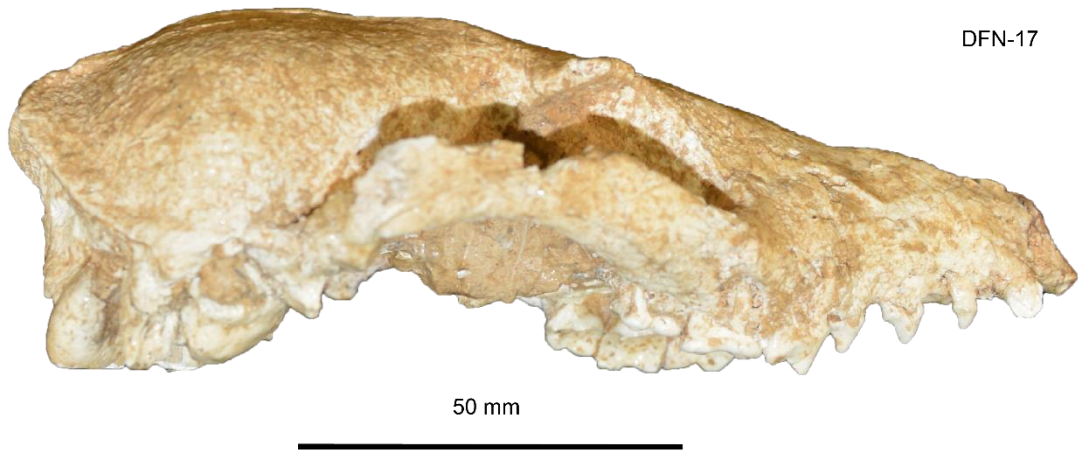


Fig. 36. DFN-17 (*N. megamastoides*) lateral view, LGPUT.

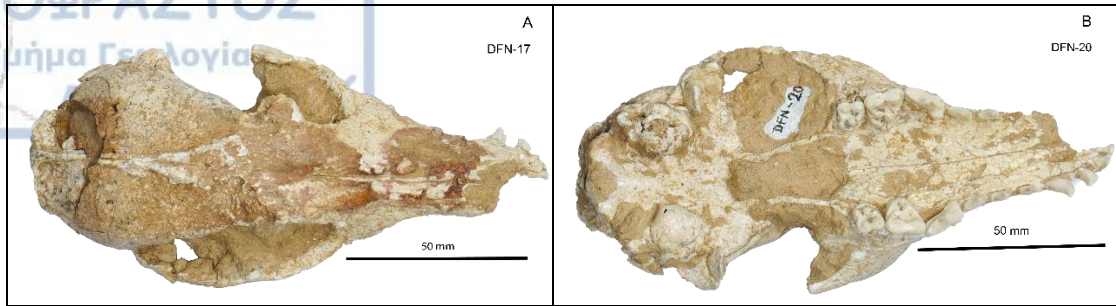


Fig. 37. DFN-20 (*N. megamastoides*), A: dorsal view, B: ventral view, LGPUT.

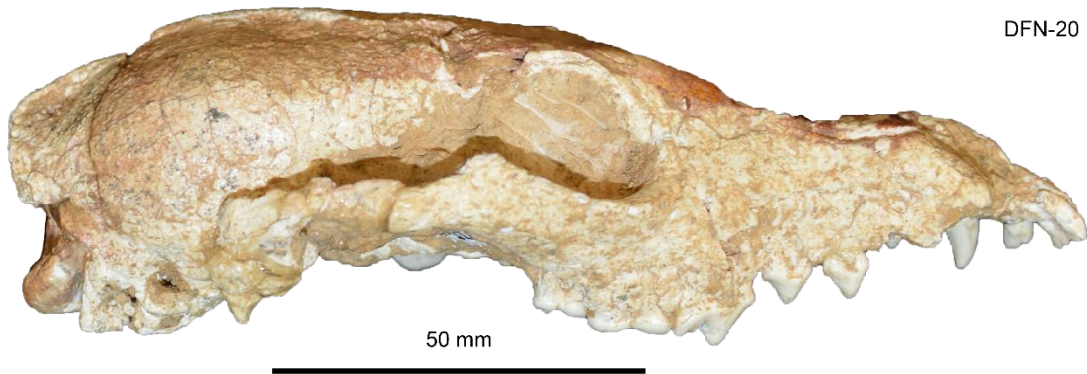


Fig. 38. DFN-20 (*N. megamastoides*) lateral view, LGPUT.

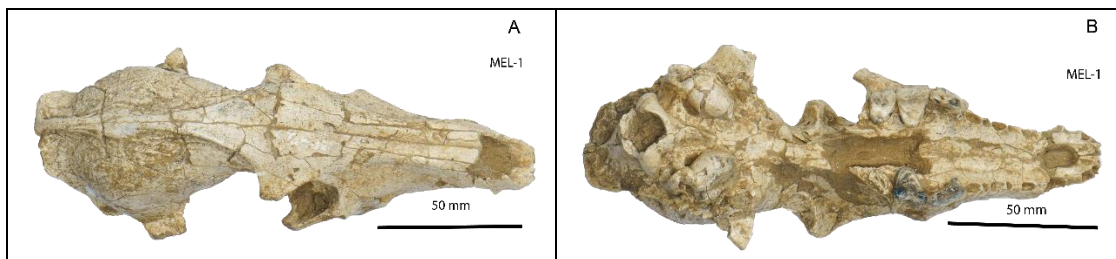


Fig. 39. MEL-1 (*N. tingi*), A: dorsal view, B: ventral view, LGPUT.



Fig. 40. MEL-1 (*N. tingi*) lateral view, LGPUT.

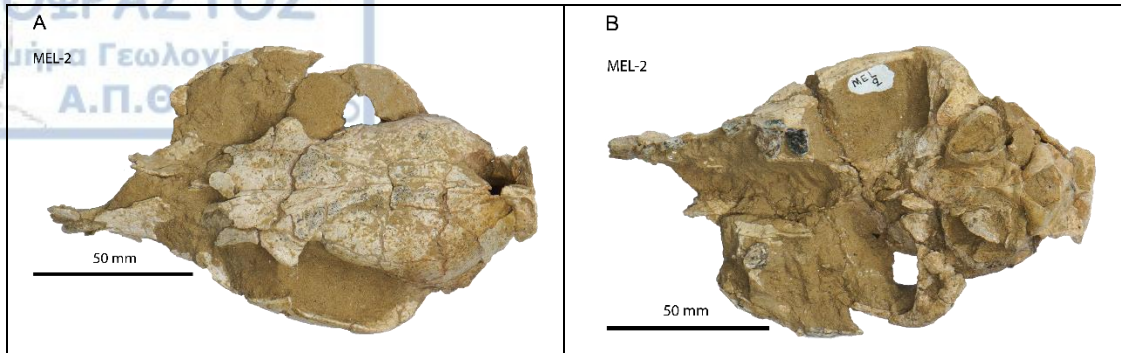


Fig. 41. MEL-2 (*N. tingi*), A: dorsal view, B: ventral view, LGPUT.

MEL-2

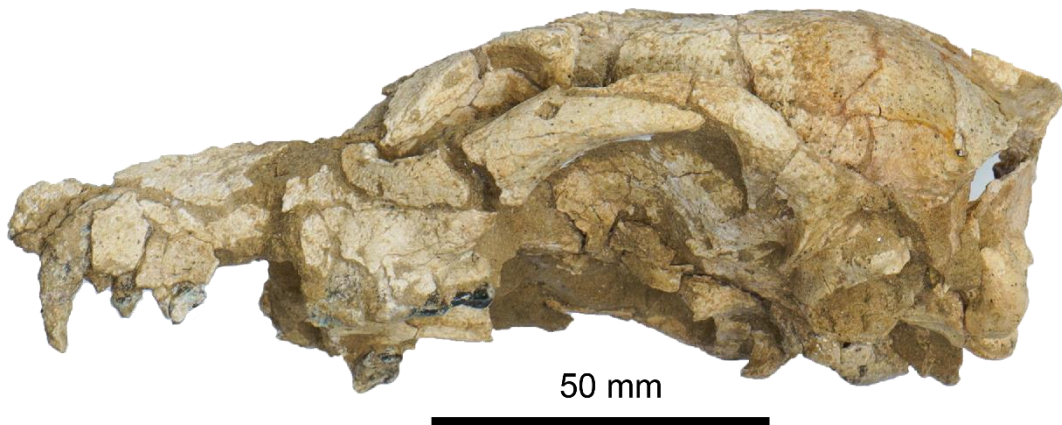


Fig. 42. MEL-2 (*N. tingi*) lateral view, LGPUT.